AUTOMATING RIPARIAN HEALTH ASSESSMENT USING HIGH-RESOLUTION REMOTELY SENSED IMAGERY

BY

GABRIELLE MARIE LEO

A Thesis submitted to the Faculty of Graduate Studies of
the University of Manitoba in partial fulfilment of the
requirements of the degree of

MASTER OF SCIENCE

Department of Environment and Geography
University of Manitoba
Winnipeg, Manitoba

ABSTRACT

Riparian areas are ecologically and economically critical habitats in the Canadian Prairies. An estimated 80% of riparian zones in North America are threatened by anthropogenic development. While riparian conservation is integrated into agricultural, watershed, and forestry best management practices across Canada, existing riparian health assessments are reliant on resource-intensive field surveys. The objective of this thesis was to develop a riparian health assessment using high-resolution remotely sensed imagery. Riparian health surveys were conducted along the La Salle River. High-resolution imagery and LiDAR data were integrated into an object-based image analysis of vegetation. Topographic analysis was conducted using a high-resolution DEM. These data were input into a linear discriminant classifier to model riparian health. Riparian health models containing both vegetation and topographic variables, and only vegetation variables, produced good agreement with field assessments. LiDAR data and the object-based image analysis method were successfully used to develop a remote riparian health assessment.

ACKNOWLEDGEMENTS

Completion of this project would not have been possible without the assistance of many people. I would first like to thank my committee, particularly my advisor, Dr. David Walker, for support, constructive criticism, and many hours of meetings and thought-provoking discussion during all stages of the project. In addition, thanks to Dr. Rick Baydack and Dr. Nicola Koper, for valuable discussion of methods and feedback on drafts.

Thank you to the University of Manitoba and the Natural Sciences and Engineering Research Council of Canada for needed funding.

Thanks to Agriculture and Agri-food Canada, especially to Jarrett Powers, Grant Wiseman, Melanie Dubois, and Evan Rodgers for providing access to data, software, training, and field support, without which this project could never have been completed. Thanks also to Megan Krohn and Amanda Shave for assistance during the three months of field data collection.

Thank you to Marilena Kowalchuk for valuable consultations regarding field methodology.

Finally, I would like to thank my family: my parents, Lorraine Leo de Jong and Christopher Leo, for unwavering moral support and proofreading; and my fiancé Brian Miller, for his love, encouragement, patience, and for keeping me sane throughout the process.

TABLE OF CONTENTS

LIST OF TABLES

LIST OF FIGURES

CHAPTER 1: INTRODUCTION

1.1 Overview

Riparian zones are fundamentally important, both economically and ecologically, but are also among the most sensitive and the most threatened habitats on a global scale (Nilsson and Svedmark, 2002; Naiman and Décamps, 1997). They are ecotonal habitats, representing an abrupt transition in biotic, geomorphologic, and hydrologic gradients. The components of riparian zones are inextricably interconnected; they represent habitat and food sources for terrestrial and aquatic wildlife, geomorphologic and fluvial interactions affecting bank stability, floodplain evolution and sediment transport, and the transfer of energy and nutrients between aquatic and terrestrial environments (Merritt et al., 2010; Nilsson and Svedmark, 2002; Gregory et al., 1991). However, they also readily transport non-point source pollution, excess nutrients and sediment, and agricultural chemicals from surface and subsurface runoff. Anthropogenic activities, such as river flow regulation, forestry, ditch construction, and pollution derived from agricultural and community sources, cause flooding and sedimentation, undermine bank stability, and compromise the integrity of the biotic community (Manitoba Water Stewardship, 2011; Nilsson and Svedmark, 2002).

The health of riparian zones can have a substantial impact on surrounding natural and anthropogenic environments. Assessing, monitoring and managing riparian areas is essential (Makkeasorn et al., 2009; Mayer et al., 2005; Nilsson and Svedmark, 2002). However, characterizing riparian health can be difficult, as it pertains not only to the current physical and biotic characteristics of the ecosystem, but also to their relationship

to the historical condition of the same area. Riparian health has historically been assessed and monitored using ground inventories and manual aerial photo-interpretation (Gergel et al., 2007; Johansen et al., 2007a). Although this approach provides detailed information, it is costly, time-consuming, and often logistically infeasible in remote or inaccessible areas. Automated approaches based on high-resolution aerial and satellite imagery, Light Detection and Ranging (LiDAR), and digital elevation models (DEMs) have the potential to facilitate landscape-level monitoring by reducing the resources required and providing access to remote areas (Forzieri et al., 2010; Makkeasorn et al., 2009; Johansen et al., 2008b; Johansen et al., 2007a).

1.2 Physiographic and Biological Characteristics of the Riparian Zone

The riparian zone is characterized by complex interactions between its hydrologic, geomorphologic, and biotic components (Camporeale et al., 2013; Merritt et al., 2010; Naiman and Décamps, 1997; Hughes, 1997; Gregory et al., 1991). The narrow, linear form of riparian habitat, combined with frequent natural disturbance resulting from seasonal and stochastic flooding, produces an extremely dynamic system, exhibiting abrupt topographic, soil type, nutrient, and moisture gradients (Steiger et al., 2005; Hughes, 1997). The stochastic nature of riparian areas and their linear form also create habitat connectivity and a wide variety of micro-habitats, resulting in disproportionately high biodiversity (Décamps et al., 2004; Nilsson and Svedmark, 2002).

Riparian geomorphology can be reliably predicted as a function of channel width, depth and slope, and flow velocity (Nanson and Gibling, 2003). Consequently, hydrologic regime and stream geomorphology are primary forces determining riparian zone

topography. Terracing results from cyclical channel evolution (Ilhardt et al., 2000). The initial channel, formed by downcutting, is typically narrow and deep (Hicken, 2003). Over time, owing to variable shear stress and erodibility of bank materials, the channel widens and the thalweg (deepest portion of the channel) is offset in the direction of more rapid erosion. A hydrologic shift, such as an increase in precipitation, causes the stream to begin downcutting in the region of the thalweg. Subsequent lateral cutting erodes the stream banks, resulting in a meandering channel form and producing a wide, flat channel at a lower level than the initial channel and a river terrace at the initial bankfull elevation. The wide, shallow stream experiences increased shear stress, resulting in the formation of sand bars and channel braiding. When water inputs increase, downcutting recommences at the new, lower level, and the cycle of terrace formation continues.

The hydrologic and geomorphologic regimes heavily influence riparian plant community composition (Merritt et al., 2010; Steiger et al., 2005; Naiman and Décamps, 1997; Gregory et al., 1991). Moisture gradients, minimum and maximum flow levels, the duration of the period of inundation, and the variability of the flow regime can all influence species presence and abundance (Auble et al., 2005; Nilsson and Svedmark, 2002; Hughes, 1997; Auble et al., 1994). Plants inhabiting the riparian zone must be tolerant of changing water levels and mechanical disturbance resulting from current and wave action (Hughes, 1997; Roberts and Ludwig, 1991). The majority of plant species are extremely sensitive to changes in maximum and minimum flood levels, even if mean annual water levels remain unchanged (Merritt et al., 2010; Auble et al., 1994). Similarly, many species are unable to withstand mechanical disturbance. Thus, a stochastic flood regime supports plant communities that are distinctly different from those found in

adjacent terrestrial and aquatic habitats. In addition, the hydrologic regime controls the availability of substrates, nutrients and moisture required by plant communities (Camporeale et al., 2013). Riparian gallery forests are characterized by spatial topographic variation resulting from terracing (Red River Regional Council, 2006).

There is a strong association between the geomorphologic environment and vegetation community composition (Lenhart et al., 2013; Osterkamp and Hupp, 2010; Richards et al., 2002; Tabacchi et al., 1998; Hughes, 1997; Hupp and Osterkamp, 1996; Harris, 1988). Erosion and sedimentation are natural parts of the riparian habitat disturbance regime, allowing species to colonize and stabilize, and thereby increasing species diversity and acting as primary forces controlling vegetation composition in the riparian area (Camporeale et al., 2013; Steiger et al., 2005; Bendix, 1994; Hupp and Osterkamp, 1996). The stratigraphic characteristics of deposited sediment influence many aspects of plant habitat, including soil water retention and balance, hydraulic conductivity, oxygen availability, nutrient retention, and physical disturbance (Hupp and Osterkamp, 1996). Vegetation community type is heavily influenced by moisture availability, soil type, and nutrient availability. Consequently, riparian vegetation exhibits spatially driven topographic succession associated with the elevation change between terraces, wherein the bank zone, terraces, and upper slopes are characterized by distinct vegetation communities (Figure 1.1) (Smith et al., 1998; Hughes, 1997).

Riparian vegetation can also reciprocally influence channel morphology, flow velocity, and transport of sediment, nutrients and contaminants (Camporeale et al., 2013). Vegetation contributes to bank stability both through physical stabilization and through

increased soil cohesion caused by matric suction (water tension) resulting from soil water uptake by plants and evapotranspiration (Pollen-Bankhead and Simon, 2010; Wynn and Mostaghimi, 2006; Micheli et al., 2004; Tabacchi et al., 2000; Hicken, 2003). Established root systems and above ground biomass protect deposited sediment from fluvial erosion and overland flow, thereby increasing accretion rates (Lenhart et al., 2013; Osterkamp and Hupp, 2010; Corenbilt et al., 2009; Van Pelt et al., 2006; Tabacchi et al., 1998). Plants also provide a temperature buffer, thereby reducing the amount of bank weakening caused by freeze-thaw cycles (Wynn and Mostaghimi, 2006). Vegetation reduces flow rate by increasing channel roughness, resulting both from living vegetation and from deposited woody debris, thereby reducing erosion (Tabacchi et al., 1998). Vegetation deposits downed woody debris in the channel and regulates water temperature through the effects of shading, creating a range of microhabitats exploited by aquatic biota (Tabacchi et al., 1998; Naiman and Décamps, 1997).

1.3 Spatial Extent of the Riparian Zone

Defining the spatial extent of the riparian zone is difficult owing to the complexity of interactions among the biotic and physical components of the habitat, as well as with adjacent terrestrial and aquatic ecosystems (Ilhardt et al., 2000; Naiman and Décamps, 1997). There is no consensus as to how the riparian zone should be defined; several instances in the literature can be found in which the terms “riparian zone” and “floodplain” are employed without any reference to a specific definition (Fischer et al., 2001; Ilhardt et al., 2000; Harris, 1988). Some differences of opinion are inevitable, as the manner in which the riparian zone is defined necessarily reflects the aims of the

analysis in question (Ilhardt et al., 2000). A variety of methods for defining the riparian zone have been used for different applications; these can be broadly grouped as methods based on predefined measurements applied indiscriminately to all riparian areas, and methods based on functional characteristics of the particular riparian area in question. The latter category is modified for appropriate application to individual habitats.

One of the oldest and most common methods of delineating the riparian zone using predefined measurements is the fixed-width buffer method (Mayer et al., 2005; Ilhardt et al., 2000). Watercourses are buffered to form a strip of a set width on either side of the watercourse. This approach is most often applied to conservation planning and water quality regulations (Qiu, 2009; Dixon et al., 2006). A single buffer width can be used along the entire watercourse, or a series of widths determined based on threshold values for measurable parameters may be laid out. The latter approach is employed by the USDA Forest Service, which assigns pre-defined buffer widths based on soil hydrologic group, source area, and soil capability class (Qiu, 2009; Narumalani et al., 1997). Qiu (2009) developed a topographic index, predicting base flow and runoff, to identify target areas requiring buffers and corresponding appropriate buffer widths. These methods, while often preferred for ease of use and applicability to water quality management, do not provide an ecologically meaningful delineation of riparian habitat. Several studies have shown that uniform buffers correspond poorly to the actual extent of the riparian zone (Abood et al., 2012; USDA, 2004; Skally and Sagor, 2001). Holmes (2011) found that fixed-width buffers can both underestimate riparian habitat, and include upland areas, and disagreed with a buffer based on an ecosystem function definition of the riparian zone 40% of the time. Defining the riparian zone in terms of the functional

interactions of its constituent parts represents a more holistic approach (Ilhardt et al., 2000; Gregory et al., 1991). In this vein, Ilhardt (2000) proposed a definition incorporating stream geomorphology, flood levels, and the presence of riparian vegetation, which has been widely referenced since in ecologically-focused riparian studies. Using this method, the riparian zone includes the watercourse, all adjacent areas that may be flooded for all or part of the year, and the extent of associated riparian vegetation (Holmes and Goebel, 2011; Verry et al., 2004; Ilhardt et al., 2000; Swanson et al., 1982). While it presents an ecosystem perspective, defining the riparian zone based on functional relationships requires that professional judgement be incorporated into the process of delineation (Ilhardt et al., 2000).

Delineating the riparian zone functionally using GIS technology presents further challenges, as it requires that both riparian topography and flood levels be obtainable. Several approaches have been developed within the last ten years. Holmes and Goebel (2011) used the stream geomorphology approach developed by Ilhardt et al. (2000) and Verry et al. (2004) to manually delineate the extent of the riparian zone from topographic maps, with an additional buffer of one average tree height extending outward. This approach requires significant ecological knowledge, and is more costly and time-consuming to develop than a fixed-width buffer. Also in 2011, Clerici et al. built a riparian habitat detection model using the coincidence of modelled 50-year flood levels, based on a 100 m DEM, and path distance (lateral cost of movement) indices calculated from 10 m and 30 m DEMs along digitized river/stream networks, and a 25 m buffer around ephemeral streams to contain possible riparian area. Within this boundary, they used a fuzzy membership classifier to identify riparian habitat based on classified Landsat

ETM+ imagery and an existing forest cover map. Mason and Maclean (2007) and Abood et al. (2012) modelled riparian zone extent using a 10 m DEM and the 50-year flood level. While these approaches accurately delineated the riparian zone, they require that 50-year flood levels be obtainable. This project used a method modified from Mason and Maclean (2007) and Abood et al. (2012), wherein a high-resolution DEM and maximum mean monthly flood level were used to approximate the riparian zone, owning to the lack of availability of 50-year flood level records.

1.4 Riparian Health, Threats to Riparian Habitat and Health Assessment

There is no universal definition for riparian health, and, when described, it is usually associated with applied practical assessments (Norris and Thoms, 1999). Consequently, it is often defined in accordance with the interests of the organization conducting the assessment, with a disproportionate focus placed on a single component (biological, ecological, hydrological, or geomorphological) of riparian habitat, without regard for the remaining components and their interconnectedness. To obtain a more holistic perspective, riparian health should be defined based on the degree of similarity between a given riparian habitat and its historical condition prior to anthropogenic or natural disturbance (Jansen, 2005). Riparian habitats are inherently dynamic ecosystems, subject to frequent disturbance in the form of changing water levels, erosion and channel migration; therefore, processes of degradation, such as bank instability due to undercutting, do not necessarily reflect poor riparian health (Nilsson and Svedmark, 2002; Naiman and Décamps, 1997). Historical fluvial regimes, erosional processes and vegetation composition should be considered in assessing riparian health. As detailed

ecological information regarding the historical condition of riparian habitats is often not available, the condition of adjacent, relatively undisturbed riparian habitats can be used to assess the probable natural state of modified riparian area, as regards its capacity to support ecosystem functions and biotic communities (Jansen, 2005).

Globally, riparian zones are among the most sensitive and vulnerable habitats (Millenium Ecosystem Assessment, 2005; Nilsson and Svedmark, 2002; Narumalani et al., 1997). The riparian zone is affected by the nutrient, chemical and sediment inputs, moisture retention capacity, and biotic species composition of adjacent uplands (Naiman and Décamps, 1997). Consequently, anthropogenic modification of surrounding habitats can have a detrimental effect on the health and function of riparian habitats. Anthropogenic factors influencing the riparian zone are primarily related to land use (Harris, 1988). The key influences include agricultural activities, water regulation, and urban development (Arroyo, 2010; Merritt et al., 2010). Agricultural production introduces chemicals, nutrients and sediment into the river system through surface and subsurface runoff (Leclaire, 2011). In addition, mechanical disturbance from land clearing for agricultural and urban development, and grazing pressure from livestock, disrupt riparian biota, undermine bank stability, and increase erosion and sediment load in streams and rivers (Arroyo et al., 2010). Municipal water systems can pollute riparian habitat through the discharge of wastewater and effluent. Water control structures such as dams interfere with natural water levels, causing flooding and sedimentation, and undermining bank stability.

While anthropogenic factors can negatively influence riparian health and functionality, the health of riparian habitat also has implications for human well-being (Steiger et al., 2005). Functioning riparian habitat regulates water quality by trapping nutrients, chemicals and sediment, and controls flooding through water retention (Steiger et al., 2005; Décamps et al., 2004; Tabacchi et al., 1998; Hughes, 1997). When this functionality is lost, human communities experience poor water quality as a result of chemical and wastewater transport, fisheries and recreation are disrupted by nutrient loading to lakes, and areas adjacent to the riparian zone are subject to increased flood levels.

Riparian vegetation also plays an important role in preventing soil erosion (Zaimes et al., 2008). While undisturbed riparian forest provides the best protection, any deep-rooted vegetation cover represents an improvement in bank stability as compared with unvegetated areas or those characterized by shallow-rooted vegetation. In North America, riparian zones adjacent to annual row crops are associated with a high rate of bank erosion. The worst bank erosion is seen in cattle pastures; however, pastures including riparian forest are less damaged than those without forest (Zaimes et al., 2008). Sediment trapping and rate of soil erosion are inversely proportional to root density through binding effects of roots, and through an increase in channel roughness, which increases flow resistance (Steiger et al., 2005; Hughes, 1997).

Riparian zones are important refuges for biodiversity. They provide critical habitat for two thirds of Canada's endangered species (Saunders, 2000). They are disproportionately plant species-rich, owning to the broad range of micro-habitats created by the sharp

hydrological, geological and soil gradients by which they are characterized (Décamps et al., 2004) (Décamps et al., 2004; Nilsson and Svedmark, 2002). These micro-habitats are also utilized by fish, birds, mammals, and terrestrial and aquatic invertebrates. In addition, riparian zones serve as corridors between habitats for wildlife, and for organic and inorganic material influencing plant communities (Levick et al., 2008; May, 2003; Nilsson and Svedmark, 2002).

Riparian health is assessed for purposes of management using health indicators. Indicators are observable characteristics of the ecosystem, from which less the visible components of healthy ecosystem function can be reliably inferred (Young and Collier, 2009). While individual structural and functional characteristics do not necessarily exhibit linear relationships, the goal of riparian habitat inventories is to identify several easily observable characteristics, which, in combination, provide a reasonable indication of total ecosystem health. As riparian inventories have traditionally been conducted in the form of detailed field surveys, the majority of riparian health indicators comprise characteristics which can be easily observed from the ground, such as: vegetation species composition; canopy cover and age class; vegetation removal by herbivore browsing or anthropogenic means; channel form and substrate composition; fluvial landforms, undercutting and human alterations affecting bank stability; and proportion of exposed soil (Dixon et al., 2006; Dixon et al., 2005; Fitch and Ambrose, 2003).

While ground monitoring provides detailed information pertaining to riparian habitat function, survey methods are costly and time-consuming (Forzieri et al., 2011; Johansen et al., 2010a; Makkeasorn et al., 2009; Johansen et al., 2008b; Johansen et al., 2007b).

Consequently, resource availability often limits the riparian monitoring efforts to small or particularly sensitive areas. In addition, conducting surveys in remote and inaccessible regions can be difficult or infeasible. As watersheds can occupy hundreds of square kilometres, there is a need to develop automated assessment methods, which can be used to monitor riparian condition over large areas and to identify problem areas requiring the application of management prescriptions. Recent research has begun to assess a variety of approaches for delineating and assessing riparian zones using remotely sensed data, including aerial and satellite imagery, DEMs, and LiDAR (Aguirre-Gutiérrez et al., 2012; Johansen et al., 2011; Abood et al., 2012; Johansen et al., 2010a; Johansen et al., 2010b; Johansen et al., 2008a; Johansen et al., 2008b; Platt and Rapoza, 2008; Gergel et al., 2007; Johansen et al., 2007a; Johansen and Phinn, 2006a; Johansen and Phinn, 2006b; Jansen, 2005).

1.5 Remote Sensing Overview and Data Types

Remote sensing is the term used to describe the observation and collection of information across the Earth's surface, using a device situated at a distance from the target surface being observed (Campbell, 2002; Barrett and Curtis, 1999). Objects on the Earth's surface emit electromagnetic energy at wavelengths as a function of their internal temperature. Information is collected by measuring the electromagnetic energy reflected by, or emitted from, the land or water surface of interest. Remote sensing is widely used tool in environmental studies and conservation, which allows information to be captured across large areas at a frequency not possible using in-field assessments, and has great utility in riparian applications (Campbell, 2002; Muller, 1997). The combination of high-

resolution aerial imagery, high-resolution multispectral and panchromatic satellite imagery, a digital elevation model (DEM), and light detection and ranging (LiDAR) data, has the potential to greatly improve riparian health detection and automation.

Aerial imagery typically consists of visible-spectrum panchromatic light captured using a camera mounted on an aircraft, though sensors able to detect infrared bands may also be carried (Campbell, 2002). Panchromatic imagery comprises a single band, usually displayed as a greyscale image, which covers a wide range of wavelengths. Aerial imagery can be converted to digital format and orthorectified using a DEM, stereo pairs, or topographic data, to correct for error introduced by the tilt of the camera, as well as relief displacement resulting from topographic variation. The corrected imagery can then be used in spatial analyses (Campbell, 2002). Aerial imagery capture can be scheduled to optimize the collection of features of interest such as vegetation data, and to accommodate adverse weather conditions (Gruen, 2012). Aerial imagery is typically high-resolution (<1m), and is usually available at a lower cost than high-resolution satellite imagery. The fine-scale spatial resolution offered by aerial data is beneficial for ecological studies, including riparian health assessment (Campbell, 2002).

Satellite imagery is captured from space using either an active sensor, which emits artificially generated electromagnetic radiation and measures the reflected returns from terrestrial features, or a passive sensor, which records emitted and reflected electromagnetic imagery originating from natural sources (Campbell, 2002). Multispectral imagery comprises several spectral bands, each of which covers a relatively small increment of the electromagnetic spectrum (e.g. blue, green, red, and infrared

wavelengths), resulting in a high spectral resolution (Dhore and Veena 2014). As different objects and surfaces such as soil, water, and vegetation are each associated with a particular spectral signature, multispectral imagery is useful for deriving indices and for environmental analyses. Despite the greater spectral resolution, multispectral imagery is usually captured at a coarser resolution than panchromatic data (Campbell, 2002). Consequently, multispectral and panchromatic imagery can be used in combination to utilize the benefits of both spectral differentiation and high spatial resolution.

The use of aerial and satellite imagery to map and classify the riparian zone is applied mainly to the vegetation component, and to physical characteristics, such as channel width, that can be easily observed using optical data (Jansen, 2005; Johansen et al., 2006a; Johansen et al., 2006b; Gergel et al., 2007; Johansen et al., 2007a; Johansen et al., 2008a; Johansen et al., 2008b). The use of DEMs to delineate riparian areas has value in that DEMs detect fluvial landforms that can be incorporated with recorded water levels to identify areas affected by mean and maximum flood levels (Abood et al., 2012). A DEM depicts a continuous three-dimensional elevation surface, commonly the elevation of a topographic surface (Podobnikar et al., 2000). DEMs are constructed using measured values, either in a grid format or at a series of survey point locations; the latter is known as a Digital Terrain Model (DTM) point dataset. These data can be collected in the field, or derived from aerial or satellite imagery, or LiDAR data. Slopes connecting known point values are interpolated using one of a variety of methods, such as kriging, inverse distance weighting, or nearest neighbour (ESRI, 2010). Several studies suggest that recorded flood levels provide the most reliable method to delineate the riparian zone (Abood et al., 2012; Ilhardt et al., 2000). DEMs enable the delineation of areas

submerged at a given flood level, and also facilitate the identification of landforms, such as terraces.

While aerial and satellite imagery can be classified to identify features visible from the air, and DEMs are useful for delineating geomorphologic structures, neither can accurately detect the vertical structure of vegetation communities. As the structure of both the understorey and the canopy change rapidly between the water's edge and the forested upper slopes marking the edge of the riparian zone, the ability to detect these characteristics has the potential to dramatically improve automated riparian assessments (Naiman and Décamps, 1997). Light Detection and Ranging (LiDAR) systems have the capacity to provide the necessary data. LiDAR, also known as laser altimetry, is an active sensor remote sensing technology, which derives elevation data by emitting short duration laser pulses light and measuring the return time of backscattered light to the sensor (Wandinger, 2005; Lefsky et al., 2002). Recent developments in LiDAR research have demonstrated that this technology has the capacity to improve the accuracy of classifications derived from optical imagery through the addition of structural information, and to augment spatial analysis by the provision of three-dimensional data (Hudak et al., 2009; Wulder et al., 2008; Wandinger, 2005; Lefsky et al., 2002). Vegetation height can be determined by subtracting the ground-level return time from the return time for the top of various understorey and canopy levels (Johansen et al., 2011; Johansen et al., 2010a; Johansen et al., 2010c; Goetz, 2006; Dowling and Accad, 2003). From these data, canopy and stand vertical structure can be described. Vegetation height and stand structure can be incorporated with classified imagery to more accurately characterize the riparian zone (Chen et al., 2012). In addition, the enhanced vegetation

community information can be used to estimate channel flow based on vegetation characteristics that affect channel flow resistance (Forzieri et al., 2010).

1.6 Application of Remote Sensing to Riparian Studies

Vegetation mapping and classification of the narrow riparian zone has historically been conducted using aerial photo-interpretation from high-resolution stereo imagery (Johansen et al., 2007a; Johansen et al., 2007b; Muller, 1997). While manual photo-interpretation is time-consuming and, consequently, is limited to small areas, riparian studies have continued to rely heavily on field surveys and photo-interpreted aerial imagery, owing to the coarse resolution (20-30 m) of satellite imagery available for broader coverages (Dilts et al., 2010; Johansen et al., 2007a). Automated classification of imagery prior to 2000 used a pixel-based classification system, in which individual pixels were classified according to spectral reflectance values. Pixel class values are defined based on training datasets. A pixel of a given resolution represents a fixed unit of area on the ground, regardless of the scale of the objects of interest in the image to be classified (Hay et al., 2003). This is particularly problematic in riparian habitat classification, as the riparian zone is often too narrow to be detected at a coarse resolution (Johansen et al., 2007a; Muller, 1997). Riparian classification studies conducted using pixel-based classification techniques have had limited success in differentiating vegetation characteristics (Nagler et al., 2001; Lonard et al., 2000).

While riparian areas are too narrow to be mapped using medium resolution imagery, such as Landsat, the advent of high-resolution satellite imagery (<5 m) provided the raw material necessary to detect riparian features (Alencar-Silva and Maillard, 2010).

However, the use of pixel-based methods to classify high-resolution imagery often results in a "salt and pepper" effect, as each pixel covers a very limited area and individual pixels are often characterized by outlier spectral values, interfering with the ability to detect features composed of multiple pixels (Blaschke, 2010; Yu et al., 2006; Bock et al., 2005). This effect is more pronounced when pixel-based classification is applied to a heterogeneous surface, such as riparian area, which represents an abrupt gradient in physical and vegetation features. Object-based image analysis, an alternative classification method, minimizes this effect using image segmentation to group pixels into objects based on spatial, textural, and spectral characteristics prior to classification (Yu et al., 2006). The resultant reduction in image noise provides for a smoother visualization and more accurate classifications.

Image segmentation is an iterative routine that first divides the image by detected underlying spatial and spectral patterns, then further segments the base objects, applying rules defined by expert knowledge (Blaschke et al., 2002). Segmentation is completed when all pixels have been assigned to objects according to a user-defined scale. A wide variety of segmentation algorithms have been developed, including region-, field- and edge-based segmentation, and multi-scale and multi-date segmentation, among others (Aguirre-Gutiérrez et al., 2012; Desclée et al., 2006; Blaschke et al., 2002; Pal and Pal, 1993). These algorithms incorporate spatial and textural quantifiers, such as nearest neighbour distances, shape metrics, texture descriptors and hierarchy with spectral reflectance values such as mean brightness to provide context for image classification and emphasize different image elements associated with features inherent to the objects being analysed (Im et al., 2008; Hay et al., 2003). Thus, selecting appropriate algorithms is

essential to accurately discriminating between objects of interest. Because pixel values are grouped to form objects, statistics describing spectral information such as: median values; minimum and maximum values; and mean ratios and variance can be calculated for each object (Blaschke et al., 2002). The statistics available for individual pixels, such as mean bandwidth, are much more limited. More importantly, spatial statistics such as distances, neighbourhoods and topologies can be computed for each object. Because OBIA utilizes spatial, geometrical, and textural attributes, it can be used to extract valuable information from panchromatic imagery that would not accessible using a pixel-based classification, which considers only spectral values (De Kok et al., 1999). As panchromatic imagery is available for larger areas and at higher resolutions than multispectral imagery, it is essential that methods able to access this valuable source of information be developed. OBIA is currently the only viable method for this task (De Kok et al., 1999).

Object-based image analysis produces significantly higher classification accuracies than traditional pixel-based classification when applied to high-resolution imagery (Aguirre-Gutiérrez et al., 2012; Platt and Rapoza, 2008). Several riparian classification studies based on object-based image analysis were conducted between 2000 and 2005. These produced relatively poor results, as only medium resolution (5-30 m) imagery was available (Yang, 2007; Congalton et al., 2002). Many researchers concluded that, while some characteristics, such as channel scour and deposition, and vegetation density could be identified, the riparian zone was too narrow for vegetation structure and composition to be accurately detected using medium resolution imagery (Brooks and Knight, 2008; Congalton et al., 2002). Post 2005, the increasing availability of high-resolution satellite

imagery has produced several advances in the use of object-based image analysis as an assessment tool. Studies have indicated that a wide variety of riparian health indicators, such as density of tree crowns, tree clearing, percent foliage cover, vegetation communities, organic litter, vegetation overhang, riparian zone width, channel width, width of exposed stream banks (an indicator of bank stability), distance between cleared areas and the stream channel, flood damage, and canopy continuity, can be detected using objected-based image analysis (Johansen et al., 2008a; Johansen et al., 2008b; Gergel et al., 2007; Johansen et al., 2007a; Johansen and Phinn, 2006a; Johansen and Phinn, 2006b; Johansen and Phinn, 2006b; Jansen, 2005). Recent research also indicates that riparian forest structure can be detected through the inclusion of both optical and LiDAR imagery in an object-based image analysis (Alencar-Silva and Maillard, 2010; Wang et al., 2008). Incorporating optical and LiDAR datasets, and object-based classification methods into existing riparian health assessments has the potential increase the efficiency and effectiveness of habitat management planning and implementation, by allowing problematic riparian areas to be targeted with comparatively minimal cost and time. This will allow the majority of resources to be reserved for the development and implementation of management prescriptions.

1.7 Statement of Problems and Objectives

Riparian areas are among the most biodiverse habitats in the Canadian prairies, and are critical to soil conservation. However, they are also among the most ecologically vulnerable habitats. Therefore, assessing, monitoring, and managing riparian areas is essential. Currently, riparian health assessments remain heavily reliant on ground-based

surveys. This approach to assessment is inherently prone to subjectivity, and, considering the length and number of river systems in the Canadian prairies, is impractical from a resource availability perspective. The primary goal of this research is to develop an objective, automated riparian health assessment to target problematic riparian areas for management planning without the need for intensive field surveys. Sub-objectives include:

1. determining the potential of object-based image analysis and canopy structure data to remotely detect riparian health;
2. developing an automated riparian health assessment using remotely sensed vegetation and topographic data; and,
3. suggesting a management protocol for the automated assessment of riparian health.

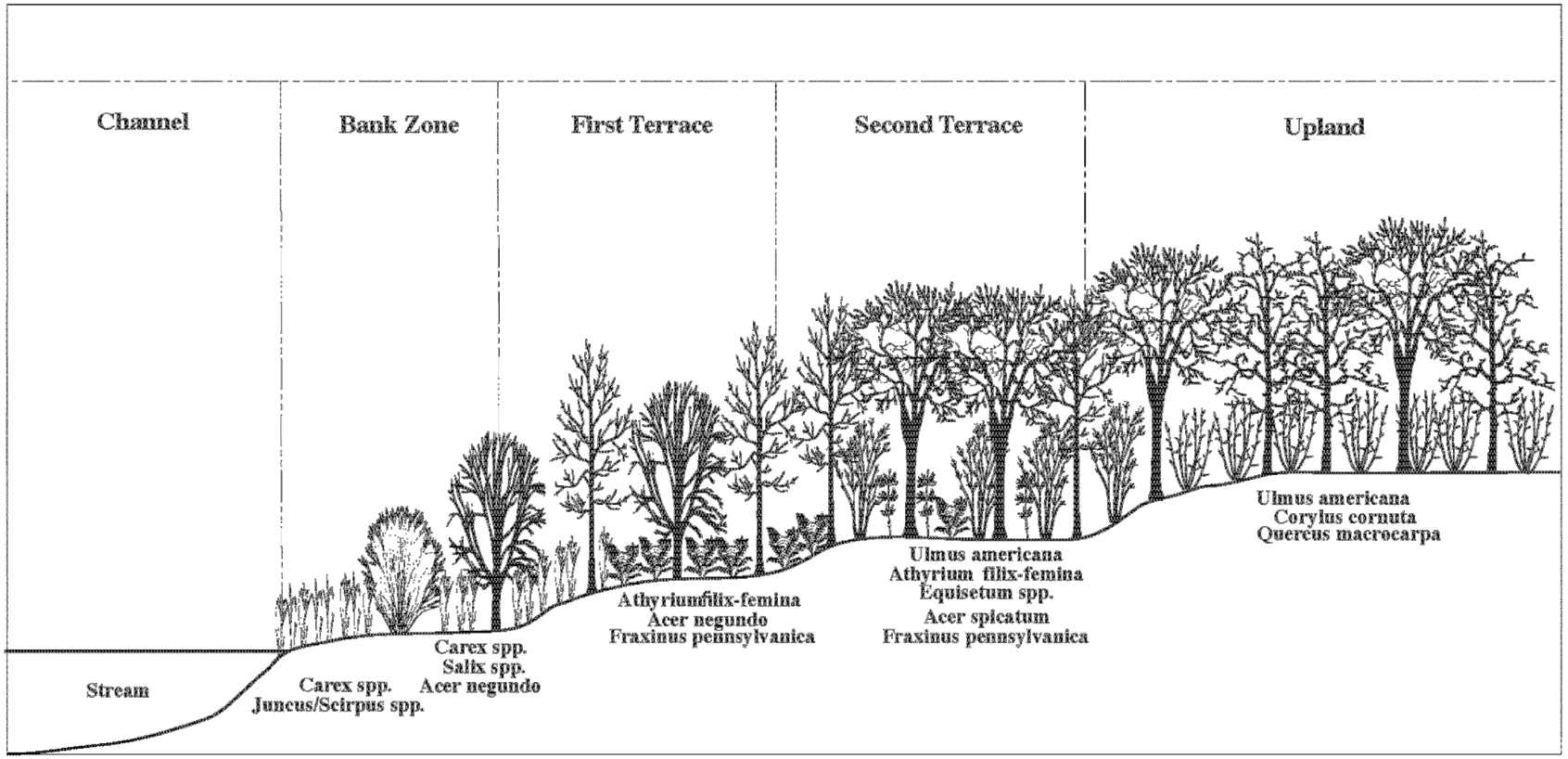

Figure 1.1. Spatially-driven topographic succession in vegetation communities typical of a riparian corridor in the La Salle River region.

CHAPTER 2: STUDY AREA

The study area comprised the majority of the La Salle River and adjacent riparian corridor in Manitoba, Canada (Figure 2.1). Riparian health field surveys were conducted along the La Salle in August, 2011 and June, 2012.

2.1 Geographic Location

The La Salle River is located in southern Manitoba, west of Winnipeg. It is the primary watercourse in the La Salle Watershed, and intersects the Winnipeg and Portage Ecordistricts in the Lake Manitoba Plains Ecoregion, contained in the Prairies Ecozone (Smith et al., 1998). The area surveyed extended 75 km along the river, from the headwaters (49°55'53"N, 98°11'18"W) to a point approximately 17 km (along the channel) west of its confluence with the Red River (49°53'11"N, 97°46'03"W).

2.2 Climate

The La Salle River is situated in the Grassland Transition Ecoclimatic Region, in the warmest and most humid portion of this climate zone (Smith et al., 1998). The Grassland Transition is characterized by long, severe winters and short, mild summers. The growing season is approximately 181-183 days, and the number growing-degree days ranges from 1700 to 1720. The dominant soil climate is subhumid Boreal, ranging from cool to moderately cold, and transitioning to Cryoboreal in the Winnipeg Ecodistrict. Weather stations in Portage la Prairie and Marquette provide climate records representing the western edge and central regions of the study area, respectively (Environment Canada, 2012a). The Portage weather station reports a mean annual temperature of 3.1°C, and a

total 514.6 mm of precipitation. Marquette records a mean annual temperature of 2.9°C, and 538.8 mm of precipitation. Up to 25% of the annual precipitation is deposited in the form of snow (Smith et al., 1998). The majority of precipitation in the area occurs between May and September (Figure 2.2). The annual moisture deficit ranges from 170 mm to 200 mm.

2.3 Soils and Geology

The La Salle River is situated on the Red River Plain in the Lake Manitoba Lowlands. The area occupied by the river is primarily underlain by Palaeozoic bedrock including, from east to west: Ordovician dolomites and limestones; Silurian dolomites; and Devonian limestones (Welsted et al., 1996; Teller, 1984). The westernmost reach of the river, near the headwaters, is associated with Jurassic shales and carbonates. The surficial geology overlying this foundation is the result of the most recent glaciation, and consists mostly of glaciolacustrine and alluvial sediments (Smith et al., 1998). The dark clays and overlying lighter calcareous silty clays, which comprise the majority of the watershed's surficial geology, were deposited following the formation of Glacial Lake Agassiz in approximately 13000 BP (Teller, 1984). Clay depth is variable, ranging from <5m to 50 m on an east-west gradient. The most eastern portion of the watershed is characterized by a gently rolling ridge and swale topography with a southeast orientation (La Salle Redboine Conservation District, 2007). The ridges, 1-3 m in height and spaced 1-3 km apart, formed when glaciolacustrine clays were deposited on glacial till ridges laid down by the Red River glacial lobe. The western third of the La Salle watershed crosses the Assiniboine delta, an alluvial deposit formed by the glacial spillway then occupied by the

Assiniboine River as it drained into Lake Agassiz. This region is characterized by a layer of medium to fine sand, with an average depth of 3 m, overlying the clay deposits. Elevation varies from approximately 259 masl on the Assiniboine Delta to 236 masl in the east (Smith et al., 1998). Topography in the area ranges from gently sloping in the west to flat on the Red River Plain in the east. Slope gradients are low, ranging from 0.3-1.0 m/km, though steeper gradients (3-10 m/km) are sometimes found immediately adjacent to the La Salle, Red and Assiniboine Rivers.

Soils in the eastern portion of the watershed are dominantly Gleyed Humic Vertisols, Gleyed Vertic Black Chernozems, Gleysolic Humic Vertisols and Humic Gleysols, with imperfect to poor drainage (La Salle Redboine Conservation District, 2007; Smith et al., 1998). Surface drainage has been enhanced in the majority of poorly drained soils in the area. These enhancements cause poorly drained soils to exhibit imperfect drainage characteristics. As a result of the higher sand content, Rego Black Chernozems with by imperfect drainage are the predominant soil type along the western portion of the La Salle. The high clay content of the majority of the soils along the La Salle is a concern with regard to water erosion, as poor infiltration results in increased ponding and surface runoff (La Salle Redboine Conservation District, 2007). The flat local topography largely mitigates this risk, resulting in a water erosion designations of negligible or low for most of the area. However, transport of soluble nutrients and chemicals from agricultural areas remains a concern. The risk of wind erosion is considered to be moderate in the clay-dominated eastern two thirds of the area; however, the sandy soils to the west have been classified as being at a high to severe risk of wind erosion.

2.4 Hydrology

The La Salle River watershed is part of the Red River drainage division, a component of the Nelson River Drainage Basin (Smith et al., 1998). The La Salle has a total drainage area of 2407 km^2 and an approximate channel length of 108 km. It is a turbid, slow-moving river, exhibiting defined meanders, meander cutoffs and oxbows, as well as significant bank undercutting associated with meander development (Graveline and Larter, 2006). It occupies a paleochannel of the Assiniboine River, which was carved by the Assiniboine approximately 2980 BP and abandoned by 1300 BP (Welsted et al., 1996).

Hydrometric data, including flow rates and water levels, have been collected at various times at 12 stations along the La Salle River operated by (Environment Canada, 2012b). Data summarized below were drawn from a station located in Sanford, Manitoba, as it reports both flow rates and levels, and has the longest record of 1915-2010. However, only data collected between 1967 and 2010 are included, as collected prior to this period is very incomplete. Peak flows occurred in April in all recorded years, with the exception of 1979, 2005 and 2010, in which the peaks took place in May, July, and June, respectively. The rate of flow is highly variable on both an annual (Figure 2.3) and a monthly (Figure 2.4) basis; April flow rates ranged from 0.345 m^3/sec in 2000 to 55.3 m^3/sec in 2001, which also represents the peak flow rate for the entire recorded period. As seen in Figure 2.4, the La Salle has had a flow rate of 0 m^3/sec in all months except April during the period of 1967-2010. Consequently, it is classified as an intermittent stream (Graveline and Larter, 2006). A direct comparison of flow rates pre- and post-dam

and pump construction (Graveline and Larter, 2006) is not possible, as sufficient data recorded prior to 1940 are not available. However, reports indicate that, with the implemented flow regulation measures, flow rates are significantly less during flood periods, owning to the presence of water retention structures, and flow conditions have become considerably more homogenous as a result of flow augmentation during low water periods (La Salle Redboine Conservation District, 2007; Graveline and Larter, 2006).

2.5 Vegetation, Land Use and Disturbance

Historically, the La Salle watershed consisted predominantly of tall-grass prairie with occasional stands of trembling aspen (*Populus tremuloides*) (Smith et al., 1998). The majority of forest cover was situated along river and stream corridors. Currently intensive agriculture dominates the La Salle watershed and consequently, the majority of the natural vegetation has been replaced with cropped agricultural land. In addition, pasture is utilized for livestock operations, primarily pig and cattle production (La Salle Redboine Conservation District, 2007). Adjacent to the La Salle, narrow strips of natural riparian habitat remain along portions of the river. These riparian corridors are typically wider and less disturbed in the lower reaches of the La Salle. Emergent species colonize the shallow edge of the channel. Soils immediately adjacent to the channel are often saturated, owing to frequent inundation and imperfect drainage. These soils support willows (*Salix* spp.), Manitoba maple (*Acer negundo*), red osier dogwood (*Cornus sericea*), reed canary grass (*Phalaris arundinacea*) and sedges (*Carex* spp.). At the level of the first terrace, periodically inundated soils are colonized by Manitoba maple, green

ash (*Fraxinus pennsylvanica),* sedges and ferns. The second terrace is better drained, and is dominated by green and black ash (*Fraxinus nigra*) and American elm (*Ulmus americana*), with chokecherry (*Prunus virginiana*) and regenerating tree species representing the main understorey component. The herbaceous layer typically includes ostrich fern (*Matteuccia sthruthiopteris*), stinging nettle (*Urtica dioica*), wood nettle (*Laportea canadensis*), and moonseed (*Menispermum canadense*). Well-drained upland soils above the second terrace are characterized by an American elm and bur oak (*Quercus macrocarpa*) forest, with an understorey dominated by American and beaked hazel (*Corylus americana, Corylus cornuta*), and hawthorn (*Crataegus chrysocarpa*). Although the vegetation composition is primarily indigenous, exotic species, such as invasive reed canary grass (*Phalaris arundinacea*) smooth brome (*Bromus inermis*), quackgrass (*Agropyron repens*), Canada thistle (*Cirsium arvense*), sow thistle (*Sonchus uliginosis*), motherwort (*Leonurus cardiaca*), field bindweed (*Convolvulus arvensis*), lesser burdock (*Arctium minus*), and dandelion (*Taraxacum officinale*), invade from adjacent agricultural areas, often displacing native species.

Historically, fire cycles allowed native tall-grass prairie to remain dominant, preventing the spread aspen stands (La Salle River Watershed Planning Authority, 2010). Because much of the land base is in agricultural production natural ecological processes, particularly fire, are largely supressed. However, owning to its physical setting in a large glacial floodplain, characterized by low relief and considerable runoff during the spring thaw, it is often subject to severe flooding in the spring. Agricultural lands comprise approximately 90% of the region, including 75% annual cropland, 10% grassland and pasture, and 4% forage (La Salle Redboine Conservation District, 2007). Agricultural

development consists primarily of cereals, with some forage crops and a trend of increasing canola production. In addition, large-scale livestock operations have recently shown considerable growth, with the greatest increase being seen in pig production, followed by cattle (La Salle River Watershed Planning Authority, 2010). Livestock operations are more prevalent in the upper portion of the watershed, owing to the higher wind erosion risk associated with the sandy soils of the Assiniboine Delta, which make this region less suitable for cropping.

2.6 Anthropogenic Impacts

Surface water quality in the La Salle Watershed currently ranges from marginal to fair (La Salle River Watershed Planning Authority, 2010). Stressors affecting water quality are primarily anthropogenic, and include both point and non-point sources associated with agricultural operations, municipal uses and recreation (Graveline and Larter, 2006). Since 1975, nutrient loading to the La Salle River has intensified, with increases of 145.5% and 193.8% in total dissolved nitrogen and phosphorus, respectively, between 1974 and 1999. The heavy agricultural usage that characterizes the watershed is the primary cause of these increases. Concentrations of broadleaf herbicides often exceed recommended guidelines (La Salle River Watershed Planning Authority, 2010). In addition, manure inputs from livestock operations contribute to nutrient enrichment. These inputs can result in algal blooms, leading to oxygen depletion along the La Salle, particularly during the winter months. Nutrient loading in the Red River downstream of its confluence with the La Salle has also been exacerbated, though to a far lesser degree (Graveline and Larter, 2006). Proportional increases in nitrogen and phosphorus observed

in the Assiniboine River over the same period have been significantly lower, indicating that factors contributing to poor water quality present a larger problem on the La Salle. The level of nutrient increase is also indicative of the deterioration of riparian habitat along the La Salle River, supporting the results of a riparian health assessment commissioned by the La Salle Redboine Conservation District in 2006 (La Salle Redboine Conservation District, 2007), which assessed qualitative classifications of channel morphology, bank stability and riparian zone function (Graveline and Larter, 2006). The survey found that only 6% of the land area within 50 m of watercourses in the La Salle watershed had native cover, and identified 119 riparian sites requiring habitat restoration. Lack of vegetative cover on stream banks and excessive tillage in agricultural areas are the primary causes of riparian habitat deterioration, and exacerbate soil and bank erosion.

The flow regime of the La Salle River has been considerably altered by dam construction and flow augmentation (Graveline and Larter, 2006). Beginning in the 1940s, eight dams were constructed by the Prairie Farm Rehabilitation Administration (PFRA, now a part of the integrated Agri-Environment Services Branch), a branch of Agriculture and Agri-Food Canada. These dams have transformed the river into a series of reservoirs, interfering with fish movements, promoting sedimentation, and creating homogenous flow conditions along the length of the river. To ensure adequate water availability for agricultural applications (e.g. livestock watering and crop irrigation), as well as domestic consumption, flow augmentation has been implemented. Significant volumes of water from the La Salle's three active pumping sites in the RM of MacDonald augment river flow rate by 0.70 m^3/sec, using water drawn from the Assiniboine River.

2.7 Management

Recognition of the water quality and management issues affecting the La Salle watershed led to the preparation of an Integrated Watershed Management Plan (IWMP), completed in October 2010 through the cooperative efforts of the La Salle Redboine Conservation District, Manitoba Conservation, and the RMs of Cartier, Grey, Macdonald, Portage la Prairie, Richot, and South Norfolk. The plan identifies riparian health as a concern and cites improving riparian and river health as one of its four goals, in addition to improving the state of water management (including flood reduction and ensuring adequate water supply), improving water quality, and increasing public participation in water stewardship. In addition, the La Salle Redboine Conservation District offers eight major programs that are directly or indirectly beneficial to riparian health, including: 1) a buffer strip program, which prescribes planting of a strip 10-200 feet wide of a forage crop along agricultural fields adjacent to designated drains to reduce soil erosion; 2) a grassed waterway program, under which vegetative cover is established and maintained along waterways to reduce erosion of the channel and of adjacent agricultural soils; 3) a gully erosion program, which subsidizes physical alterations along gullies to repair existing erosion and reduce future stream bank deterioration; 4) placement of sediment barriers to trap eroded sediment at its point of origin, thereby reducing sediment loading downstream and maintaining local soil health; 5) pasture pipeline and alternative watering system assistance; 6) riparian fencing and relocation of livestock facilities programs, which prevent livestock access to riparian areas and provide water for livestock pastured away from water sources, thereby preventing damage associated with pugging and hummocking in riparian areas, preserving wildlife habitat, and reducing

nutrient inputs to the stream from manure; 7) a farmyard runoff control program, which subsidizes the rerouting of farmyard runoff around pollution sources to reduce nutrient inputs to streams; and, 8) constructed wetland, water retention, and flood protection diking programs, all of which reduce pollution inputs to stream through leaching and overland flow (La Salle Redboine Conservation District, 2012). These programs are intended reduce erosion, improve water quality, and preserve wildlife habitat.

Figure 2.1. Map showing the extent of the La Salle River study area, survey sites, and its location in Manitoba (Data Sources: Manitoba Land Initiative (2014)).

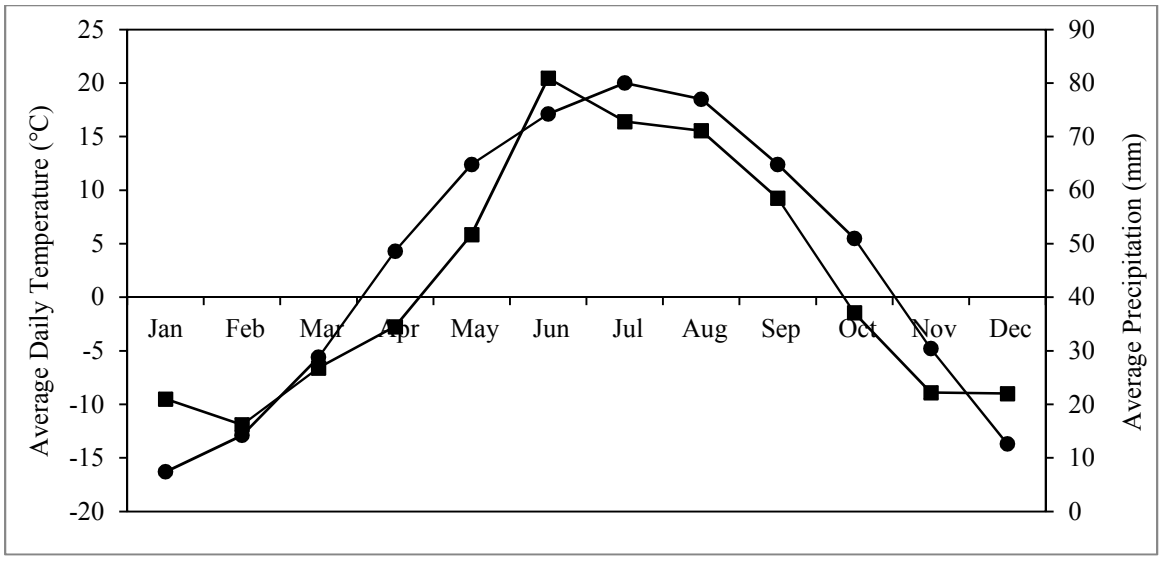

Figure 2.2. Mean monthly precipitation (mm), denoted by a square symbol, and temperature (°C), denoted by a circle symbol recorded at the Marquette weather station (Environment Canada, 2012a).

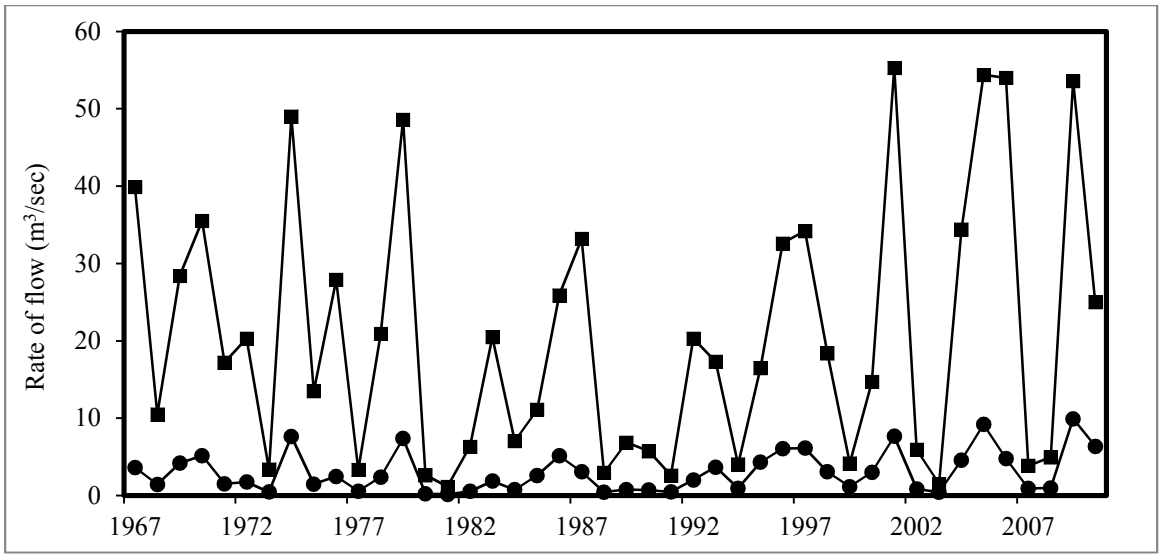

Figure 2.3. Mean, denoted by a circle symbol, and maximum, denoted by a square symbol, annual flow rates (m^3/sec) for the La Salle River at Sanford (Environment Canada, 2012a). Minimum values are near zero and not shown.

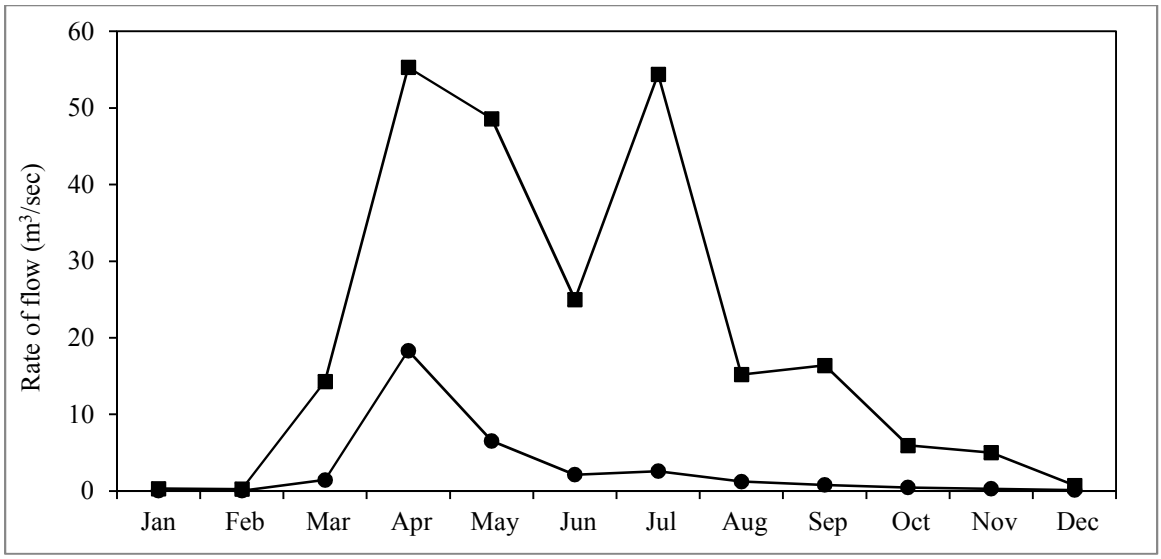

Figure 2.4. Mean, denoted by a circle symbol, and maximum denoted by a square symbol, monthly flow rates (m^3/sec) for the La Salle River at Sanford between 1967 and 2010 (Environment Canada, 2012b). Minimum values are near zero and not shown.

CHAPTER 3: EMERGING TECHNOLOGIES IN RIPARIAN HEALTH ASSESSMENT

Abstract

Riparian zones are narrow, heterogeneous habitats characterized by structurally diverse gallery forests. Traditional riparian health assessment methods rely on resource-intensive field surveys. Recent advances in remote sensing have potential in the development of remote riparian health assessment methods. The objective of this research was to explore the potential of emerging technologies, including object-based image analysis (OBIA) and light detection and ranging (LiDAR), in remote riparian health assessment. Riparian health surveys were conducted along the La Salle River in Manitoba, Canada. An OBIA was conducted on high-resolution imagery and canopy structure data derived from LiDAR data. A cluster analysis was preformed to identify natural groupings of objects in the image object dataset, and to assess their relationship to the riparian health scores determined in the field. Vegetation species composition was similar across all surveyed polygons. Healthy polygons were characterized by a dense understorey. The two-group level of the cluster analysis corresponded strongly to sites determined to be healthy or unhealthy during field reconnaissance, especially when LiDAR were used to generate canopy structure. The study shows that OBIA detects habitat elements relevant to riparian health, and canopy structure data derived from LiDAR contribute significantly to improving the accuracy of riparian health detection.

3.1 Introduction

Riparian zones are narrow, heterogeneous habitats, and are often characterized by gallery forests in the Northern United States and Canada (Naiman and Décamps, 1997). Gallery forests exhibit spatially driven topographic succession, wherein vegetation species composition changes rapidly on a gradient from the river's edge to the upland slopes, owing to the differential moisture and nutrient availability, and soil type associated with elevation above the river. These gradients result not only in vegetation species variability, but also in canopy structural diversity. Canopy structural diversity is a fundamental component of the riparian zone, contributing to many essential ecosystem functions, such as: provision of habitat and food sources for terrestrial and aquatic wildlife; nutrient and energy cycling; and sediment transport, deposition, and bank stability (Merritt et al., 2010; Nilsson and Svedmark, 2002; Gregory et al., 1991).

Healthy riparian areas are essential ecosystem components, both economically and ecologically. However, in a compromised state they can contribute to the transport of non-point source pollution, excess nutrients and sediment, and agricultural chemicals. Anthropogenic activities exacerbate damage to riparian areas, leading to flooding and sedimentation, bank erosion, and loss of wildlife habitat and biodiversity (Leclaire, 2011; Nilsson and Svedmark, 2002). Given the impact of riparian condition on surrounding environments, mitigating damage to riparian areas is essential (Makkeasorn et al., 2009; Mayer et al., 2005; Nilsson and Svedmark, 2002). In order to properly manage these habitats, it is necessary to assess their current degree of health and identify problem areas.

Riparian health has historically been assessed and monitored using ground inventories and manual aerial photo-interpretation (Gergel et al., 2007; Johansen et al., 2007a). This approach provides detailed information, but is costly, time-consuming, and often logistically infeasible in remote or inaccessible areas. Riparian areas are too narrow to be assessed using the medium- and low-resolution satellite imagery available prior to 2000 (Dilts et al., 2010; Johansen et al., 2007a; Muller, 1997). In addition, current generations of satellite platforms lack sensors that provide simultaneously high spatial and spectral resolution, frequently limiting multispectral analyses to the visible and near-infrared portions of the electromagnetic spectrum. Furthermore, the pixel-based spectral classification methods widely used in landscape mapping often produce a scale-dependent "salt and pepper" effect in riparian areas when high-resolution data are used. This occurs when spectral values in high-resolution data detect sub-elements of a single target feature (e.g. the sunny and shadowed portion of a single tree crown) that may have highly variable intensities but are not independent elements (Blaschke T. , 2010; Bock, Xofis, Mitchley, Rossner, & Wissen, 2005). This effect is problematic in the classification of narrow riparian zones, as the scale of many elements, as well as the zone itself, is spatially heterogeneous over small areas. However, following recent developments in image processing, semi-automated assessment approaches based on high-resolution aerial and satellite imagery, light detection and ranging (LiDAR), and digital elevation models (DEMs), have the potential to facilitate landscape-level monitoring (Forzieri 2011; Johansen et al., 2008; Makkeasorn et al. 2009; Johansen et al., 2007a). Object-based image analysis (OBIA), an alternative classification method, minimizes these problems

by using image segmentation to group pixels into objects based on spatial, textural, and spectral characteristics prior to classification (Yu et al., 2006). The resultant reduction in image noise provides for a smoother visualization and more accurate classifications. Although few studies have examined the application of OBIA to the assessment of riparian health, significant potential exists.

A key issue associated with remote riparian health assessment is the condition of the understorey (Johansen, 2006a). The understorey contributes to several essential riparian functions, including: bank stability and erosion control; regulation of pollutants and nutrients; and structural complexity, which results in increased biodiversity and available wildlife habitat (Fortier, 2014; Eskelson et al., 2010; Munro et al., 2009; König, 2000; Richards and Chirman, 1994). Jansen (2005) found that the majority of information lost in remote sensing-based riparian health assessments pertains to the understorey. Consequently, a method to evaluate the state of the understorey needs to be a component of automated remote sensing approaches for riparian health assessment. Unfortunately, understorey attributes cannot be easily detected using above canopy imagery in the visible portion of the spectrum. LiDAR imagery, while unable to provide detailed spectral classifications of floristic composition, can be used to calculate the height of the canopy and understorey levels, and to derive understorey and canopy densities (structure) (Johansen et al., 2011; Johansen et al., 2010a; Johansen et al., 2010c; Goetz, 2006; Dowling and Accad, 2003). Integrating LiDAR data with optical imagery has strong potential for detecting riparian health indicators, but, to date, little research has explored this application. The objective of this study was to determine the potential of object-based image analysis and canopy structure data to remotely detect riparian health in the field.

3.2 Methods

3.2.1 Riparian Health Field Survey Methods

Field data collection was undertaken along the La Salle River to identify riparian health indicators detectable using remotely sensed imagery, and to obtain training and testing datasets for use in riparian health model development and validation. Data collection included detailed vegetation and physical feature surveys conducted in August of 2011 and June and July of 2012 within the riparian zone, in cooperation with Agriculture and Agri-Food Canada (AAFC). The protocol employed was the Riparian Health Assessment developed by AAFC, modified from methods used by the Alberta Lotic Wetland Inventory, a comprehensive ground inventory developed by the Alberta Riparian Habitat Management Society (AAFC, 2004; Fitch and Ambrose, 2003). The Alberta Lotic Wetland Inventory characterizes the riparian zone based on the presence of wetland hydrology, hydric soils and hydrophytic vegetation.

Prior to the field campaign, riparian survey units were delineated using a DEM to identify the boundary of the riparian zone. All areas adjacent to the river and sloping toward it were included. This riparian zone was then segmented into polygonal survey units, using eCognition Developer object-based image analysis software to identify topographically homogenous regions on the DEM. The segmented polygon boundaries were manually adjusted using topographic maps and aerial photography to produce polygons derived from observable vegetation or physical features. Because polygons were based initially on an automated DEM segmentation, they were irregular in shape and length. Polygons between 100 m and 300 m in length were surveyed. Hundreds of polygons along the 75

km study area fit these criteria; however, the majority were physically inaccessible or located on private land. A total of 100 polygons were selected for the survey, based on physical accessibility and landowner permission. A few sites were situated on Crown land. To ensure only one management regime was present in each polygon, polygons with boundaries crossing property or fence lines were excluded. As the delineated polygon boundaries frequently fell well beyond the actual limits of the riparian zone, polygon boundaries were validated in the field, and polygons with inappropriately located boundaries were recorded.

The riparian health survey consisted of eleven metrics of riparian health, comprising vegetation, physical and anthropogenic attributes, including: 1. percent vegetation cover on the floodplain and stream banks; 2. percent cover, density and distribution of invasive species; 3. percent cover of undesirable disturbance-adapted herbaceous species; 4. establishment and regeneration of preferred tree and shrub species; 5. browsing of woody species; 6. percentage of standing decadent and dead woody material; 7. percentage of root mass for stream bank stabilization; 8. percent cover of bare ground of anthropogenic origin; 9. anthropogenic structural alteration of stream banks; 10. anthropogenic physical alteration to the rest of the polygon; and, 11. stream channel incisement or vertical stability (AAFC, 2004; Fitch and Ambrose, 2003). The riparian survey polygons were assigned a numerical score for each riparian health metric. All metrics were tallied to produce an overall riparian health score for each polygon, which was converted to a percentage value. The polygons were then assigned the ranked categories ‘Unhealthy’ (<60%), ‘Healthy with Problems’ (60%-80%), or ‘Healthy’ (>80%)(AAFC, 2004; Fitch and Ambrose, 2003). In addition to the riparian health survey, observations about the

state of the understorey were made at each site. For the purposes of this study, the understorey was considered well developed when shrubs and woody vegetation were the dominant ground cover, and poorly developed when bare ground or shallow-rooted herbaceous vegetation dominated.

3.2.2 Riparian Flood Zone Delineation

During the course of the field surveys, it was observed that the riparian survey polygons delineated using desktop methods did not correspond well to the actual boundaries of riparian habitat, frequently extending well into adjacent upland habitat. Consequently, following field work and prior to conducting analyses, additional criteria and rules were developed to identify the actual limits of riparian habitat. For the purposes of defining the riparian zone for this study, areas adjacent to the river, situated at a lower elevation than the maximum mean monthly flood level and including a buffer of adjacent riparian vegetation, were considered to be flooded with sufficient frequency to be classified as riparian (Abood et al., 2012; Mason and Maclean, 2007).

Flood zone modelling was conducted using a 1 m-resolution LiDAR-based DEM, captured in May of 2009, to delineate areas adjacent to the river at a lower elevation than the maximum monthly flood level, i.e. those areas that would be submerged during the period of highest water level in a normal flood year and could therefore be assumed to constitute riparian habitat. To accomplish this, it was first necessary to determine the elevation of the river surface along the length of the channel at both normal and flood levels. A river centre-line was manually digitized in an ArcGIS environment at a scale of 1:2500, using 50 cm orthorectified true colour aerial imagery captured in 2009 and 2011,

obtained from the Manitoba Land Initiative (MLI) via AAFC (2012). All segment vertices were situated on the actual river centre-line, preserving their exact location. As the small, straight-line segments comprising the digitized centre-line could potentially affect the results of geometric analyses, such as the calculation of sinuosity, the centre-line was smoothed using a Bézier curve function (Artyszuk, 2002; Farin, 2002. The smoothed centre-line was subsequently split into 15-m segments. The vertices of the segmented line were converted to point feature classes and mean elevation values were extracted from the LiDAR-based DEM at each point location, producing a series of point elevations 15 m apart along the length of the channel centre-line. In 2009, flood levels peaked between mid- and late-April, and had returned to normal flow conditions by the time the DEM dataset was captured between May 6 and May 23 of 2009 (Environment Canada, 2012b). Therefore, these point elevations represent the level of the water in normal flow conditions. To create a continuous surface across the study area, a 1 km buffer was generated for the river centre-line. As per the centre-line, the left and right sides of the buffer were split into 15-m segment vertices and converted to point feature classes. Coordinates were calculated for each point location in the Universal Transverse Mercator (UTM) North American Datum (NAD) 1983 Zone 14 projection. Polylines connecting the paired point locations were generated and split into 15-m segments. The segment vertices were converted to a point feature class and clipped to the extent of the DEM, producing a 15-m grid of points across the study area. The centre-line point dataset was spatially joined to the 15-m grid points to assign river surface elevation values to the grid using a nearest neighbor rule. A radial basis function method was applied to

interpolate a river elevation surface across the grid extent (Sterling, 2003; Mitášová and Mitás, 1993; Mitás and Mitášová, 1988).

To delineate areas at lower elevation than the maximum mean monthly flood level, the difference between the maximum mean monthly flood level and the water level under normal flow conditions was determined using flood records and a DEM. The mean elevation value extracted from the river surface elevation layer at the Sanford hydrometric station was subtracted from the highest mean monthly water level for the period of record (2002-2011). The interpolated river surface was then subtracted from the ground-surface DEM. The delineated riparian flood zone includes all areas situated below the threshold flood increment and connected to the river channel. This flood zone boundary was used in all subsequent analyses. The generated flood zone extent was visually compared to the observed riparian zone extents recorded in the field to ensure the modeled area corresponded to actual riparian zone boundaries.

3.2.3 Vegetation and Canopy Structure Indices

Several image datasets were utilized in the object-based image analysis. A 50 cm, 24-bit, orthorectified, multispectral aerial image dataset, including red, green, and blue bands, was the primary dataset. The imagery was captured in 2007 and 2008 by Manitoba Conservation at a scale of 1:40,000 using a digital camera module (DCM). Despite the high resolution of the aerial image dataset, however, portions of the image were found to be of insufficient quality for the analysis; portions of the image were flown during leaf-off, and contrast was variable between image tiles. As vegetation-based studies require leaf-on data, and OBIA requires consistent contrast across the entire image, additional

datasets were acquired to mitigate these problems. A 2.5 m, 8-bit panchromatic image, captured by the satellite SPOT-5 in the summer of 2012, was included to detect the extent of leaf-on vegetation cover. In addition, a vegetation productivity map was produced using the Normalized Difference Vegetation Index (NDVI), a measure of photosynthetic wavelength reflectance used to infer plant productivity (Tucker, 1979). A 5 m, 12-bit, multispectral image, including red, green, blue, near infrared (NIR), and "red edge" (a narrow bandwidth between the red and NIR bands, normally applied to vegetation studies) bands, captured by the satellite RapidEye in September 2012, was used for the NDVI calculation. All image datasets were obtained from AAFC in an orthorectified and radiometrically corrected format. Before being input into the object-based software, all datasets were converted to 8-bit (0-255) format using ArcGIS software, to streamline OBIA processing.

In addition to the spectral imagery, raw LiDAR data were obtained from AAFC to provide information about the riparian forest structure and understorey. The data were collected in May of 2009, with an average post spacing of 1.7 m and vertical accuracy (root mean square error) of 0.036. The raw LiDAR points were coded with land cover types, including ground, low, medium and high vegetation, buildings, and water, prior to being distributed by the producer. The raw data were input into FUSION, a LiDAR processing, analysis and visualization software (McGaughy, 2003). Outlier values were removed from the dataset and ground and canopy points were extracted, and used to generate a digital terrain model (DTM) and canopy surface model (CSM). A canopy height model with a resolution of 2 m was generated by subtracting the DTM from the CSM. A canopy cover model was generated from first vegetation returns, which reflect

off the top of the canopy, at a resolution of 15 m. This resolution approximates average crown area, ensuring an appropriate grid size for sampling canopy cover (McGaughy and Carson, 2003). Finally a vegetation density model was calculated using all vegetation returns, representing the different levels of canopy and understorey structure. The vegetation density model was generated at resolution four times greater than the input data (8 m), which is considered appropriate for vegetation structure modelling (ESRI, 2011).

Each of these datasets describe an element of the vegetation component: aerial and satellite imagery show the canopy surface; NDVI approximates vegetation productivity; and the canopy models describe vertical canopy structure. Consequently, in subsequent analyses, they will be referred to as vegetation variables.

3.2.4 Object-based Image Analysis

An object-based image analysis (OBIA) was carried out using eCognition Developer software to segment the study area into statistically meaningful riparian zone polygons. The high-resolution aerial imagery (red, green and blue bands), SPOT imagery, NDVI model, and canopy cover, height, and structure models were input into eCognition. Prior to conducting the image segmentation, a number of analysis variables must be set, including scale, colour, shape and compactness parameters. The scale parameter represents a unitless value, indirectly related to the size of the created objects, such that a larger scale parameter produces larger objects. Scale is variable among images, depending upon image resolution, contrast and data type, and must consequently be selected separately for different images and study areas. The scale parameter was selected

using a method developed by Drăguţ et al. (2010), in which segmentation is conducted at a variety of scales, using a bottom up approach. The local variance for each spectral band at each scale, and rate of change between scales, are calculated. Local variance and rate of change are then plotted against scale to identify scales that are meaningful for objects at different levels of spatial complexity. This method operates on the principal that the variance among segmented image objects will be small if the spatial resolution being measured is finer than the scale of actual landscape elements, and increases with decreasing resolution until the scale of the segmentation is the same as the scale of the landscape elements of interest (Drăguţ et al., 2010). Consequently, meaningful scale levels are denoted by a break in slope in the rate of change. There are several meaningful scale levels for a given image, associated with different scales of landscape complexity (e.g. individual tree scale, stand scale, forest scale). Using the local variance-rate of change method, several meaningful scales were identified, and an appropriate scale associated with riparian habitat was identified visually.

Colour, shape, and smoothness/compactness parameters are weighted to control the relative importance of each in determining image object homogeneity (eCognition Developer, 2012). Colour (digital number of the spectral signature) and shape (textural homogeneity of image objects) are weighted relative to one another to produce a total weight of one. In addition, the shape criterion can be modified by changing the relative weighting between smoothness of the image object borders and the compactness of the image object. Finally, the relative importance of image layers in the segmentation can be modified. Colour, shape, smoothness/compactness, and layer weight parameters were selected through an iterative trial and error process to produce polygonal objects

(hereafter referred to as image objects, to avoid confusion with the riparian field survey polygons) that corresponded well with visually identified riparian habitat features.

Once objects were delineated, a variety of spectral, geometrical, and textural metrics were calculated for each. Spectral metrics included: brightness, mean brightness, brightness standard deviation (SD), and maximum difference. Geometrical metrics comprised: area, length, border length, border index, asymmetry, roundness, compactness, length:width ratio, shape index, and density. Textural statistics were calculated based on a grey-level co-occurrence matrix. Texture metrics included mean, SD, contrast, homogeneity, entropy, correlation, angular second moment, and dissimilarity, calculated for the grey-level co-occurrence matrix. Spectral and texture metrics were calculated within each image object individually for each layer and spectral band, and globally for all layers and bands in combination, resulting in a total of 98 metrics. Image objects associated with the riparian zone were selected, including objects contained within the generated riparian flood zone, and overlapping with its boundary to ensure that riparian vegetation on the upper slopes was captured. The selected image objects and associated metrics were exported for use in further analyses.

3.2.5 Analysis of Riparian Vegetation and Canopy Structure

A hierarchal cluster analysis using Wards method was conducted to assess the relationships between segmented image objects, LiDAR variables (canopy cover, canopy height, vegetation density), and riparian habitat condition. To reduce dataset size prior to carrying out the cluster analysis, a Spearman's rank correlation matrix was used to identify redundant variables, and a total of 57 variables were selected for use in the

cluster analysis (Table 3.1). Cluster analysis is a data exploration method that identifies natural groupings in a dataset, and is used to describe datasets that are assumed to contain distinct populations (Legendre and Legendre, 2012; Ferreira and Hitchcock, 2009). The method is described in detail in Legendre and Legendre (2012). The cluster analysis was conducted for all segmented image objects that intersected the riparian field survey polygons, 1193 objects in total. Cluster solutions were calculated for two to 20 groups. The results were plotted against the riparian field survey health ranks ('Healthy', 'Healthy with Problems', 'Unhealthy'), to determine the optimal group solution corresponding to riparian habitat condition. This cluster analysis was performed two separate times: once for image objects with all OBIA variables; and once excluding LiDAR canopy layers, but retaining all other variables. This procedure was followed to assess the contribution of canopy and understorey structure metrics to detecting riparian health. The results of the cluster analyses were displayed in contingency tables, which plotted the frequency cluster groups against riparian health field survey categories to evaluate the association between the two (Legendre and Legendre, 2012). A chi-square test was performed to assess the significance of the group separations. Finally, to identify differences between cluster groups, mean and SD values were calculated for each variable within each cluster group and visually compared. Student's *t*-test was used determine whether the differences between cluster group variable values were significant.

Principal Coordinates Analysis (PCoA) was used to visualize separability of the cluster groups. PCoA is an ordination method used to project variables in reduced space, which facilitates the interpretation of relationships between image objects and environmental gradients, and reduces dataset noise (Legendre and Legendre, 2012). PCoA is a useful

method for ecological descriptors because, unlike many ordination methods, it can handle a mix of quantitative and qualitative variables, mixed levels of precision, and can be computed using any type of distance metric (Legendre and Legendre, 2012). These attributes made it an appropriate method for the image object dataset, which was derived using a variety of unrelated indices and imagery, collected at different scales. The results of both cluster analyses (including and excluding canopy structure variables, respectively), which included the 1193 image objects and each object's group assignment, were analysed separately using PCoA. The first two axes of each PCoA were displayed as a biplot. Points on the biplot were colour-coded according to their cluster group assignment, and 95% confidence ellipses were drawn for each group to facilitate a visual assessment of both the degree of separability based on clustering, and the influence of canopy structure variables. Outliers on the biplots were examined to determine whether they matched their expected riparian health category based on group membership ('Healthy', 'Healthy with Problems', 'Unhealthy').

For the purpose of discussing and interpreting the contribution of canopy structure to delineating cluster groups, canopy structure profiles were developed using the following method. Four representative field survey polygons, two ranked as healthy and two as unhealthy, were chosen. In a GIS environment, a cross-sectional line was drawn across the riparian area from the channel to the adjacent upland. Elevation points were extracted from a 2 m DEM along this line and used to construct a topographic profile. Raw LiDAR vegetation point cloud data were also summarized along the cross-section and plotted on the elevation profile. In a separate panel, the LiDAR point cloud plot, and species data

recorded during the field survey, were used to construct a detailed illustration of canopy and understorey structure along the riparian profile.

3.3 Results

3.3.1 Riparian Health Field Survey

Forty-nine of the 100 riparian polygons surveyed were assigned to the 'Healthy' category. Of the remaining 51 polygons, 50 were categorized as 'Healthy with Problems', while only one polygon scored less than 60%, placing it in the 'Unhealthy' category. Community composition was relatively uniform throughout the study area, consisting of and overstorey dominated by Manitoba maple, American elm, green ash, and bur oak, an understorey of chokecherry, red osier dogwood, and willow species, and a mix of native and invasive herbaceous species. In general, it was observed that vegetation species composition was not notably different between polygons ranked as 'Healthy' and those with lower scores, although species abundances and density of the understorey differed (Leo, personal observation). The riparian health survey does not contain specific reference to the density of the understorey; however, in a second riparian ecosystem surveyed as part of this project (Turtle River, unpublished data) polygons categorized as 'Healthy' were observed in the field to possess a dense understorey

3.3.2 Riparian Zone Delineation

In the majority of cases, the surveyed riparian polygon extents corresponded well with the delineated riparian area extent. However, the survey polygons were found to be either wider or narrower in a few cases. The delineated riparian flood zone corresponded well both with visual observations of the flood zone as seen on aerial imagery, and with documented field observations from surveyed polygons. In addition, extending the riparian area by including all image objects overlapping the outer boundary of the

delineated flood zone was representative of the true extent of riparian habitat as observed in the field. Consequently, the delineated riparian zone, including the generated flood zone and overlapping vegetation-based image objects provided a better representation of the extent of riparian habitat than the original survey boundaries. Figure 3.1 shows an example of riparian survey polygons that agreed well with the delineated riparian zone extent. Figure 3.2 shows survey polygons that are aligned with the delineated flood zone along the western bank, but are narrower than the actual extent of riparian habitat along the eastern bank. The survey polygons shown in Figure 3.3 extend beyond the actual riparian zone on the southwestern bank.

3.3.3 Object-based Image Analysis

A workflow detailing the steps the OBIA is shown in Figure 3.4. The following segmentation parameters were chosen iteratively through trial and error: colour and shape weights of 0.9 and 0.1, respectively; and smoothness and compactness weights of 0.9 and 0.1. Because of pronounced the differences in contrast between several high-resolution aerial image tiles, different segmentation scales were required to produce equivalent riparian habitat sub-component objects across the study area (Figures 3.5-3.6). Segmentation scales of 75 and 175 were used for high and low contrast tiles, respectively. The segmentation was refined further by assigning weights to image layers to adjust the degree of influence each layer had on the segmentation. A weight of two was applied to green, red, and NDVI layers. Blue, panchromatic, and canopy height layers were given a weight of one. Finally, canopy cover and canopy structure layers were assigned a weight of 0.25. These parameters were visually confirmed to produce image objects at an appropriate scale for detecting sub-components of riparian habitat (Figures 3.5-3.6).

3.2.1 Analysis of Riparian Vegetation and Canopy Structure

Cluster solutions ranging in size from two to twenty clusters were examined. The two-group solution was found to best correspond to riparian health categories measured in the field. In addition, the cluster analysis that included canopy structure variables provided a better correspondence to riparian health survey results than the dataset that excluded these data (Tables 3.2 and 3.3). In the dataset including canopy structure variables, 90% of the image objects in Group 1 were found to belong to polygons classified as 'Healthy' in the field (Table 3.2). In addition, 90% of the image objects contained in polygons classified as 'Healthy with Problems' or 'Unhealthy' in the field were captured in the Group 2 cluster. Conversely, in the dataset excluding canopy structure, 50% of image objects in 'Healthy with Problems' polygons were placed in each cluster group (Table 3.3). Eighty-seven percent of 'Healthy' image objects were clustered in Group 1; however, 100% of 'Unhealthy' image objects were also included in Group 1. The cluster group separations were found to be significant for both datasets including ($\chi^2 < 0.001$) and excluding ($\chi^2 = < 0.001$) canopy structure variables. As can be seen in Figures 3.7 and 3.8, the classification groups including canopy structure variables are more also more evenly distributed, with approximately half of the image objects falling in each cluster group. The cluster analysis was applied, not as a classifier, but rather, as a data exploration tool to assess the relationship between field-derived riparian health categories and OBIA-derived image objects, as well as evaluating the contribution of LiDAR variables to this relationship. Consequently, a full accuracy assessment was not conducted. However, it should be noted that 77% and 71% of image objects were placed in the correct cluster group ('Healthy' image objects in Group 1, 'Unhealthy'/'Healthy

with Problems' in Group 2) with canopy structure variables included and excluded, respectively.

Examination of the mean and SD of variables in each group revealed that the canopy height model had no overlap between mean and SD for most texture metrics. In addition, the canopy structure model stood out strongly in the grey-level co-occurrence mean texture metric. Two texture metrics (grey-level co-occurrence matrix contrast and mean values) also showed a noticeable difference between mean and SD values for Groups 1 and 2, while grey-level co-occurrence of SD and correlation showed smaller but still visible differences. Finally, mean image brightness also showed noticeable differences between groups. However, no variables were significantly different between groups according to Student's t-test.

The results of the PCoA are displayed in Figures 3.9 and 3.10. While both canopy structure-inclusive and canopy structure-exclusive plots show visible overlap between Groups 1 and 2, the overlap among points was greater for the canopy structure-exclusive dataset. In addition, a larger number of outliers were present. While group separation was significant both with and without canopy structure variables, the inclusion of canopy structure variables produces a much clearer visualization of the separation between Groups 1 and 2. Group 1 and Group 2 PCoA outliers for canopy structure-inclusive dataset had a moderately higher expected riparian health category misclassification rate (31%) than the total misclassification rate for the dataset (23%) (Section 3.3.3). Group 1 and Group 2 outliers displayed on the canopy structure-exclusive dataset biplot were

usually (65%) misclassified, and had a far greater misclassification rate for than the full dataset (29%).

3.4 Discussion

3.4.1 Riparian Health Survey

Field observations revealed that healthy polygons were generally associated with an understorey characterized by dense, well-established shrub species, suggesting that canopy and understorey structure influence riparian habitat health more heavily than vegetation species composition. Vegetation species composition was relatively uniform across all polygons and did not have a noticeable effect on health score. This is consistent with existing research, which indicates that, while functional and species diversity are often strongly correlated, habitats characterized by high species diversity often exhibit functional redundancy (Biswas and Mallik, 2011; Cadotte et al., 2011). Functional diversity is often more sensitive to environmental and disturbance gradients, making it a better measure of ecosystem health than species diversity. The riparian understorey contributes to several essential functions of healthy riparian areas. Dense root mass protects against erosion, and aids in nutrient cycling and pollutant filtration (Eskelson et al., 2010; Richards and Chirman, 1994). Understorey structural complexity is associated with higher species diversity, and increased habitat complexity (Fortier, 2014; Munro et al., 2009). Conversely, a poorly developed understorey is often indicative of colonization by herbaceous invasive species and relatively recent disturbance. Multiple canopy layers provide habitat for a larger number of wildlife species (König, 2000). The observed correlation between the state

of the understorey and riparian condition demonstrates the importance of a well-developed understorey to riparian health.

3.4.2 Riparian Zone Delineation

The delineated riparian area, generated as function of the highest mean monthly flood level and vegetation objects overlapping the flood zone boundary, was agreed well with riparian zone boundaries identified in the field. Studies by Abood et al. (2012) and Mason and Maclean (2007) have produced accurate flood zone delineations using a 10 m DEM to map the extent of the 50-year flood level. Highest mean monthly flood level was used in place of the 50-year flood in this study, owing to the lack of available 50-year flood data for the La Salle River. Given its observed success, this method has potential for application in areas where 50-year flood data are not available. In addition, the Abood et al. (2012) and Mason and Maclean (2007) studies did not consider the extent of riparian vegetation beyond the flooded area. As discussed by Verry et al. (2004) and Ilhardt et al. (2000), riparian vegetation extends horizontally an average of one tree-height beyond the perimeter of the flooded area. The additional vegetation extent was successfully approximated in this study through the inclusion of the vegeation objects that overlapped the outer boundary of the flooded area.

3.4.3 OBIA and Canopy Structure in Riparian Health Assessment

This study found that canopy structural and vegetation characteristics derived from object-based segmentation correspond to riparian habitat condition observed in the field (Figures 3.5-3.6). These findings agree with numerous existing studies, which have successfully predicted a wide range of riparian habitat attributes using object-based

methods (Kollár et al., 2013; Arroyo et al., 2010; Johansen et al., 2008b; Johansen et al., 2007a; Johansen et al., 2007b; Gergel et al., 2007; Johansen and Phinn, 2006a). However, existing research has focused on predicting specific attributes, such as: vegetation structure, successional stage and overhang; riparian zone and channel width; bank stability; flood damage; percentage canopy and organic litter cover; and canopy continuity and tree clearing, while this study sought to link image objects directly to the overall health of the riparian area, defined as the results of the ground-based health assessment. This objective was achieved using descriptive methods.

The correspondence between understorey density and overall health score observed in the field reinforces the established importance of the understorey to riparian habitat health (Johansen and Phinn, 2006a; Jansen, 2005). The higher misclassification rate observed on the PCoA biplot for the cluster group outliers of both canopy structure-inclusive and canopy structure-exclusive datasets suggests that the object-based image segmentation detects variables that reflect habitat characteristics, which influence riparian health, but are not directly captured by the ground-based health assessment. Similarly, the lower cluster group-riparian health category misclassification rate observed for the canopy structure-inclusive dataset implies that at least some of this missing information, probably pertaining to the state of the understorey, can be captured when vegetation structural data are included in the assessment. While no individual variable included in the OBIA was significantly different between cluster Groups 1 and 2, the canopy height and structure models had no overlap between mean and SD values for the two groups, and showed more separation than any other image layers used in the analysis. This assessment reinforces the importance of structural attributes to overall riparian health. The fact that

two texture metrics (grey-level co-occurrence matrix contrast and mean) produced the better separation between Groups 1 and 2 for all data layers than either geometrical or spectral metrics also emphasizes the importance of including texture metrics in the assessment of fine-scale heterogeneous habitats.

The value of LiDAR (in isolation and in combination with spectral data) for detecting specific structural attributes of riparian areas, such as: vertical stream erosion and bank stability; canopy height, structure and continuity; understorey establishment and structure; vegetation overhang; total plant biomass; and dead wood abundance, is well established (Fortier, 2014; Chen et al., 2012; Johansen et al., 2011; Johansen et al., 2011; Arroyo et al., 2010; Johansen et al., 2010a; Johansen et al., 2010c; Dowling and Accad, 2003). This study found that the inclusion of structural information can also improve the correspondence between segmented vegetation-based image objects and overall riparian health.

Figures 3.11-3.14 show cross-sections of four surveyed polygons. These cross-sections demonstrate that forest structural information relevant to riparian health, which is not obtainable from visible imagery, is easily derived from LiDAR data. Each figure includes an aerial overview, a profile of LiDAR returns, and a diagrammatic representation of vegetation composition and structure. The topographic profiles are derived from the 1 m DEM, and species composition is accurately portrayed according to field observations. Figure 3.11 shows a classic example of healthy riparian area, characterized by visible terracing and a well-developed gallery forest. The first terrace is dominated by mixed green ash and Manitoba maple, with a dense willow understorey and minimal herbaceous

vegetation. The second (upland) terrace is dominated by American elm and bur oak, and exhibits a more open understorey, with well-developed herbaceous vegetation interspersed with patches of hazel. The variable density of the understorey between the first and second terraces is easily distinguished in the LiDAR profile by examining the point density between the ground level and overstorey canopy. Figure 3.12 shows a healthy riparian area with less pronounced terracing and a uniformly dense understorey across its width. The overstorey is dominated by green ash and Manitoba maple near the channel, and by American elm, bur oak and green ash on the upland slope. The understorey consists primarily of chokecherry, saskatoon, and hazel. As in Figure 3.11, the understorey density is readily visible in the LiDAR profile. Figure 3.13 shows an unhealthy riparian zone with no terracing, characterized by a sparse overstorey consisting of Manitoba maple and green ash. There is no woody understorey, and the herbaceous vegetation consists almost exclusively of invasive smooth brome and quack grass. The LiDAR profile shows very few points at understorey-level, and a sparse canopy as compared with the healthy riparian areas in the previous figures. The riparian area shown in Figure 3.14 is confined to a steep bank, which lacks terracing and is dominated by invasive herbaceous species, with Manitoba maple at the top of the slope. The adjacent upland consists of a dense shrub understorey and bur oak-Manitoba maple-dominated overstorey, with large canopy gaps. As can be seen in all four figures, the aerial image shows only the overstorey canopy surface, and does not provide any information pertaining to the understorey. Given the importance of understorey structure to many elements of a healthy riparian ecosystem, the inclusion of canopy structure data derived

from LiDAR in riparian health modelling has potential to provide considerably more detailed and accurate results.

3.5 Conclusion

Based on field observations, canopy and understorey structure were found to be more important than vegetation species composition and species diversity in determining the condition of riparian areas. Modelling recorded mean flood levels using a DEM, extended to the outer edge of segmented vegetation objects overlapping the flooded area boundary, was found to provide an accurate estimate of the extent of riparian habitat. Vegetation spectral, and canopy and understorey structural information extracted from a combined dataset comprising high-resolution imagery, vegetation productivity and canopy structure indices using object-based methods can be descriptively linked to overall riparian health scores derived from an indicator-based field assessment. The inclusion of canopy structure indices derived from LiDAR significantly improves the correspondence with riparian habitat health.

Table 3.1. OBIA metrics selected for cluster analysis and riparian health modelling. Metrics are organized based on the type of vegetation information provided, and divided into groups based on the OBIA metric (spectral, textural, and geometrical) calculated.

Vegetation Productivity Information	Canopy Surface Information	Canopy Structure Information	Combined Information - All Image Datasets
Texture Metrics	**Texture Metrics**	**Texture Metrics**	**Geometry Metrics - Shape**
Contrast	*Contrast*	*Contrast*	*Asymmetry*
NDVI	Panchromatic	Canopy Height Model	*Density*
Homogeneity	Red Band	Canopy Structure Model	*Compactness*
NDVI	Green Band	Canopy Cover Model	*Roundess*
Mean	*Homogeneity*	*Homogeneity*	*Shape Index*
NDVI	Panchromatic	Canopy Height Model	
Entropy	Red Band	Canopy Structure Model	**Geometry Metrics - Extent**
NDVI	Green Band	Canopy Cover Model	*Area*
Standard Deviation	*Mean*	*Mean*	*Length:Width*
NDVI	Panchromatic	Canopy Height Model	
Correlation	Red Band	Canopy Structure Model	**Spectral Metrics - Mean**
NDVI	Green Band	Canopy Cover Model	*Brightness*
	Entropy	*Entropy*	*Max Difference*
	Panchromatic	Canopy Height Model	
	Red Band	Canopy Structure Model	**Texture Metrics**
	Green Band	Canopy Cover Model	*Contrast*
	Standard Deviation	*Standard Deviation*	*Homogeneity*
	Panchromatic	Canopy Height Model	*Mean*
	Red Band	Canopy Structure Model	*Entropy*
	Green Band	Canopy Cover Model	*Standard Deviation*
	Correlation	*Correlation*	*Correlation*
	Panchromatic	Canopy Height Model	
	Red Band	Canopy Structure Model	
	Green Band	Canopy Cover Model	

Table 3.2. Contingency table and significance statistics showing the relationship between riparian health scores and image object groups, including both spectral and LiDAR variables ($\chi^2 < 0.001$).

Group/Health Score	Healthy	Healthy with Problems	Unhealthy
Group 1	477	50	1
Group 2	222	434	9

Table 3.3. Contingency table and significance statistics showing the relationship between riparian health scores and image object groups, including only spectral variables ($\chi^2 < 0.001$).

Group/Health Score	Healthy	Healthy with Problems	Unhealthy
Group 1	607	241	10
Group 2	92	243	0

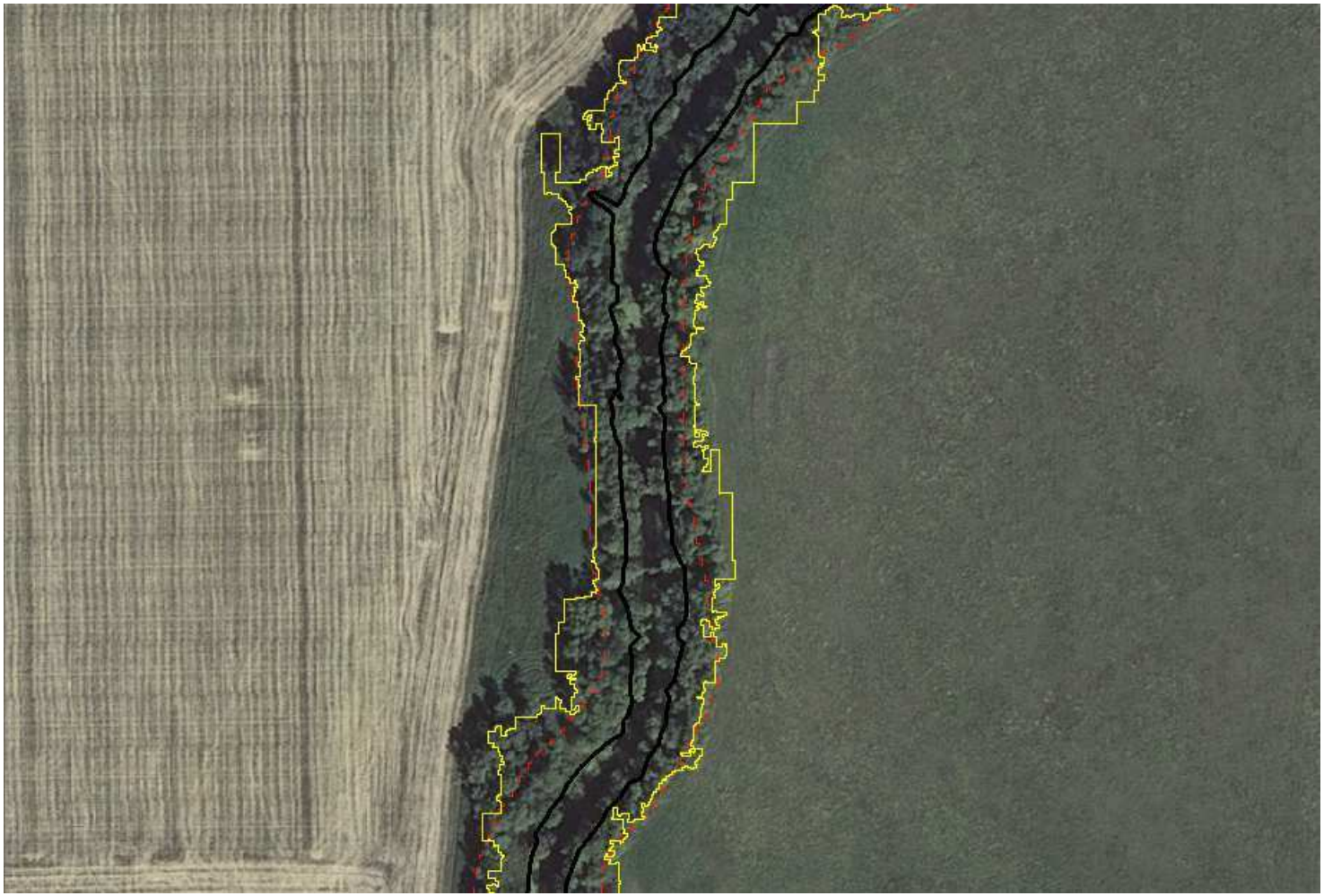

Figure 3.1. Example of survey polygons that are relatively well aligned with the delineated riparian zone extent. The dashed red line shows the extent of riparian survey polygons 58, 59, 62, 63, and 64. The solid black line shows the generated flood zone. The solid yellow line shows the extent of the riparian zone, including the generated flood zone and overlapping vegetation-based image objects.

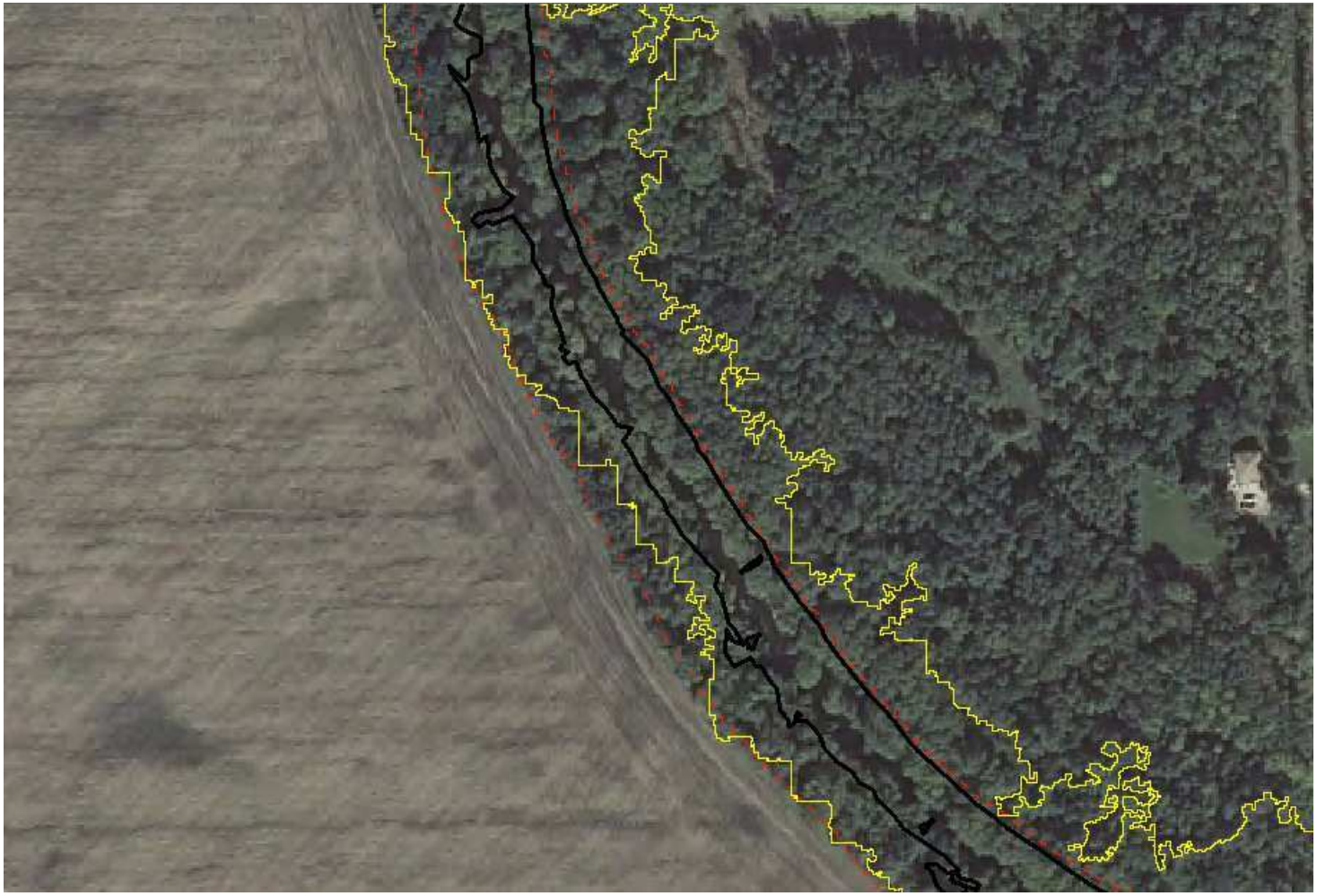

Figure 3.2. Example of survey polygons that are narrower than the delineated riparian zone extent on the eastern slope of the river. The dashed red line shows the extent of riparian survey polygons 36, 37, 38, 40, and 41. The solid black line shows the generated flood zone. The solid yellow line shows the extent of the riparian zone, including the generated flood zone and overlapping vegetation-based image objects.

Figure 3.3. Example of survey polygons that are wider than the delineated riparian zone extent on the south western slope of the river. The dashed red line shows the extent of riparian survey polygons 73, 74, 75, 76, and 78. The solid black line shows the generated flood zone. The solid yellow line shows the extent of the riparian zone, including the generated flood zone and overlapping vegetation-based image objects.

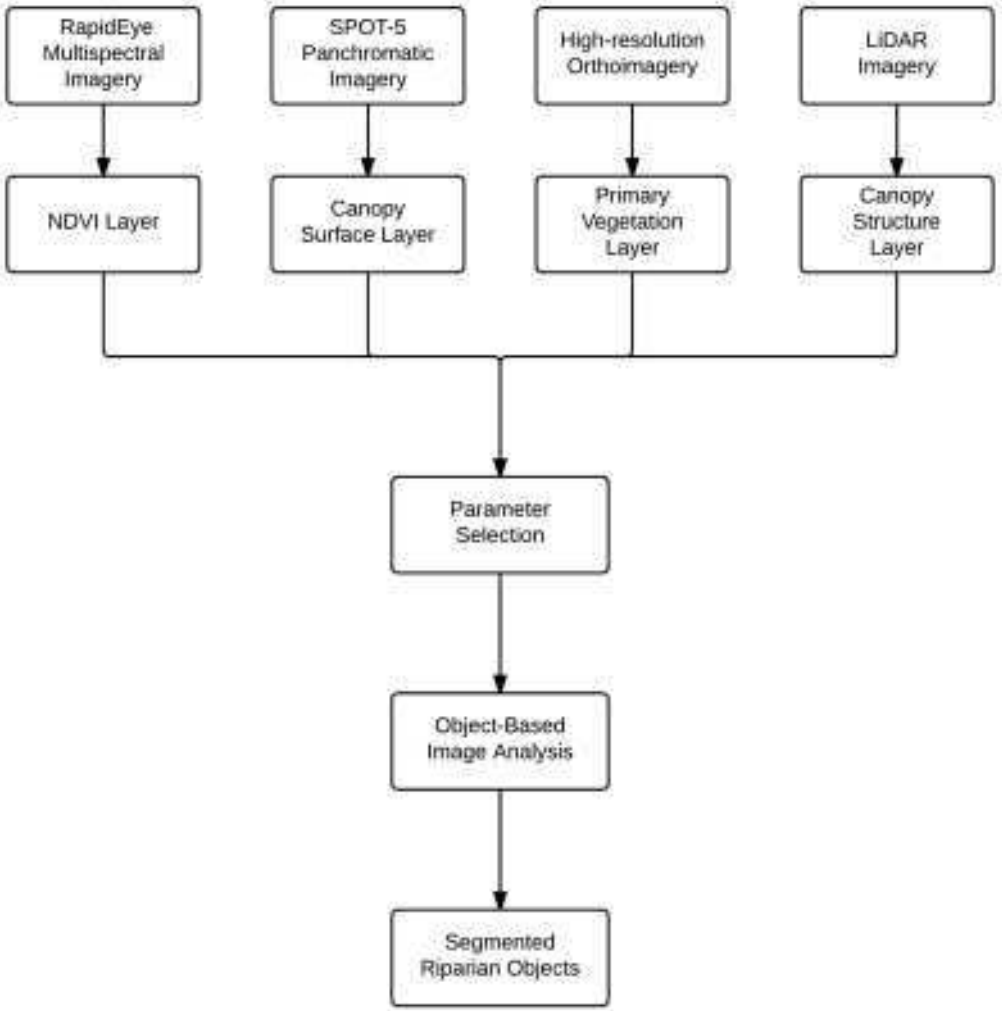

Figure 3.4. Workflow chart showing the steps followed for the object-based image analysis.

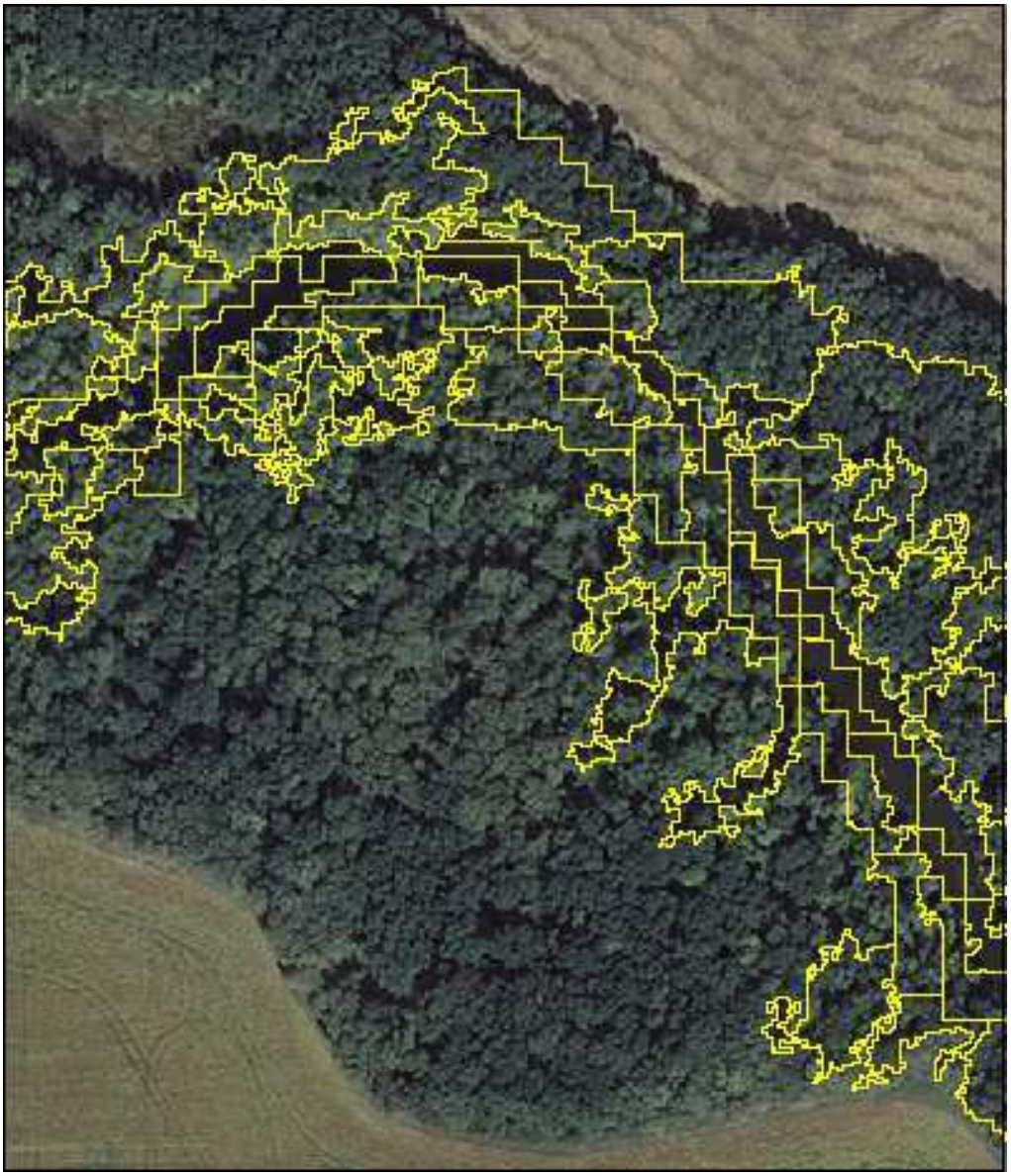

Figure 3.5. Riparian image objects overlaid on an ortho-image with good contrast, captured during leaf-on.

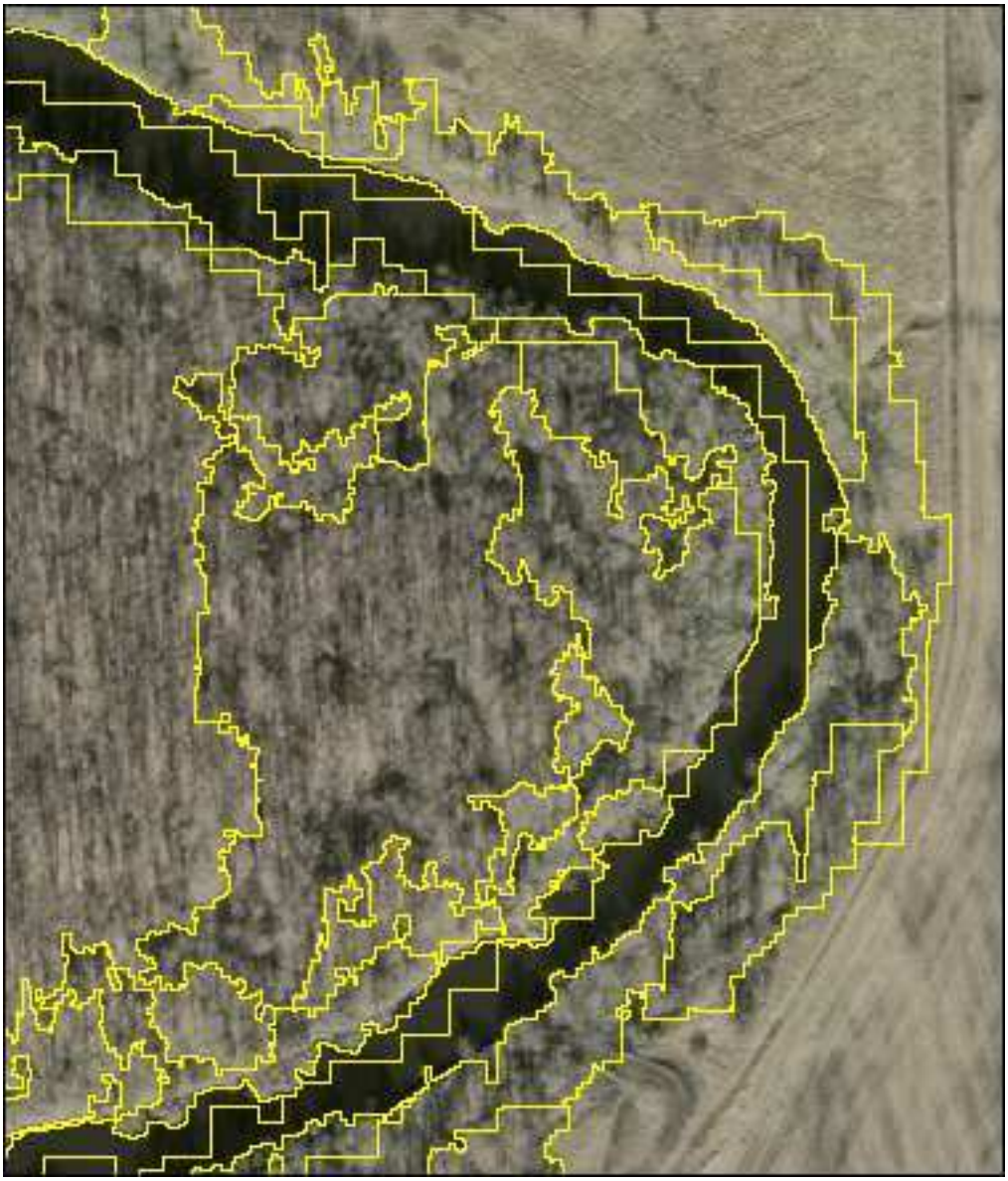

Figure 3.6. Riparian image objects overlaid on an ortho-image with poor contrast, captured during leaf-off.

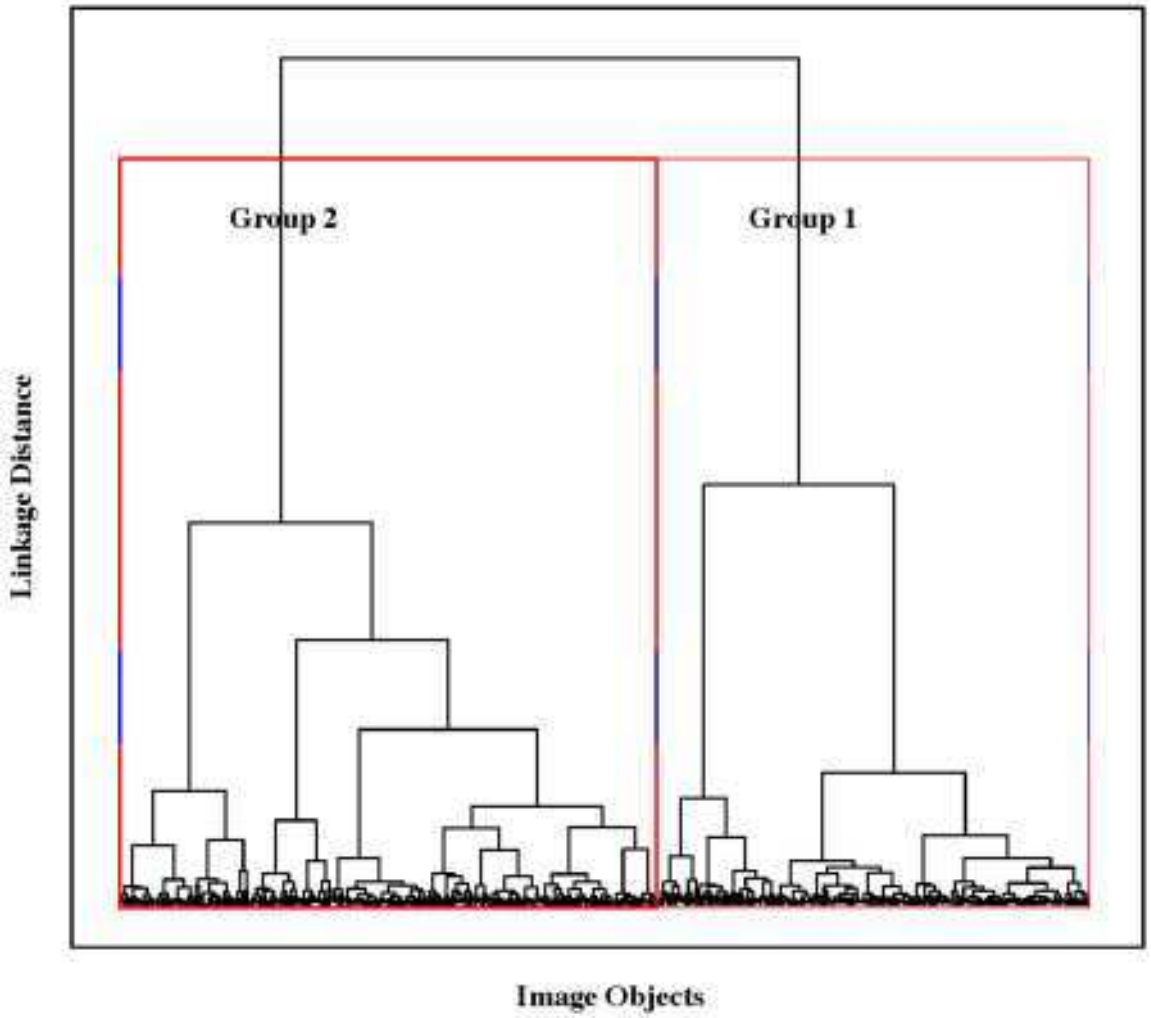

Figure 3.7. Cluster dendrogram showing the natural grouping of image objects segmented using all spectral variables and LiDAR variables within riparian survey polygons.

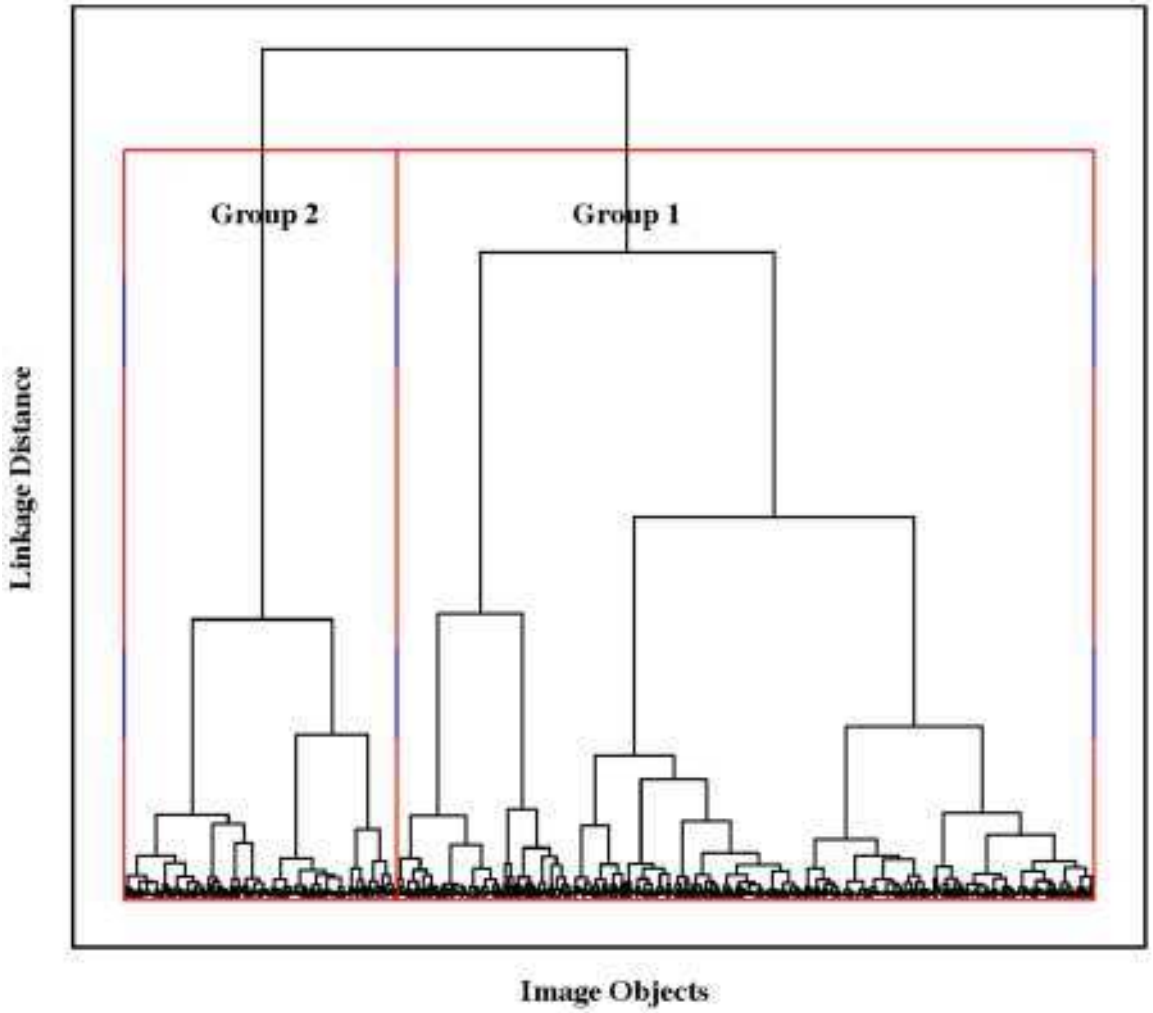

Figure 3.8. Cluster dendrogram showing the natural grouping of image objects segmented using only spectral variables, with LiDAR variables excluded, within riparian survey polygons.

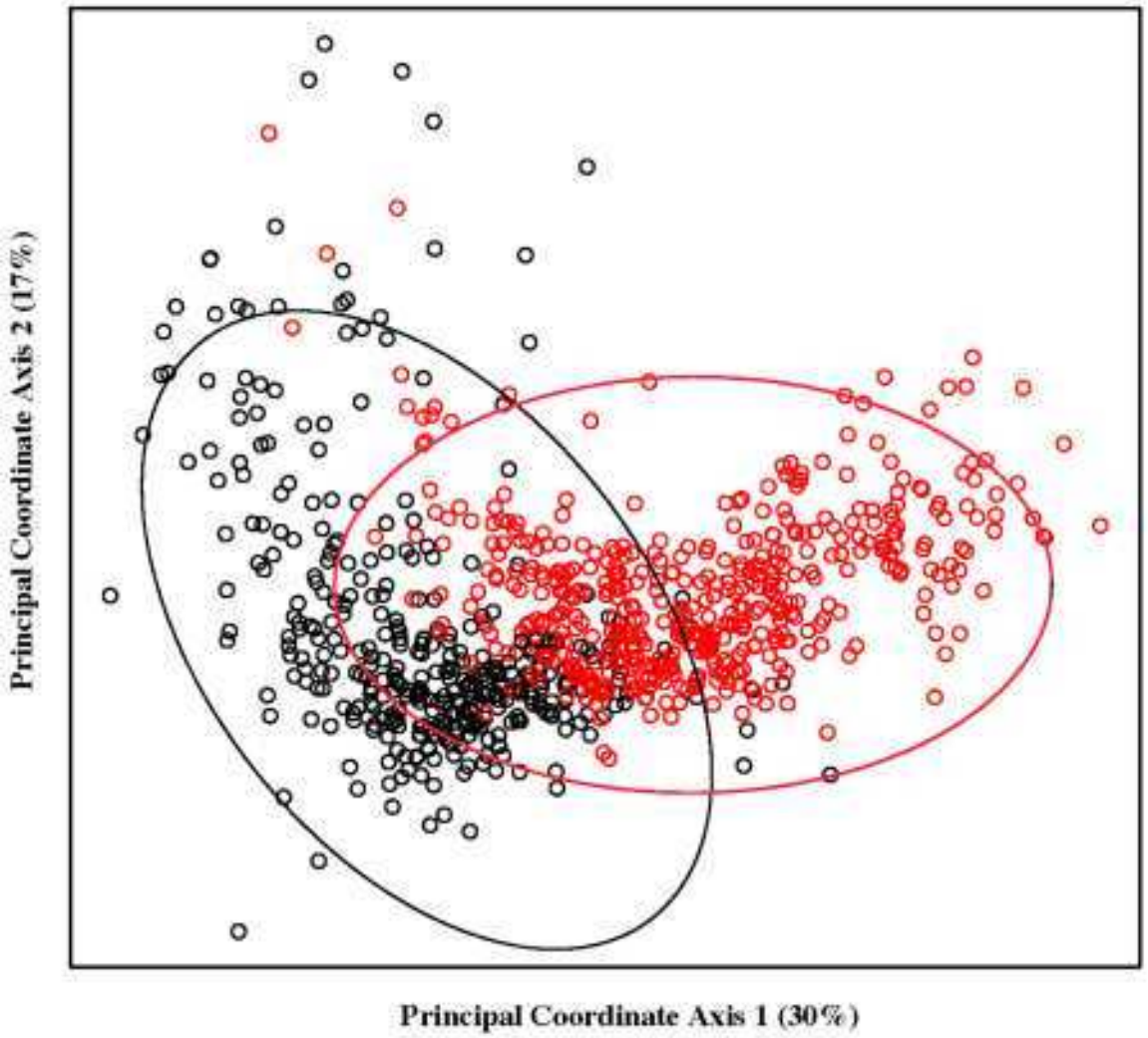

Figure 3.9. Biplot displaying the first two axes of a principal coordinates analysis with 95% confidence ellipses, conducted for image object groups derived from both LiDAR and spectral variables. Colour-coding indicates cluster-group membership (black = Group 1; red = Group 2), not riparian health category membership.

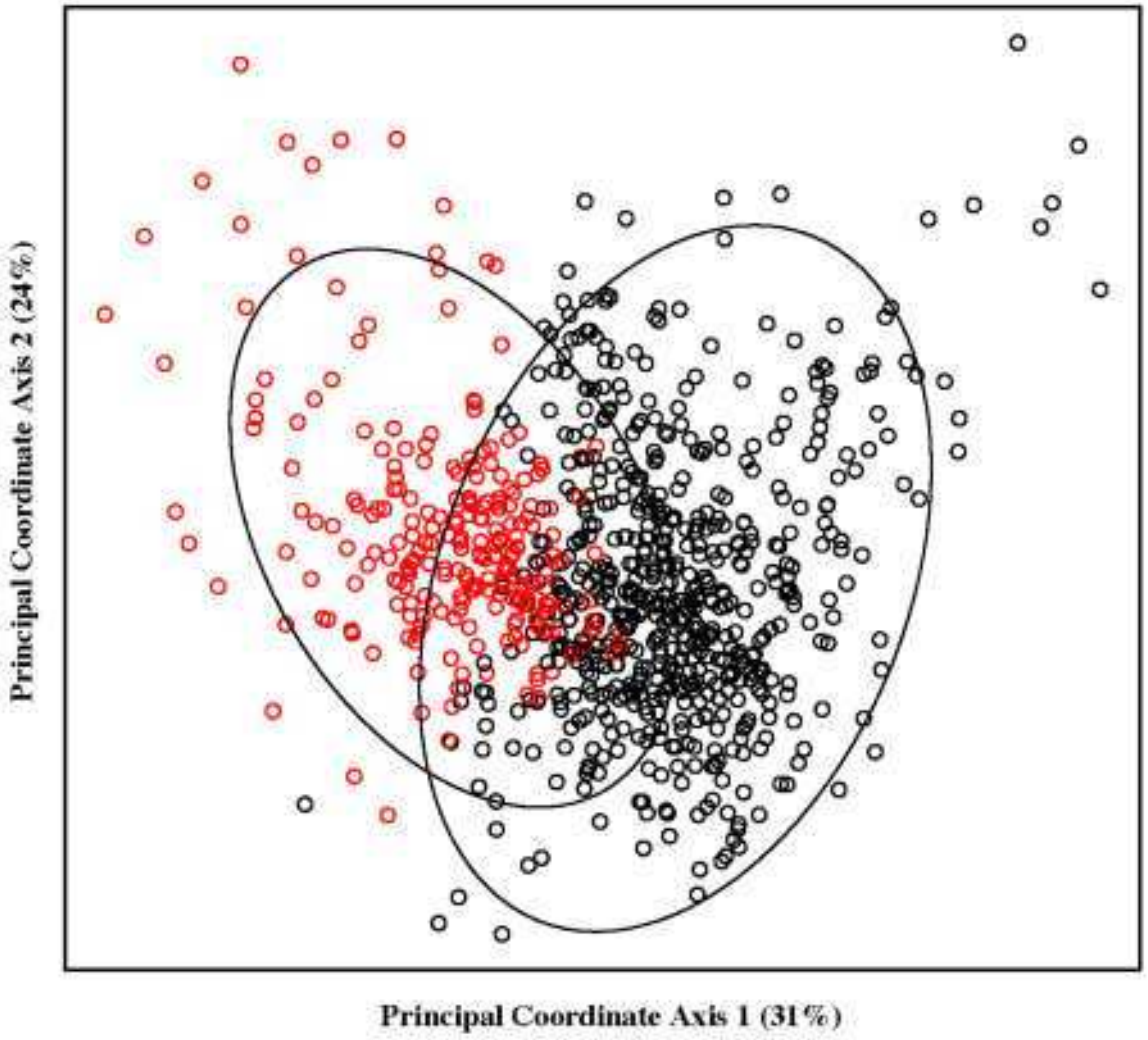

Figure 3.10. Biplot displaying the first two axes of a principal coordinates analysis with 95% confidence ellipses, conducted for image object groups derived from only spectral variables, excluding LiDAR variables. Colour-coding indicates cluster-group membership (black = Group 1; red = Group 2), not riparian health category membership.

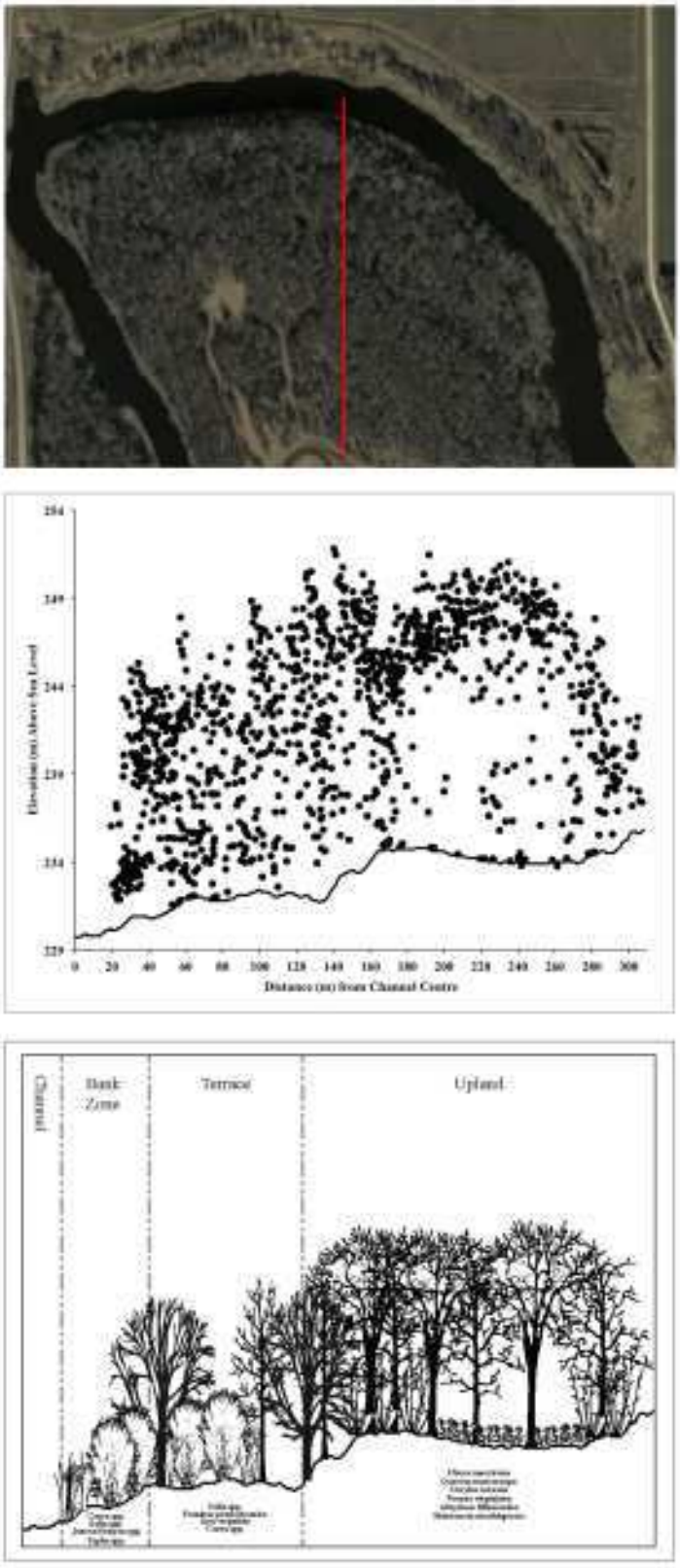

Figure 3.11. A LiDAR profile through a section adjacent to riparian health survey polygon #69. This polygon was scored as healthy.

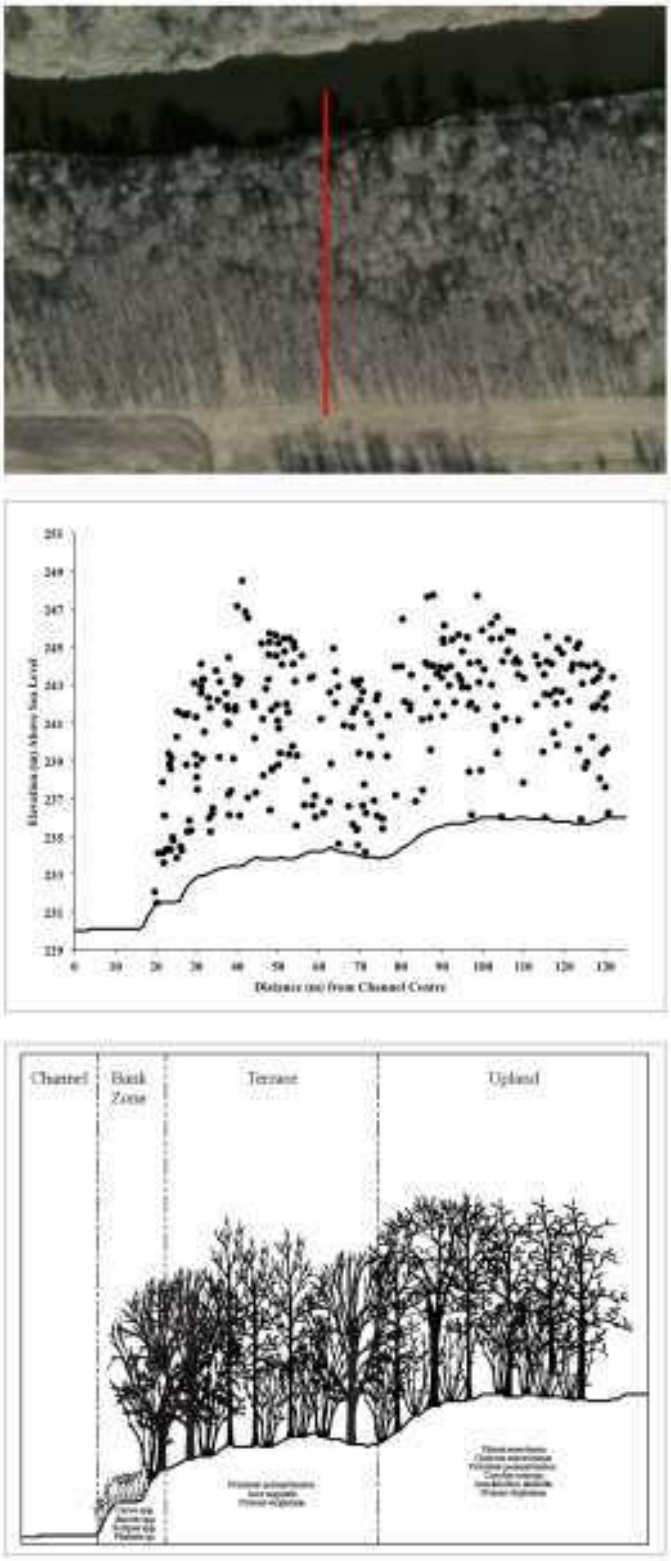

Figure 3.12. LiDAR profile through a section of riparian health survey polygon #77. This polygon was scored as healthy.

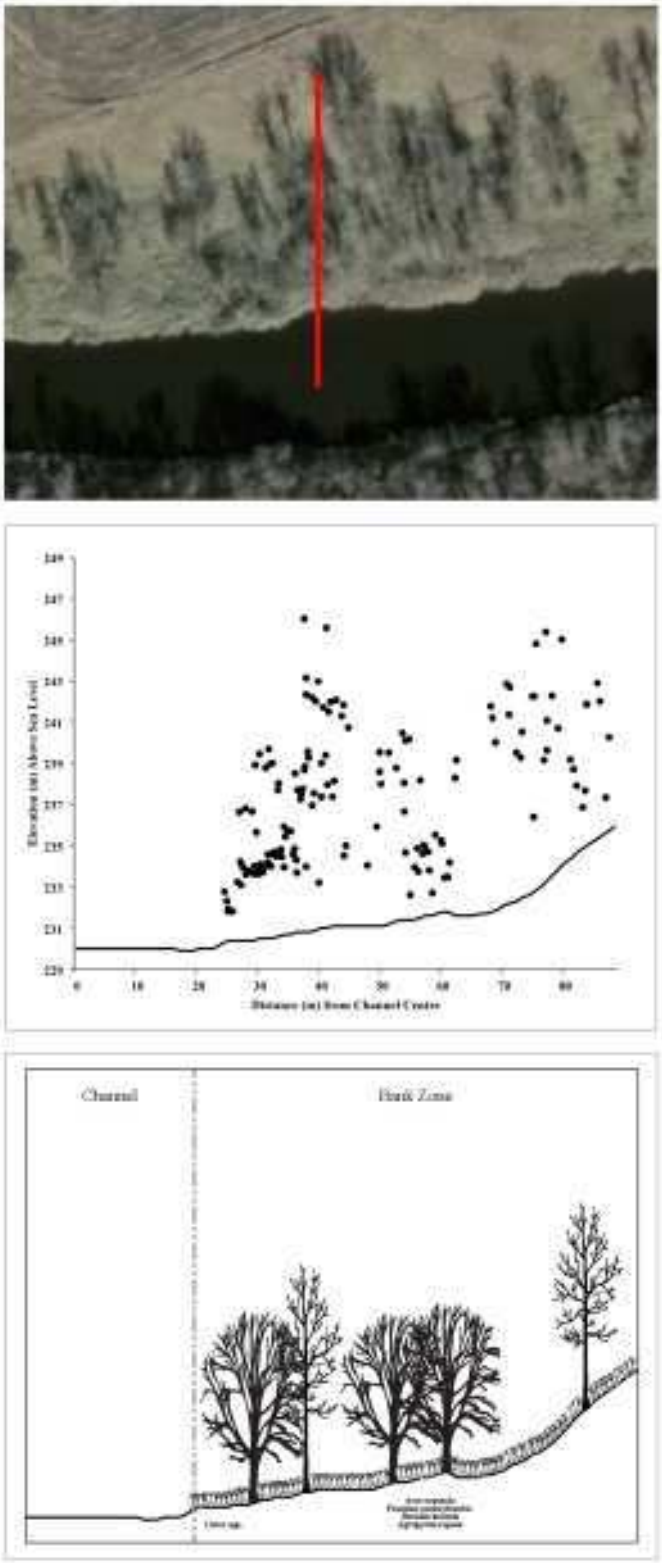

Figure 3.13. LiDAR profile through a section of riparian health survey polygon #73. This polygon was scored as unhealthy.

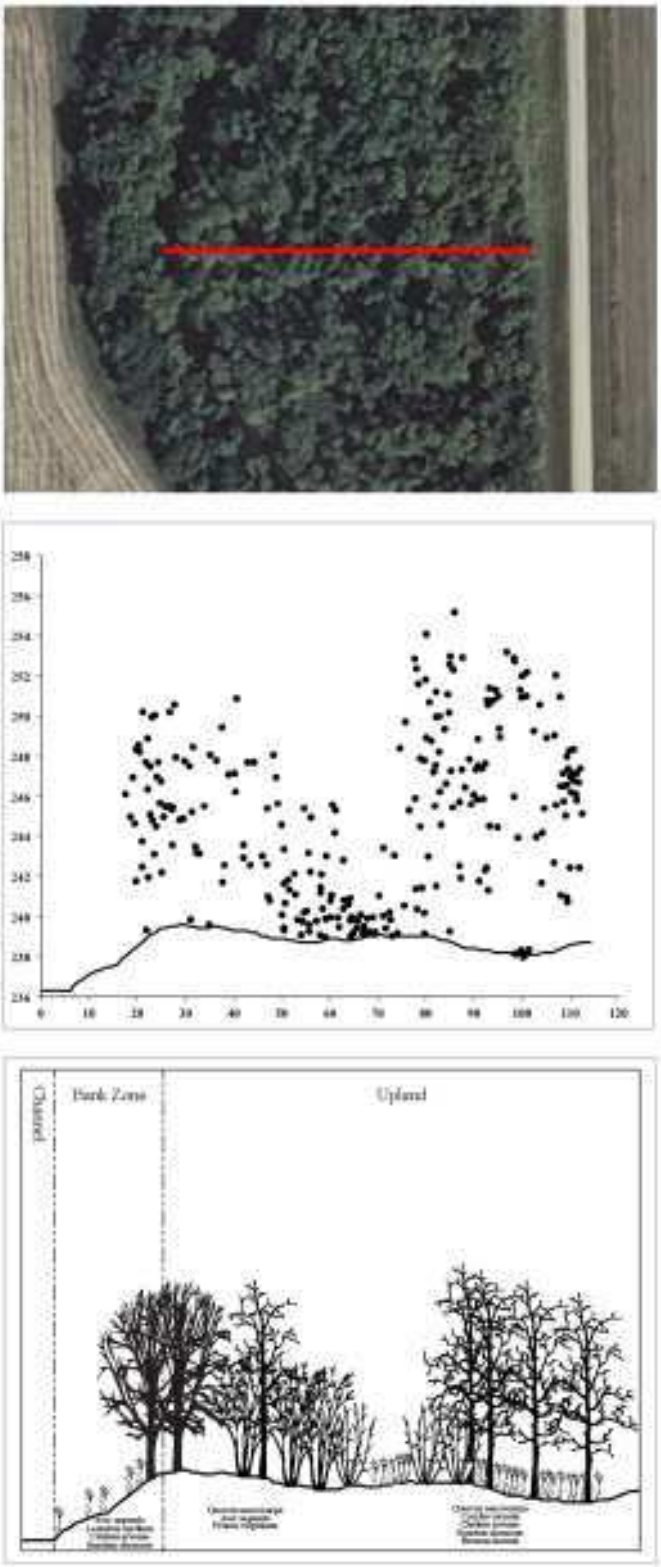

Figure 3.14. LiDAR profile through a section of riparian health survey polygon #57. This polygon was scored as unhealthy.

CHAPTER 4: RIPARIAN HEALTH MODEL

Abstract

Riparian areas are ecologically and economically critical habitats. However, they are also very susceptible to anthropogenic disturbance. Riparian health assessments have historically been conducted through resource-intensive field surveys. Recent advances in remote sensing have potential in the development of remote riparian health assessment methods. The objective of the study was to develop an automated riparian health assessment using remotely sensed data. Riparian health surveys were conducted along the La Salle River in Manitoba, Canada. Vegetation variables were derived from an object-based image analysis (OBIA). Topographic variables derived from a high-resolution DEM. Linear discriminant models were developed using topographic and vegetation, only vegetation and only topographic variables. The vegetation/topographic and vegetation models produced good results, with accuracies of 87% and 88% (kappa 74% and 75%). The topographic model produced poor results, with an accuracy of 61% (kappa 21%). The study demonstrated that riparian health can be assessed remotely, eliminating the need for field surveys and preserving resources for riparian management and conservation programming.

4.1 Introduction

Riparian areas are ecologically and economically critical habitats, providing numerous ecological services, including: wildlife habitat; bank stability and erosion control; sediment transport and deposition; energy, nutrient and pollutant regulation (Merritt et al., 2010; Nilsson and Svedmark, 2002; Naiman and Décamps, 1997; Gregory et al., 1991). However, they are also vulnerable to anthropogenic disturbance, such as urban and agricultural development. In a compromised state, riparian areas contribute to sedimentation, transport of pollutants, flooding, and a loss of wildlife habitat and biodiversity (Leclaire, 2011; Nilsson and Svedmark, 2002). Riparian health assessments are required to evaluate the degree of damage to riparian areas and aid in developing management prescriptions.

Riparian health assessments have historically been conducted through resource-intensive field surveys and manual aerial photointerpretation (Gergel et al., 2007; Johansen et al., 2007a). The narrow, linear dimensions and steep vegetation and physiographic gradients that characterize riparian areas made them unsuitable for the medium- and low-resolution satellite imagery available for landscape-level research prior to 2000 (Dilts et al., 2010; Johansen et al., 2007a; Muller, 1997). However, recent advances in remote sensing technology, including high-resolution imagery (<5m) and object-based image analysis (OBIA) have facilitated the detection of riparian attributes using remote methods. Object-based image analysis represents an advance in classification methodology for remotely sensed imagery. Traditional pixel-based methods classify individual pixels based on spectral value or digital number. Conversely, OBIA groups pixels to form objects based

on spectral, geometrical, spatial-contextual, and textural attributes, until a predefined degree of homogeneity is achieved in each object (Blaschke, 2010; Bock et al., 2005). Subsequent to this process, which is known as segmentation, the image objects are classified using algorithms that incorporate nearest neighbour distances, shape metrics, texture descriptors and hierarchy to quantify spectral, geometrical, contextual and textural attributes (Im et al., 2008; Hay et al., 2003). This methodology overcomes the speckle effect that results when a pixel-based classification is applied to a heterogeneous surface comprising a wide range of spectral values. In addition, it considers the inherent spatial structure of the natural system. Existing research overwhelmingly demonstrates that object-oriented image analysis produces significantly higher classification accuracies than traditional pixel-based classification when applied to high-resolution imagery (Aguirre-Gutiérrez et al., 2012; Platt and Rapoza, 2008).

Remotely sensed imagery has been used to detect riparian attributes in many studies since the advent of high-resolution satellite imagery in the early 2000s. Pixel-based classifications have been used to delineate the riparian zone width and extent, canopy cover and continuity, and vegetation species with varying degrees of success (Akasheh et al., 2008; Makkeasorn et al., 2009; Yang, 2007; Johansen and Phinn, 2006b; Jansen, 2005). Studies using object-based methods were able to detect a far wider range of riparian attributes, including: riparian zone and stream width; canopy cover and continuity; organic litter cover; vegetation overhang; bank stability; tree clearing; and flood damage (Arroyo et al., 2010; Johansen et al., 2010a; Johansen et al., 2010c; Johansen et al., 2008b; Johansen et al., 2007b; Johansen and Phinn, 2006a). These studies demonstrated that riparian attributes could be accurately mapped using object-based

methods to classify high-resolution spectral, LiDAR, and DEM datasets. However, no study has drawn a direct link between remotely sensed data and overall riparian health, defined as the cumulative impact of all relevant riparian health indicators. The objective of this study was to develop an automated riparian health assessment using remotely sensed imagery and topographic data.

4.2 Methods

The field methods, riparian flood zone delineation, and OBIA methods described in Section 3.2.4 were utilized in the following study. Additional data processing and analytical methods are described below. All topographic metric derivation, analysis, and modelling were conducted within the generated riparian flood zone described in Section 3.2.2.

4.2.1 Analysis of Riparian Topography

Channel sinuosity is a function of length along the channel between two points, divided by the shortest straight-line distance between the same two points. This calculation produces an index ranging from zero to one, which indicates the degree to which the channel meanders, and is indicative of the erosional regime in the riparian area. A sinuosity index value of one indicates a straight channel, while a deeply meandering stream will have a sinuosity index near zero. To calculate channel sinuosity along the La Salle, the smoothed river centerline was split into 1 km segments. A sinuosity index was calculated for each 1 km segment in ArcGIS. The derived sinuosity index was then assigned to the riparian survey polygons using a spatial join rule, which applied the index value of the intersecting or nearest centre-line segment to each survey polygon. In the

case of polygons intersected by more than one segment, the sinuosity indices were averaged and the mean value was assigned to the polygon.

While habitat condition is not necessarily correlated with riparian zone width, wider riparian areas provide more effective sediment and nutrient trapping, higher-quality fish and wildlife habitat, and a better buffer against adjacent disturbance (Wenger, 1999). The width of the riparian zone was calculated for the riparian survey polygons. Because the survey polygons were irregularly shaped and, consequently, not of uniform width, it was necessary to derive an average measure of polygon width. Straight lines 100m in length were manually digitized at 15-m intervals along each polygon, perpendicular to the river centre-line. The perpendicular lines were clipped to the riparian survey polygon extents. The clipped perpendicular line lengths were calculated and averaged for each riparian survey polygon.

Given the importance of topographically controlled moisture gradients to the vegetation component and, by extension, to riparian health, riparian zone topography was considered to be a potential indicator of habitat condition (Arroyo et al., 2010; Auble et al., 2005; Nilsson and Svedmark, 2002; Hughes, 1997; Auble et al., 1994). Instantaneous slope metrics provide a measure of topography (Blaga, 2012; Wood, 1996). Eleven slope metrics, including first and second derivatives of the elevation surface, were computed from the LiDAR-based DEM. First derivatives provide a measure of the tangent slope of a surface, while second derivatives characterize the surface curvature. First derivative slope metrics included slope and aspect. Nine measures of surface curvature, including profile and longitudinal curvatures (slope variation in the vertical plane), cross-sectional

and plan curvatures (slope variation in the horizontal plane), and minimum, maximum and mean curvatures (local minimum, maximum and mean surface curvature values in Euclidean space), as well as concavity (decreasing second derivative function) and convexity (increasing second derivative function), comprised the second derivative metrics (Blaga, 2012). Mean, maximum and minimum slope metric values were summarized for each image object contained within the riparian survey polygons. Prior to conducting further analyses, the slope variables were plotted using quantile-quantile (Q-Q) plot to assess normality (Legendre and Legendre, 2012). Non-normally distributed variables were removed, leaving a total of 12 slope variables.

Principal Components Analysis (PCA) was used to characterize spatial trends in first (slope and aspect) and second (measures of curvature) topographic derivatives and to isolate slope metrics explaining the majority of variation in the dataset. A detailed review of the PCA method can be found in Pielou (1984), Legendre and Legendre (2012) and Jolliffe (2002). Although not strictly a dimension reduction method, PCA can be used to determine main trends, variables that are important on those axes, and whether colinearity exists amongst those variables. In this study PCA was used to identify and eliminate redundant variables prior to full model development. Because the variables in the dataset comprised several units (e.g., slope (%), aspect (degrees), plan curvature (radians)), a correlation matrix was used in computing the PCA. The results of the PCA were displayed as a biplot. Topographic variables retained for the linear discriminant analysis were those that had low mutual correlation (less collinearity in multivariate space) and simultaneously the largest weights on the first and second axes.

4.2.2 Riparian Health Model Development

Linear Discriminant Analysis (LDA) was performed to assess and model the relationship between the topographic variables and the riparian health scores of the surveyed sites. LDA, also called Canonical Variates Analysis, is a linear modelling method (Legendre and Legendre, 2012). It is used to detect and quantify statistical separation between two or more predefined classes, which are described by a linear combination of several explanatory variables. In addition to determining the separability of classes and identifying the degree to which the various explanatory variables contribute to distinguishing between them, the derived linear equation can be applied as a maximum likelihood classifier, assigning objects to the class to which they maximally belong.

The image objects were randomly split into training and tests datasets for model development and validation. The training set contained 879 samples (75%), while the test set contained 249 (25%). Three separate LDAs were performed, using the training set, to assess the relationship between topographic and vegetation variables, and riparian health categories. Owing to the insufficient sample size of 'Unhealthy' polygons observed in the field (Section 3.2.1), and the tendency of 'Unhealthy' and 'Healthy with Problems' polygons to cluster together, these two categories were combined into a single riparian category, referred to in the remainder of the document as 'Unhealthy'. The first analysis included both vegetation and topographic variables. Vegetation variables included the 57 variables selected for the cluster analysis in Section 3.2.5 (Table X). Topographic variables included the 9 variables selected using the PCA and are listed in Section 4.3.1. All variables were standardized prior to conducting the LDA. Between-class separability for each LDA was tested by plotting the discriminant values for each class ('Healthy' and

'Unhealthy') on a boxplot, then examining the plot for overlap between the class mean, maximum and minimum discriminant values, upper and lower quartiles, and standard deviation. Classifier accuracy was assessed using resubstitution, which employs the same data to develop and test the classifier, to the training data. Resubstitution was considered an appropriate accuracy assessment method owing to the relatively small size of the image object dataset. While resubstitution can provide an optimistic estimate of classification accuracy, other methods of accuracy assessment, such as leave-one-out cross-validation, are prone to a high degree of variability when applied to small datasets (Braga-Neto et al., 2004). To provide a more realistic estimate of model accuracy, classification accuracy was also assessed for the test sets, which were not used in the development of discriminant functions. For both training and testing data, accuracy results were displayed using a confusion matrix, and producer, user and total accuracies were computed. Producer accuracy represents the probability that feature on the ground has been correctly classified, while user accuracy indicates the probability of a classified feature actually being found to be of the same class on the ground (Congalton and Green, 2009). Producer and user accuracies are calculated separately for each class. Total accuracy is calculated for the classifier as a whole. In addition, a kappa statistic was calculated for the training and testing sets for each discriminant function. Kappa provides a measure of agreement between two raters (the modeled class and actual class) that considers agreement occurring by random chance, thereby providing a very conservative estimate of model accuracy (Congalton and Green, 2009; Cohen, 1960). The significance of the derived discriminant functions for both training and testing sets was assessed using a Multivariate Analysis of Variance (MANOVA). The test statistic applied was Wilks'

Lambda, the ratio of the within-class sums of squares to the total sum of squares, which represents a measure of the proportion of unexplained class variance (Legendre and Legendre, 2012). Based on the results of the LDA and accuracy statistics, the best model was selected and applied to the entire La Salle study area.

4.3 Results

4.3.1 Analysis of Topographic Variables

Channel sinuosity for 1 km segments along the La Salle ranged from 0.45 to 0.96, with a mean and median values of 0.80 and 0.84, respectively. These values are indicative of a relatively straight flow path. The width of riparian polygons clipped to the generated flood zone ranged from 2.3 m to 60.7 m, with respective mean and median widths of 11.5 m and 10.3 m. After eliminating non-normally distributed variables, the slope metrics input into the PCA included: minimum mean curvature, profile curvature, longitudinal curvature, cross-sectional curvature, and concavity; maximum mean curvature, profile curvature, longitudinal curvature, cross-sectional curvature, slope, and convexity; and mean aspect.

The results of the PCA are presented in Figure 4.1. The PCA explained 81% of the total variation in the slope metrics dataset, with 67% summarized on the first axis and 14% on the second. There was almost complete overlap between objects belonging to riparian survey polygons classified as ‘Healthy’ and ‘Unhealthy’. The dataset displayed strong collinearity among minimum variables in the upper right quadrant. With the exception of maximum slope, the maximum variables showed only slightly weaker collinearity in the upper left quadrant. Aspect, the only mean variable, trended weakly in the upper left

quadrant. The relative weights of each variable on the first two axes were also compared to help identify redundancy. Based on these results, longitudinal curvature (with weights of -0.316 and -0.228 on the first and second axes, respectively), minimum profile curvature (-0.316, -0.206), and mean curvature (-0.319, -0.231) were removed from the dataset to reduce redundancy, as these metrics explained essentially same portion of dataset variability as minimum concavity (-0.323, -0.217), which was retained.

4.3.2 Riparian Health Model Development

The results of the vegetation/topographic LDA are presented in Figure 4.2. The plot clearly shows separation between the two classes; the third quartile of the 'Healthy' and first quartile of the 'Unhealthy' categories are well separated. However, there is also noticeable overlap between both mean and median standard deviation bars, and the 'Unhealthy' category mean and median. Both mean and median SDs are greater for the 'Healthy' class than for the 'Unhealthy'. 'Healthy' category LD values are weighted toward the lower end of the discriminant axis, while 'Unhealthy' category LD values are weighted toward the upper end. All outliers for both classes lie opposite to the direction in which the plots are weighted. The vegetation/topographic model achieved a training accuracy of 87% (Kappa (κ) = 74±4%) and a testing accuracy of 85% (κ = 69±8%) (Tables 3 and 4). Both training (Wilks' Lambda (Λ) = 0.41, p value (p) < 0.001) and testing (Λ = 0.34, p < 0.001) results were significant.

The results of the LDA using only vegetation variables are shown in Figure 4.3. The distribution of LD values are very similar to the vegetation/topography model; the third quartile of the 'Healthy' and first quartile of the 'Unhealthy' categories are well

separated, mean and median SD bars of the two categories overlap, and the 'Healthy' SD bars overlap with the 'Unhealthy' mean and median. 'Healthy' category LD values are weighted toward the lower end of the discriminant axis, while 'Unhealthy' category LD values are weighted toward the upper end and, like the previous model, all outliers for both classes are opposite to direction in which the plots are weighted. The vegetation model had a slightly higher training accuracy of 88% ($\kappa = 75\pm4\%$), and an equal testing accuracy of 85% ($\kappa = 69\pm8$ %). Both training ($\Lambda = 0.42$, $p < 0.001$) and testing results were significant ($\Lambda = 0.38$ $p < 0.001$) and comparable to the vegetation/topographic model.

The LDA using only topographic variables produced drastically different results to the above models. The results of the topographic LDA are presented in Figure 4.4. The median SD bars overlap almost completely. Both the third quartile and first quartiles of the 'Healthy' and 'Unhealthy' classes, respectively, overlap with the opposite class medians. The medians of both classes are virtually equal. Unlike the vegetation/topographic and vegetation models, the class distributions are not weighted in either direction along the discriminant axis, and outliers are found at both ends of each class distribution. Training and testing accuracies of only 61% ($\kappa = 21\pm7\%$) and 62% ($\kappa = 21\pm11\%$) were achieved. Both training (Wilk's $\Lambda = 0.93$, $p < 0.001$) and testing ($\Lambda = 0.90$, $p = 0.002$) results were significant; however, the higher Wilks' Lambda values indicate group differences show notably less separation than the previous models.

4.4 Discussion

4.4.1 Analysis of Topography

Strong collinearity was observed among minimum slope curvature metrics (upper right quadrant of the PCA plot), while slightly weaker, but still pronounced collinearity was observed among the maximum curvature metrics in the upper left quadrant (Figure 4.1). Collinearity among topographic metrics is a well-known phenomenon in topographic studies (Guo et al., 2010). Consequently, it was not an object of concern in this study, and was handled by retaining only one of each group of strongly collinear variables to minimize dataset redundancy.

4.4.2 Riparian Health Model Development

The results of this study demonstrate that riparian habitat health can be accurately predicted from OBIA on remotely sensed image datasets. Multiple existing studies have used OBIA of remotely sensed imagery to predict various riparian attributes, including: riparian zone and channel width; vegetation overhang; bank stability; flood damage; canopy cover and continuity; tree clearing; and organic litter cover (Arroyo et al., 2010; Johansen et al., 2008b; Johansen et al., 2007b; Johansen and Phinn, 2006a). These indicators can be assessed in combination to determine riparian health. However, no previous studies have linked segmented image objects directly to overall riparian health. In this study, the most accurate model used only spectral and structural vegetation variables. Riparian physical structural attributes are important contributors to riparian health indicators such as bank stability (Arroyo et al., 2010; Johansen et al., 2010a; Johansen et al., 2010c). Therefore, it follows that including topographic information in a

riparian health model should improve the accuracy. However, the inclusion of topographic variables was found to slightly reduce accuracy in combination with vegetation variables in this study. In addition, results for the topographic variables model were very poor, particularly as a predictor of unhealthy polygons. These results suggest that terrain variables do not contribute useful information to the model.

There are several possible reasons for these unexpected results. First, the LiDAR data used to construct the DEM from which topographic metrics were derived was not sampled at a sufficiently high point density. Several studies indicate that DEMS can be accurately constructed using relatively low point densities (Guo et al., 2010; Liu, 2008; Anderson et al., 2006). Liu (2008) found that a post spacing of at least half the DEM grid resolution was adequate. However, detection of small topographic features can require much higher sampling densities (Chu et al., 2014). In addition, the presence of forest cover also requires denser sampling, as the canopy layers deflect some LiDAR waves before they reach the ground. These factors could apply to the detection of riparian erosional features, which are often small-scale and are also usually situated beneath overhanging vegetation. Second, the topographic variables were added in subsequent step, rather being included in the image segmentation. Had the terrain variables been included in the image segmentation, they would have influenced the statistical attributes of the image objects and might have contributed more to model accuracy. An important element of the previous studies' success using topographic and vegetation data was the inclusion of a LiDAR-derived DTM and slope model in the OBIA (Arroyo et al., 2010; Johansen et al., 2010a; Johansen et al., 2010c). It is possible that a 1 m DEM is not sufficiently high-resolution to capture information required to detect riparian physical

structure-related health indicators. These indicators might be better detected indirectly through vegetation characteristics. Finally, it is possible that no relationship exists between topography and riparian health; cycles of erosion, deposition, bank collapse, and channel migration are natural elements of channel migration and habitat succession in the riparian zone (Naiman and Décamps, 1997).

To demonstrate the practical utility of the remote riparian health assessment, Figures 4.5 to 4.13 show examples of riparian zone extent and health, predicted using the vegetation and canopy structure model. Figure 4.5 shows a typical healthy riparian area, characterized by a wide band of forest on both banks. The riparian area extends 30-60 m from the channel, consistent with field observations for wider, well-forested polygons along the La Salle. Figure 4.6, also classified as healthy, shows narrower forested riparian area. Despite its lesser width, it has a well-established band of native forest on both banks, providing sufficient protection against erosion. Figure 4.7 shows an herbaceous riparian area, classified as healthy. While the majority of healthy riparian areas are treed, low-lying herbaceous communities dominated by marsh species or the invasive, but deep-rooted, reed canary grass (*Phalaris arundinacea*) can also be functional habitats. In this example, there is a wide buffer between the adjacent agricultural field and the channel, and, while some erosion is present, there is no evidence of excessive erosion along the bank. Figure 4.8 shows a forested riparian area intersected by a road. While most of the riparian area shown was classified as healthy, the section adjacent to the road intersection was classified as unhealthy, owing to disturbance resulting reduced bank stability, and the lack of native species and tree cover, and a correlative increase in the cover of invasives. Figures 4.9 and 4.10 show forested riparian areas with adjacent yard sites. These sites are

typical of much of the La Salle study, with patches of disturbed and compromised riparian habitat interspersed among predominantly healthy, well-treed habitat. Because of their small footprints, damaged habitat associated with yard sites is usually relatively localized as compared with cultivated fields. However, construction of erosion control structures (e.g. riprap) on these sites also frequently results in increased erosion downstream. Figure 4.11 exhibits a less clear classification; while both sides of the channel are well-forested, the north bank is classified as unhealthy. The yard site on the north bank does not appear large enough to influence riparian habitat along the entire reach shown. However, as aerial imagery does not show the state of the riparian area below the canopy, the unhealthy classification reflects habitat damage in the understorey detected through structural information derived from canopy structure indices. Figure 4.12 shows a narrow riparian area classified as unhealthy, with sparse tree growth and cultivated fields immediately adjacent on both sides. Sites of this type are affected by bank instability resulting from tree clearing, invasion by invasive species, and agricultural pollutants, which cannot be adequately filtered owing to the lack of tree growth. Figure 4.13 shows a similar riparian area bisecting a golf course. While not affected to the same degree by agricultural pollutants, this riparian area is similar to the previous one.

4.5 Conclusion

This study found that object-based methods applied to vegetation and canopy structure data could be used to develop a model that accurately predicts riparian habitat condition as observed in the field. The model using only vegetation spectral and canopy structural

variables was found to produce the best result, with an accuracy of 88% (κ = 74±4%). The model based on topographic variables in isolation produced very poor results. This could be a function of: the sampling density of the LiDAR data used to construct the DEM; the lack of inclusion of topographic metrics in the object-based image segmentation; or, riparian physical structural attributes might be better represented in remotely sensed datasets by vegetation indicators. These results demonstrate that riparian health can be accurately modelled using object-based methods to assess spectral and structural vegetation data. Using this method, riparian health can be assessed remotely, eliminating the need for field surveys and preserving resources for riparian management and conservation programming.

Table 4.1. Accuracy statistics for the linear discriminant model training set using topographic and vegetation variables ($\Lambda = 0.41$, $p < 0.001$).

Actual Class/Predicted Class	Healthy	Unhealthy	Total
Healthy	453	63	516
Unhealthy	47	316	363
Total	500	379	879
Producer Accuracy	91%	83%	
User Accuracy	88%	87%	
Total Accuracy	87%		
Kappa	74%		
Kappa Confidence Interval	±4%		

Table 4.2. Accuracy statistics for the linear discriminant model testing set using topographic and vegetation variables ($\Lambda = 0.34$, $p < 0.001$).

Actual Class/Predicted Class	Healthy	Unhealthy	Total
Healthy	150	22	172
Unhealthy	22	100	122
Total	172	122	294
Producer Accuracy	87%	82%	
User Accuracy	87%	82%	
Total Accuracy	85%		
Kappa	69%		
Kappa Confidence Interval	±8%		

Table 4.3. Accuracy statistics for the linear discriminant model training set using vegetation variables only ($\Lambda = 0.42$, $p < 0.001$).

Actual Class/Predicted Class	Healthy	Unhealthy	Total
Healthy	453	63	516
Unhealthy	44	319	363
Total	497	382	879
Producer Accuracy	91%	84%	
User Accuracy	88%	88%	
Total Accuracy	88%		
Kappa	75%		
Kappa Confidence Interval	±4%		

Table 4.4. Accuracy statistics for the linear discriminant model testing set using vegetation variables only ($\Lambda = 0.38$, $p < 0.001$).

Actual Class/Predicted Class	Healthy	Unhealthy	Total
Healthy	152	20	172
Unhealthy	24	98	122
Total	176	118	294
Producer Accuracy	86%	83%	
User Accuracy	88%	80%	
Total Accuracy	85%		
Kappa	69%		
Kappa Confidence Interval	±8%		

Table 4.5. Accuracy statistics for the linear discriminant model training set using topographic variables only ($\Lambda = 0.93$, $p < 0.001$).

Actual Class/Predicted Class	Healthy	Unhealthy	Total
Healthy	423	93	516
Unhealthy	247	116	363
Total	670	209	879
Producer Accuracy	63%	56%	
User Accuracy	82%	32%	
Total Accuracy	61%		
Kappa	21%		
Kappa Confidence Interval	±7%		

Table 4.6. Accuracy statistics for the linear discriminant model testing set using topographic variables only ($\Lambda = 0.90$, $p < 0.002$).

Actual Class/Predicted Class	Healthy	Unhealthy	Total
Healthy	146	26	172
Unhealthy	87	35	122
Total	233	61	294
Producer Accuracy	63%	57%	
User Accuracy	85%	29%	
Total Accuracy	62%		
Kappa	21%		
Kappa Confidence Interval	±11%		

Table 4.7. Significance statistics for linear discriminant models (training and testing sets).

Model Variables	Degrees of Freedom	Wilks' Lambda	Approximate F Statistic	Number of Degrees of Freedom	Density of Degrees of Freedom	P-value	Residuals
Vegetation and Topography - Training	1	0.40875	17.23	68	810	<0.001	877
Vegetation and Topography - Testing	1	0.34191	6.3686	68	225	<0.001	292
Vegetation Only - Training	1	0.42386	19.578	57	821	<0.001	877
Vegetation Only - Testing	1	0.37864	6.7944	57	236	<0.001	292
Topography Only - Training	1	0.92634	6.2674	11	867	<0.001	877
Topography Only - Testing	1	0.90329	2.7446	11	1161	0.002	292

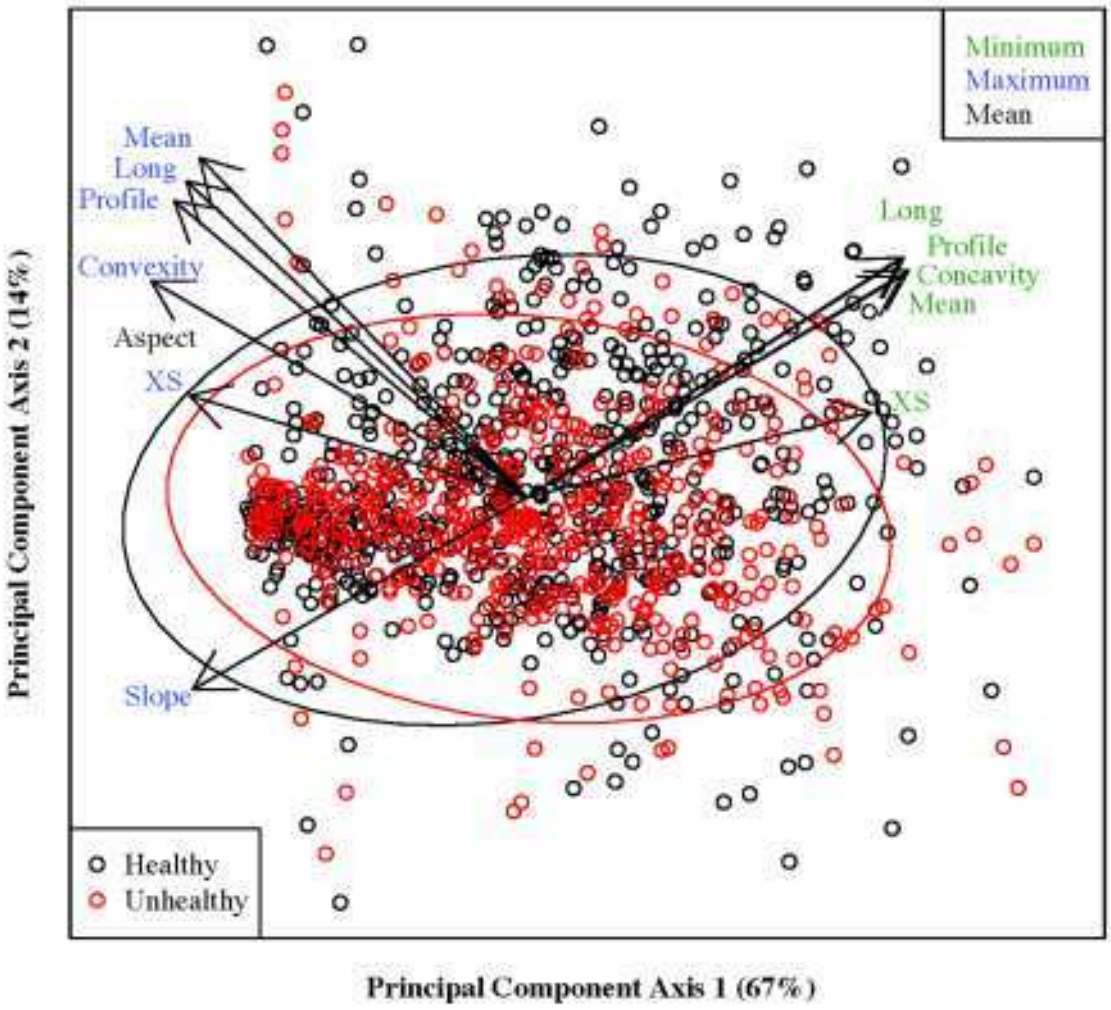

Figure 4.1. Biplot showing the first two axes of the principal components analysis conducted for the instantaneous slope variables, with 95% confidence ellipses. Circles represent segmented image objects, colour coded according to riparian health survey score. Variables abbreviated: Long=longitudinal curvature; Profile=profile curvature; XS=cross-sectional curvature; Mean=mean curvature. "Aspect" is situated in the upper left quadrant near the plot centre, trending weakly on both axes.

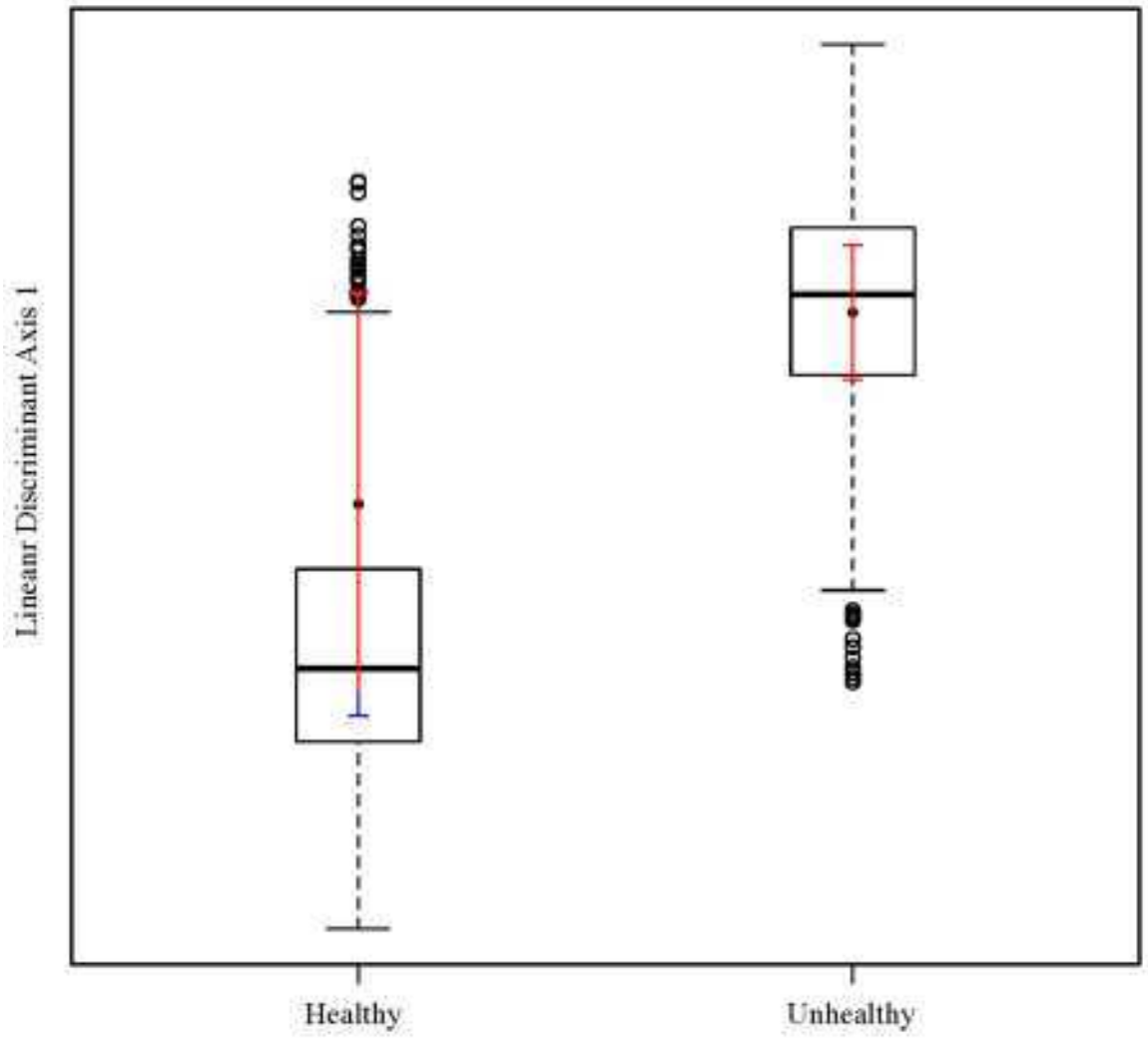

Figure 4.2. Boxplot showing the distribution of healthy and unhealthy riparian classes according to a linear discriminant model developed using both vegetation and topographic variables. The horizontal solid line depicts the median. The box contains 50% of the data, between the first and third quartiles. Dashed whiskers represent the median 95% confidence interval (CI). Solid red whiskers show the mean 95% CI. Solid and hollow circles depict the mean and outliers, respectively.

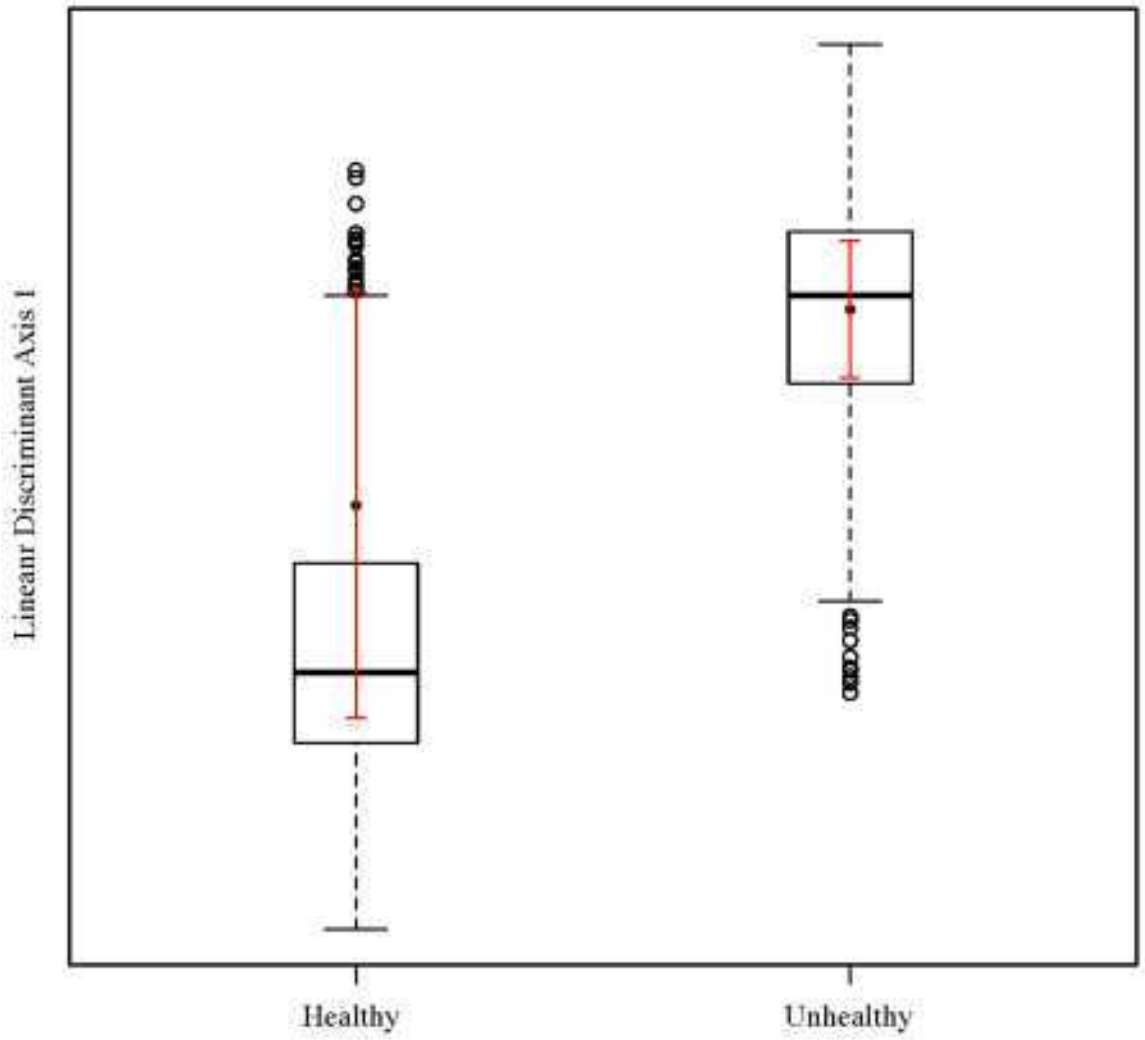

Figure 4.3. Boxplot showing the distribution of healthy and unhealthy riparian classes according to a linear discriminant model developed using only vegetation variables. The horizontal solid line depicts the median. The box contains 50% of the data, between the first and third quartiles. Dashed whiskers represent the median 95% confidence interval (CI). Solid red whiskers show the mean 95% CI. Solid and hollow circles depict the mean and outliers, respectively.

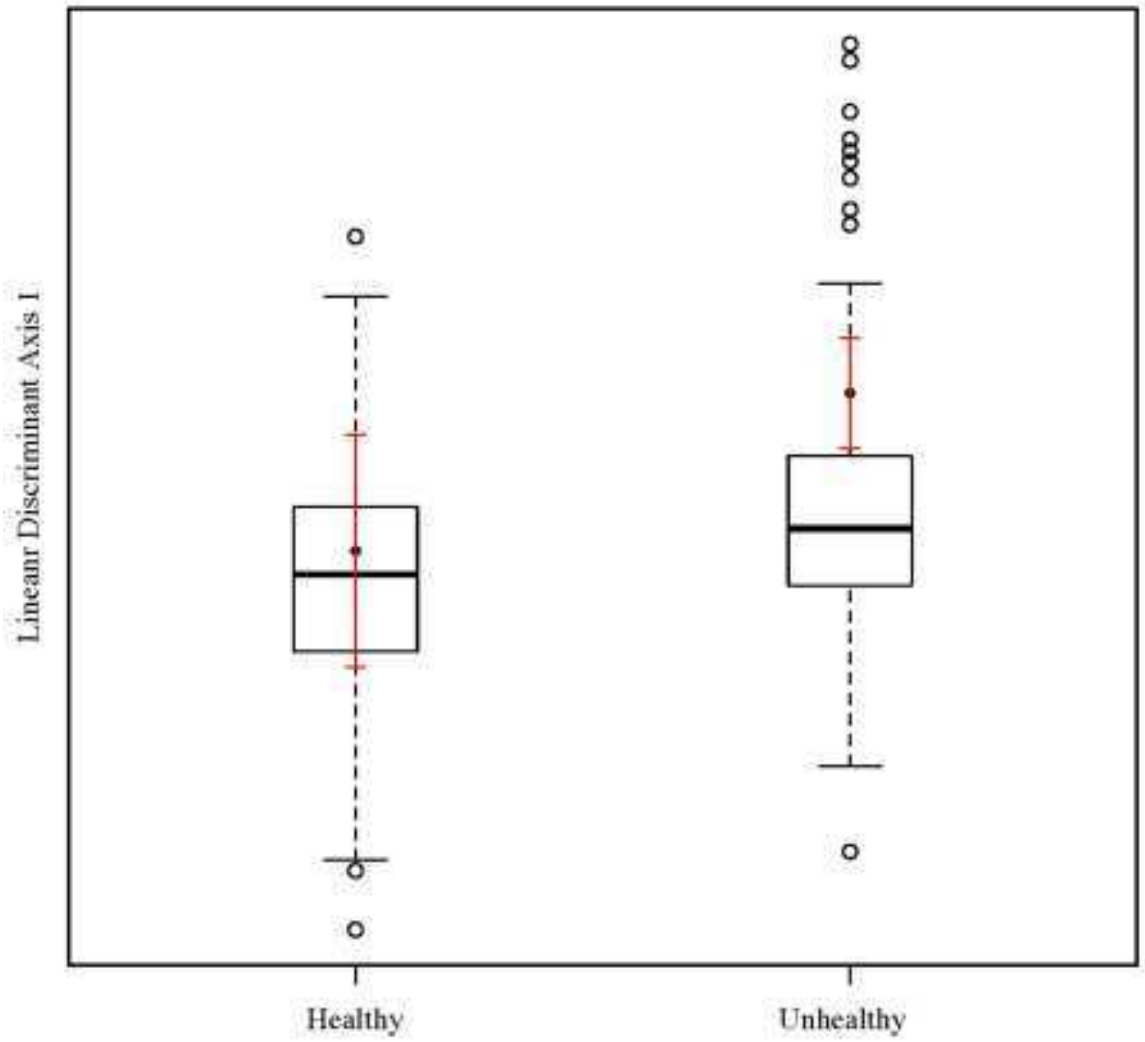

Figure 4.4. Boxplot showing the distribution of healthy and unhealthy riparian classes according to a linear discriminant model developed using only topographic variables. The horizontal solid line depicts the median. The box contains 50% of the data, between the first and third quartiles. Dashed whiskers represent the median 95% confidence interval (CI). Solid red whiskers show the mean 95% CI. Solid and hollow circles depict the mean and outliers, respectively.

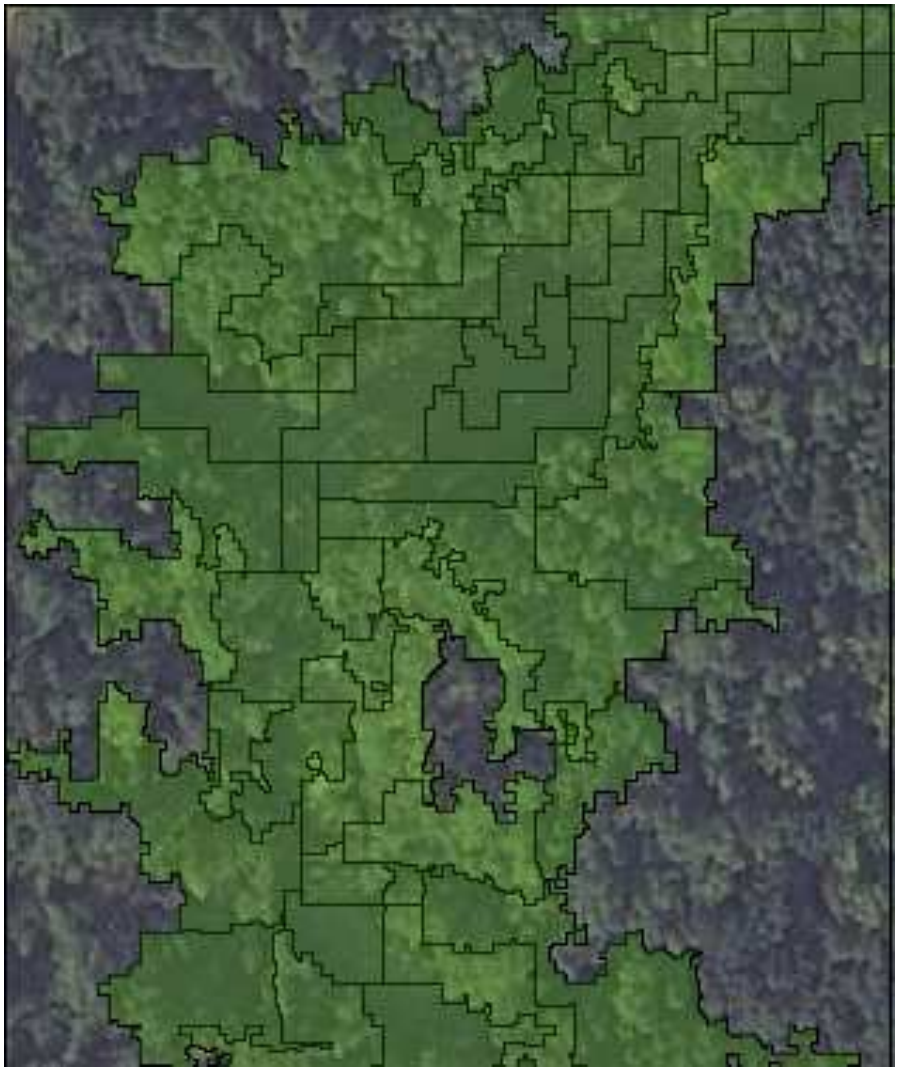

Figure 4.5. A wide, forested riparian area. Riparian health model classification: green = healthy, red = unhealthy. Image captured using a 175x210 m window at a scale of 1:2000.

Figure 4.6. A narrow, forested riparian area, surrounded by cultivated agricultural fields. Riparian health model classification: green = healthy, red = unhealthy. Image captured using a 175x210 m window at a scale of 1:2000.

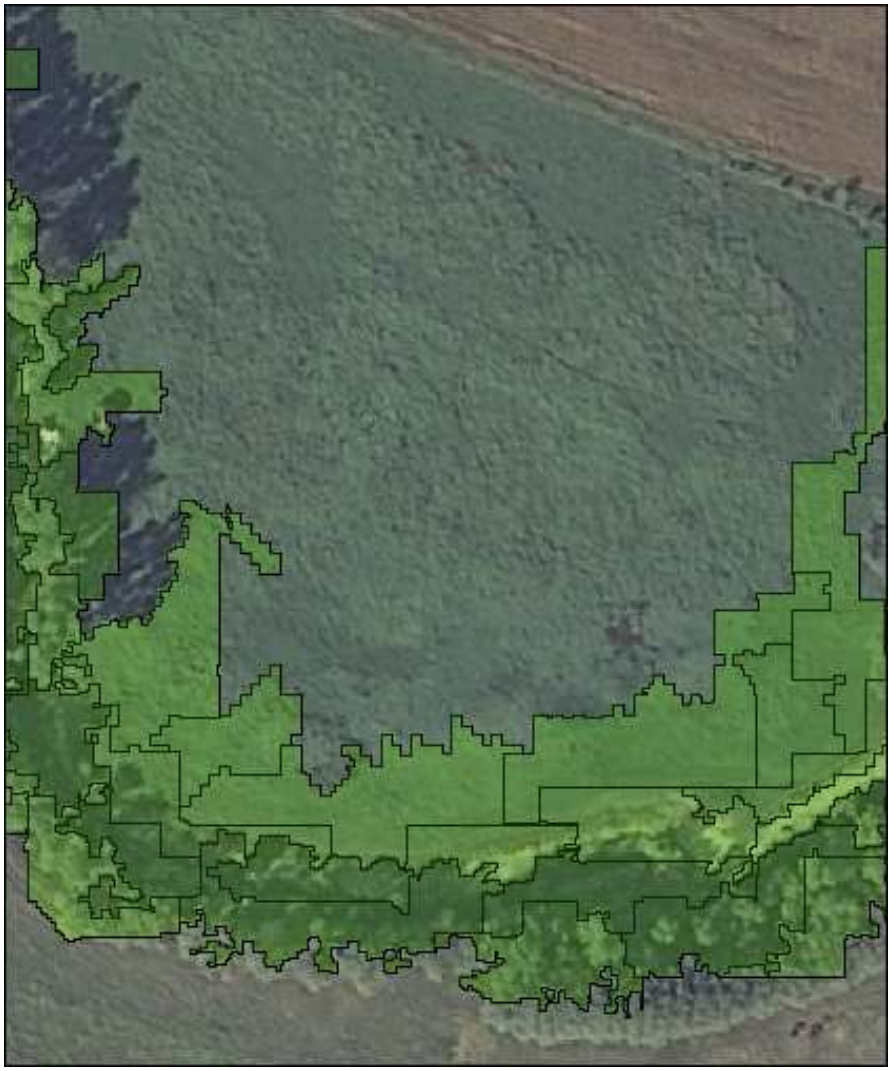

Figure 4.7. A narrow riparian area, characterized by herbaceous cover on one side of the river. Riparian health model classification: green = healthy, red = unhealthy. Image captured using a 175x210 m window at a scale of 1:2000.

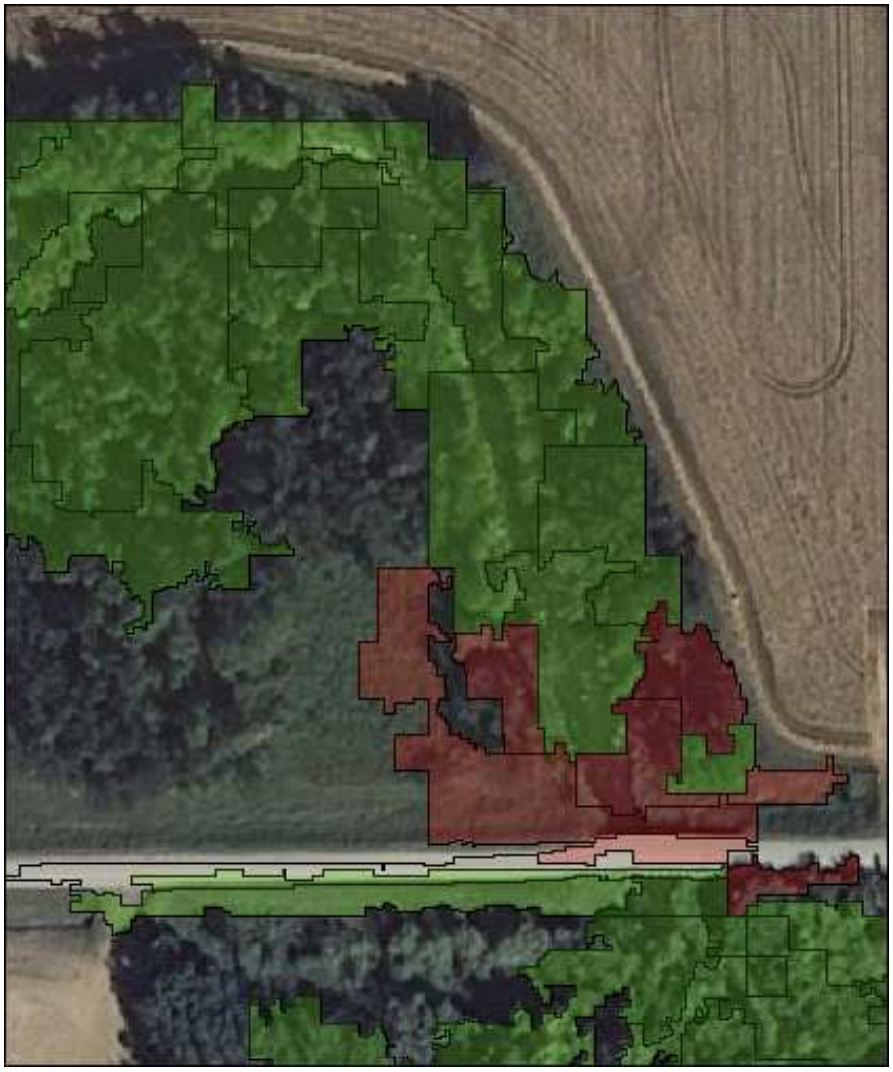

Figure 4.8. A forested riparian area intersected by a road. Riparian health model classification: green = healthy, red = unhealthy. Image captured using a 175x210 m window at a scale of 1:2000.

.

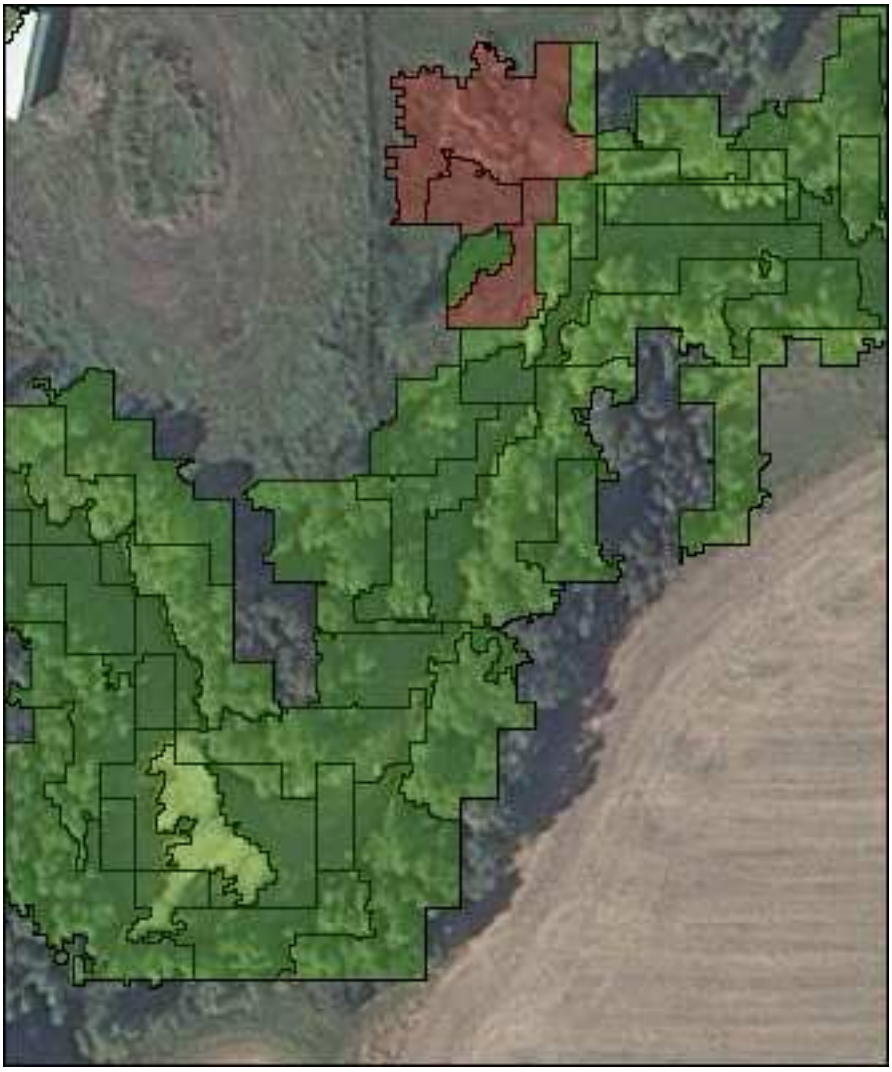

Figure 4.9. A forested riparian area adjacent to a yard. Riparian health model classification: green = healthy, red = unhealthy. Image captured using a 175x210 m window at a scale of 1:2000.

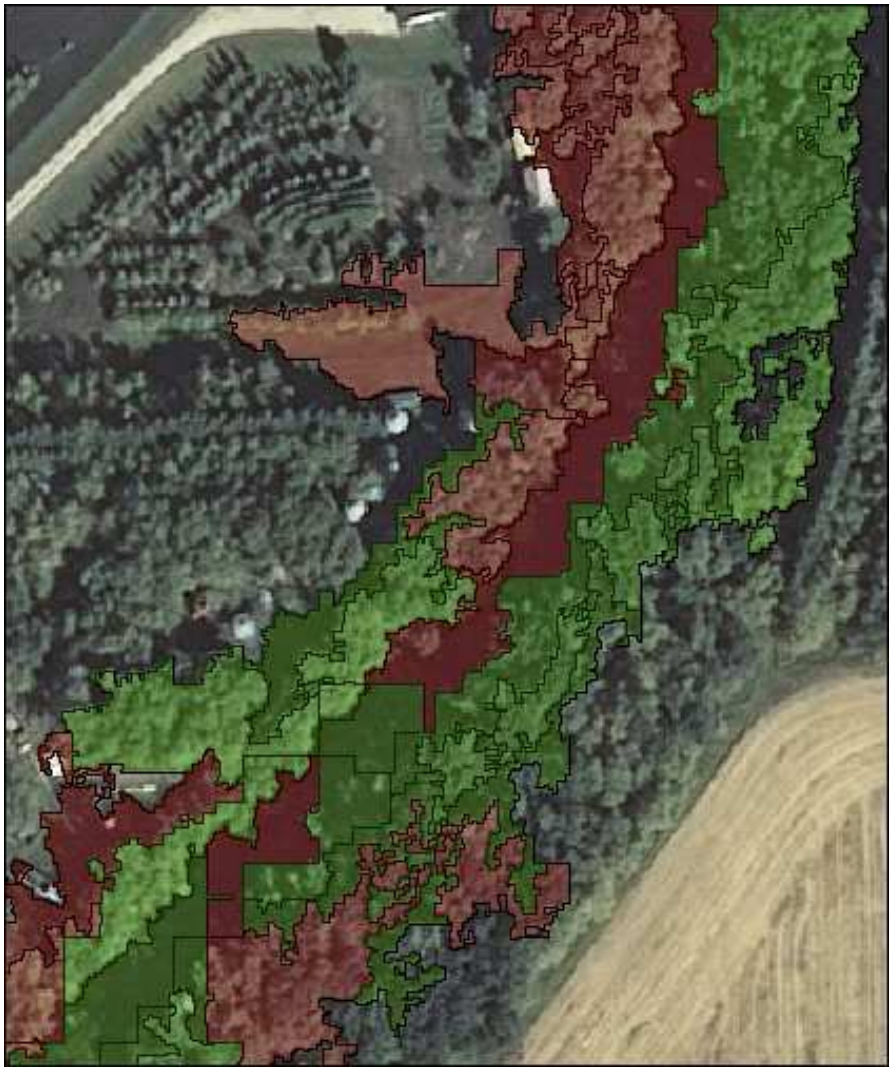

Figure 4.10. A forested riparian area adjacent to urban development. Riparian health model classification: green = healthy, red = unhealthy. Image captured using a 175x210 m window at a scale of 1:2000.

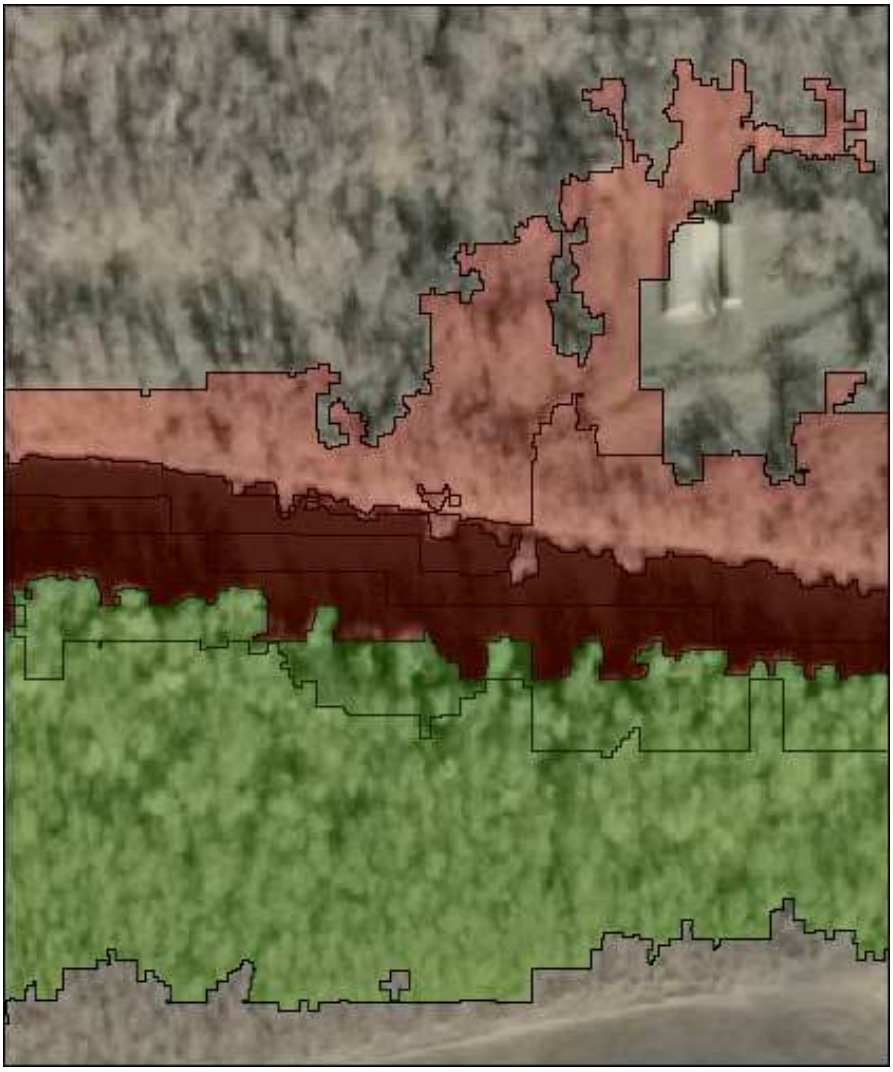

Figure 4.11. Forested riparian areas opposite one another. Riparian health model classification: green = healthy, red = unhealthy. Image captured using a 175x210 m window at a scale of 1:2000.

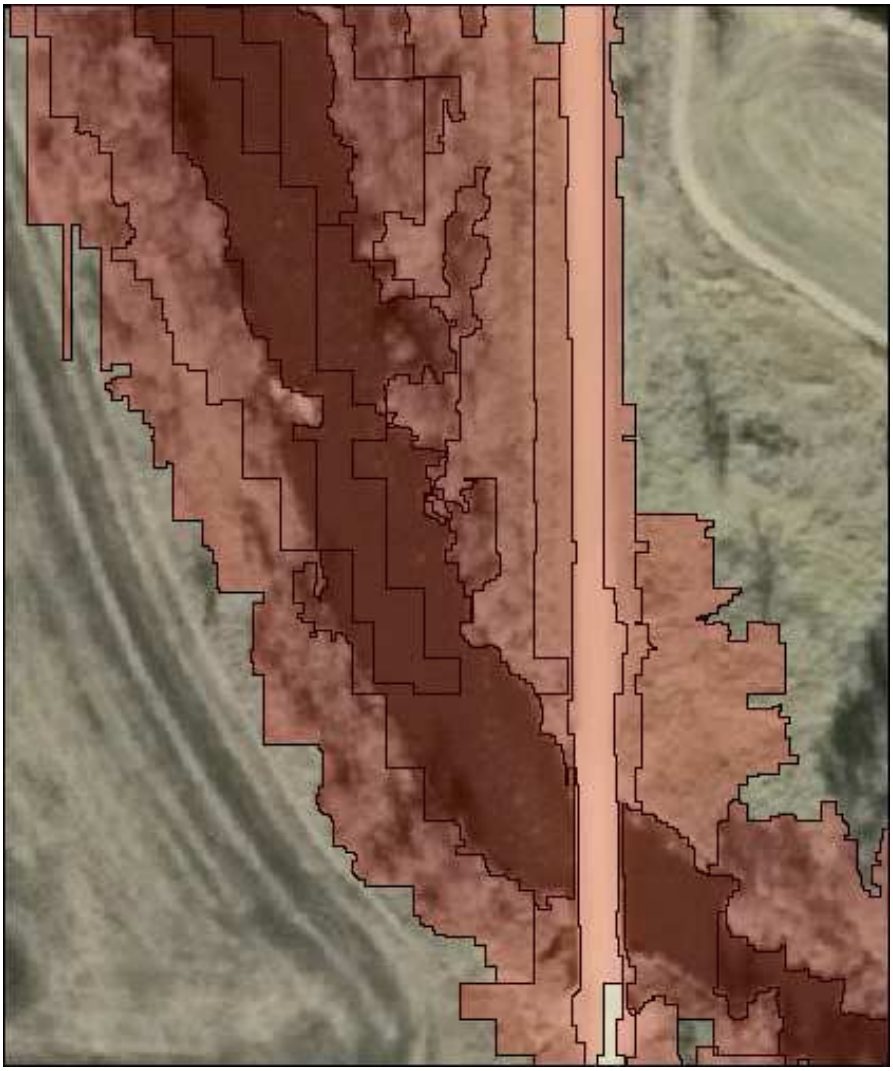

Figure 4.12. Narrow riparian area surrounded by cultivated fields and a road. Riparian health model classification: green = healthy, red = unhealthy. Image captured using a 175x210 m window at a scale of 1:2000.

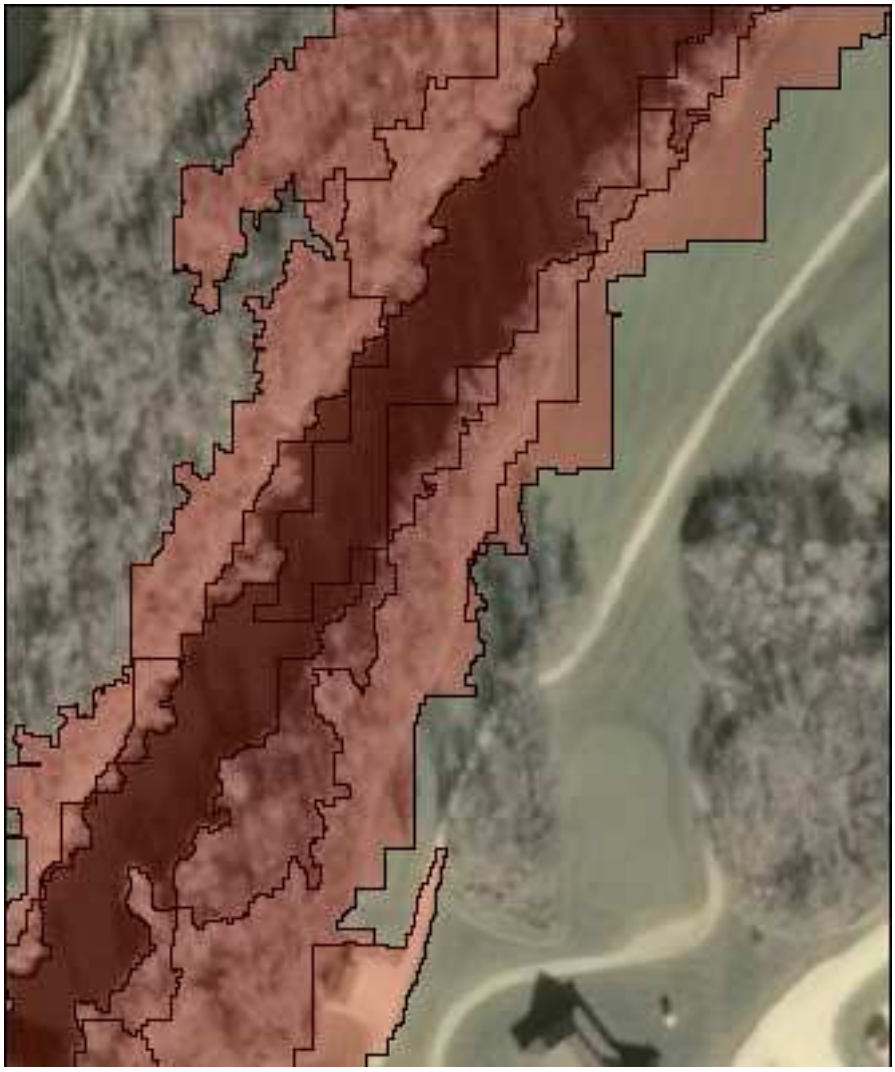

Figure 4.13. Riparian area with a narrow buffer of trees, surrounded by a golf course. Riparian health model classification: green = healthy, red = unhealthy. Image captured using a 175x210 m window at a scale of 1:2000.

CHAPTER 5: CONCLUSIONS AND MANAGEMENT IMPLICATIONS

5.1 Summary and Conclusions

1. Field observations revealed the vegetation structure, particularly the degree of establishment and density of shrubs in the understorey, was more important than community composition and species diversity in determining the health of riparian areas on the La Salle River.
2. A method was developed to model the extent of riparian habitat. Recorded maximum mean flood levels were mapped using a DEM to delineate the flood zone. To account for riparian vegetation, the flood zone was then extended to the outer edge of segmented vegetation objects overlapping the flooded area boundary. This approach provided an accurate estimate of the extent of riparian habitat, based on field observations.
3. Using hierarchical clustering, vegetation spectral and structural information extracted from a combined dataset comprising high-resolution imagery, vegetation productivity and vegetation structure indices using object-based methods were linked to overall riparian health scores derived from an indicator-based field assessment. The correlation was statistically significant.
4. The inclusion of vegetation structure indices derived from LiDAR improved both the correlation between image objects and riparian habitat health, and the separation between health categories based on image object clustering.
5. Object-based methods can be used in combination with linear discriminant modelling to accurately predict riparian habitat condition as observed in the field. Three models were

tested, using structural and spectral vegetation variables in isolation, topographic variables in isolation, and vegetation and topographic variables in combination. The model using only vegetation variables was found to produce the best result, with an accuracy of 88% (κ = 74±4%).

6. The model based on topographic variables produced very poor results. This could be a function of: the sampling density of the LiDAR data used to construct the DEM; the lack of inclusion of topographic metrics in the object-based image segmentation; or, riparian physical structural attributes might be better represented in remotely sensed datasets by vegetation indicators. These results demonstrate that riparian health can be accurately modelled using object-based methods to assess spectral and structural vegetation data.
7. Using the modelling method developed in this project, riparian health can be assessed remotely, eliminating the need for resource-intensive field surveys and thereby preserving resources for riparian management and conservation programming.

5.2 Management Implications and Further Research

5.1.1 Riparian Health Model

Figure 5.1 shows the workflow followed to produce the La Salle riparian health model. The model achieved an overall accuracy of 88%, a result comparable with other successful riparian habitat modelling endeavours (Arroyo et al., 2010; Johansen et al., 2008b; Johansen et al., 2007b; Johansen and Phinn, 2006a). As discussed in Section 4.4.2, previous studies have focused on predicting individual riparian health indicators, rather than a cumulative measure of riparian health. This approach has the advantage of simplicity, in that it provides a single classification, which does not require further assessment. However, as individual indicators cannot be

separated, it is not appropriate for detailed analyses and management prescriptions at the site level. Rather, its utility is as a watershed-level screening tool, used to identify compromised riparian areas for more in-depth field-based investigation.

The method used should be transferable to other riparian reaches in southern Manitoba, but this assumption has not yet been tested. The object-based image segmentation was carried out without training data, but it will be necessary to adjust parameters to account for image availability and quality, and physiographic variation in new areas. While field-derived training and testing data were not used for the OBIA, they were needed for model development. The discriminant functions used should be tested for applicability in another study area to assess the potential for full automation of the riparian health model in southern Manitoba. However, it is likely that the collection of training data will be necessary to modify model parameters for application in regions with significantly different physiographies.

Given the high cost associated with field surveys, this methodology has potential as a cost saving measure, allowing resources to be conserved for the application of management prescriptions. However, this assumption is dependent upon access to OBIA software, which is expensive both to purchase and to license. LiDAR is also currently expensive, though it is becoming more readily available. This study has demonstrated that LiDAR is necessary to achieve acceptable accuracy levels.

5.1.2 Ecological Challenges

The Manitoba riparian health assessment focuses on physical/topographic, vegetation and anthropogenic attributes that influence bank stability, flood regulation, and nutrient/pollutant control (AAFC, 2004). While some elements of the ecological health of the riparian zone are

addressed through the inclusion of rankings for invasive and opportunistic species, other elements, such as the presence and abundance of native species (whether rare, vulnerable or generalist), are not included. Nor is any measure of biodiversity or species richness recorded. (Moffatt and McLachlan, 2004) found that including both opportunistic (colonizing) and vulnerable (usually native) species as indicators was effective for assessing the condition of riparian areas. In particular, they found the species composition of the herbaceous component to be a valuable indicator. However, the Manitoba riparian habitat assessment does not include a ranking for the presence of specific ecologically desirable species. In addition, invasive species are not adequately represented. An example is reed canary grass (*Phalaris arundiacea*), a rhizomatous perennial grass in the taxonomic family *Poaceae*. It is native to parts of both North America and Eurasia (Lavergne and Molofsky, 2007). The Eurasian type was introduced to North America for use as a forage crop, shoreline stabilizer, and for extraction of soil and water contaminants, and subsequently hybridized with the native type, producing an aggressive invasive variant. Reed canary grass is listed as invasive by the Invasive Species Council of Manitoba, and is described as an aggressive invasive species by Fortier (2014) in report released by AAFC. In addition, there is a large body of literature devoted to managing and controlling the spread of reed canary grass in wetlands and riparian areas in North America (Gebauer, 2013; Glaser and Glick, 2012; Officer, 2012; Miller et al., 2008; Seebacher, 2008). Despite this, reed canary grass is not listed as either an invasive or a disturbance species in either the Manitoba riparian health assessment, or the Alberta assessment a more detailed inventory on which the Manitoba assessment is based.

A second ecological issue with the field assessment is the lack of emphasis on indicators that assess the state of the understorey. Understorey structural attributes of the riparian zone serve as

indicators of many facets of riparian health (Johansen and Phinn, 2006a; Jansen, 2005). However, this essential component of the riparian zone is assessed only indirectly in the field survey, through three indicators: preferred tree and shrub establishment and regeneration; browsing usage of preferred woody vegetation; and presence of deep binding root mass.

5.1.3 Field Assessment Bias

To assess the relative importance of each of the eleven riparian health indicators in determining the health score assigned to each polygon, a logistic regression was conducted. Logistic regression and its applications are described in detail in Legendre and Legendre (2012). Briefly, logistic regression is a form of generalized linear model, often used to predict the response of a binary or categorical dependent variable to one or several independent variables. It is a conditional probability classifier, predicting outcomes of a combination of independent variables or predictors based on probability. In addition to conditional probability modelling, logistic regression can be applied to assess the relative importance of predictors in determining the model outcome (Szumilas, 2010; Thompson, 2009). The results of the logistic regression indicated that percent vegetation cover had the greatest influence in predicting the overall riparian health score, followed by anthropogenic structural alteration of the river bank, and anthropogenic physical alteration to the rest of the polygon. The indicators having the least influence on the overall score included browsing and anthropogenic removal of preferred trees and shrubs, preferred tree and shrub establishment and regeneration, and presence of root mass for stream bank stabilization. These results indicate that the binary nature of the field assessment output is likely more a function of a bias inherent in the assessment protocol than it is evidence of a simple healthy-unhealthy split in riparian habitat condition. The assessment metrics having the greatest relative importance in determining the total health score – overall vegetation cover and anthropogenic

habitat alteration – are primarily binary in nature and are easier to visually estimate with consistency than less influential metrics, such as the percentage of the bank protected by deep, binding root mass. The dominance of binary metrics in the assessment results in clean division of riparian habitat into two virtually discrete health categories. However, in reality riparian areas are natural ecosystems, which exist along a continuum between fully functional, healthy habitat, and heavily modified or disturbed, non-functional habitat.

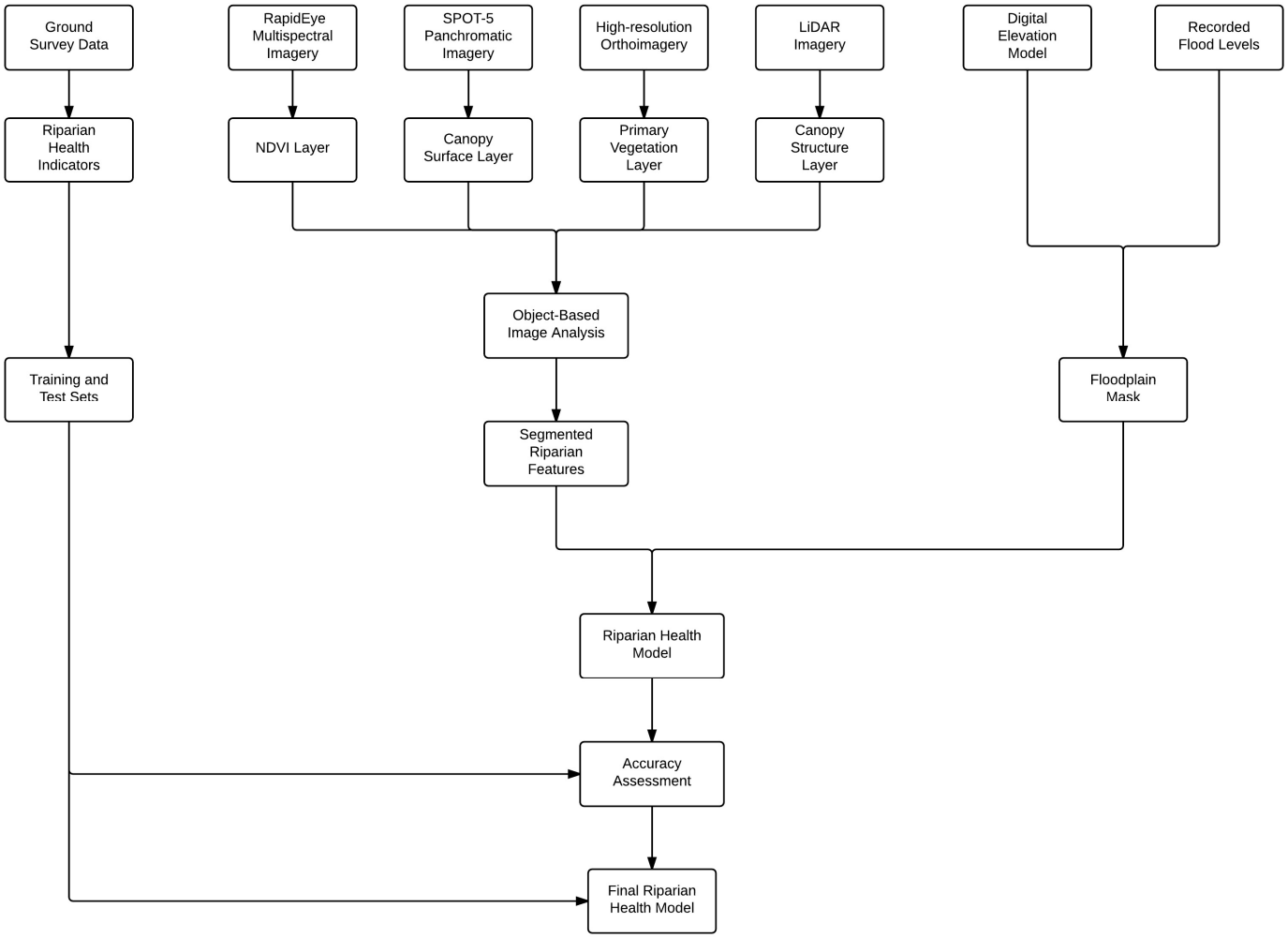

Figure 5.1. Workflow chart showing steps followed in developing the riparian health model.

LITERATURE CITED

AAFC, 2004. *Managing the Water's Edge - Riparian Health Assessment for Streams and Small Rivers*. Version 1. Winnipeg, Manitoba, Canada: Agriculture and Agri-Food Canada, 92 pp.

Abood, S.A., Maclean, A.L. and Mason, L.A., 2012. Modeling riparian zones utilizing DEMS and flood height data. *Photgrammetric Engineering and Remote Sensing*, 78(3):259-69.

Aguirre-Gutiérrez, , Seijmonsbergen, A.C. and Duivenvoorden, J.F., 2012. Optimizing land cover classification accuracy for change detection, a combined. *Applied Geography*, 34:29-37.

Akasheh, O.Z., Neale, C.M.U. and Jayanthi, H., 2008. Detailed mapping of riparian vegetation in the middle Rio Grande River using high resolution multi-spectral airborne remote sensing. *Journal of Arid Environments*, 72:1734– 1744.

Alencar-Silva, T. and Maillard, P., 2010. Assessment of biophysical structure of riparian zones based on segmentation method, spatial knowledge and texture analysis. In Wagner, W. and Székely, B., eds. *ISPRS TC VII Symposium – 100 Years ISPRS*. 5–7 July 2010. Vienna, Austria: 26-31, 2010.

Anderson, E.S., Thompson, J.A., Crouse, D.A. and Austin, R.E., 2006. Horizontal resolution and data density effects on remotely sensed LIDAR-based DEM. *Geoderma*, 132:406–15.

Arroyo, L.A., Johansen, K., Armston, J. and Phinn, S., 2010. Integration of LiDAR and QuickBird imagery for mapping riparian biophysical parameters and land cover types in Australian tropical savannas. *Forest Ecology and Management*, 259:598–606.

Artyszuk, J., 2002. Bezier approach to smoothing zig-zag data for use in ship maneuvering model identification. *Annual of Navigation*, 4:5-12.

Auble, G.T., Friedman, J.M. and Michael , S.L., 1994. Relating riparian vegetation to present and future streamflows. *Ecological Applications*, 4(3):544-54.

Auble, T., Scott, M.L. and Friedman, M., 2005. Use of individualistic streamflow-vegetation relations along the Fremont River, Utah, USA to assess impacts of flow alteration on wetland and riparian areas. *Wetlands*, 25(1):143–54.

Barrett, E.C. and Curtis, L.F., 1999. *Introduction to Environmental Remote Sensing*. 4th ed. New York, NY, USA: Routledge, 457 pp.

Bendix, J., 1994. Scale, direction, and pattern in riparian vegetation-environment relationships. *Annals of the Association of American Geographers* , 84(4): 652-665.

Biswas, S.R. and Mallik, A.U., 2011. Species diversity and functional diversity relationship varies with disturbance intensity. *Ecosphere*, 2(4):1-10.

Blaga, L., 2012. Aspects regarding the significance of the curvature types and values in the studies of geomorphometry assisted by GIS. *Studies in Mathematical Sciences*, 6(1):327-37.

Blaschke, T., 2010. Object based image analysis for remote sensing. *ISPRS Journal of Photogrammetry and Remote Sensing*, 65:2-16.

Blaschke, et al., 2002. Object-Oriented Image Processing in an Integrated GIS/Remote Sensing Environment and Perspectives for Environmental Applications. In *Environmental Information for Planning, Politics and the Public*. Metropolis Verlag. pp.555-70.

Bock, M. et al., 2005. Object-oriented methods for habitat mapping at multiple scales – case studies from northern Germany and Wye Downs, UK. *Journal for Nature Conservation*, 13:75-89.

Braga-Neto, U. et al., 2004. Is cross-validation better than resubstitution for ranking genes? *Bioinformatics*, 20(2):253-58.

Brooks, A. and Knight, J., 2008. *Development of a Riparian Condition Assessment Protocol for Northern Gulf Rivers using Remote Sensing and Ground Survey: Final Report*. Project No – GRU38. Canberra, ACT, Australia: Land and Water Australia, Australian Government, 16 pp.

Cadotte, M.W., Carscadden, K. and Microtchnick, N., 2011. Beyond species: functional diversity and the maintenance of ecological processes and services. *Journal of Applied Ecology*, 48:1079–87.

Campbell, J.B., 2002. *Introduction to Remote Sensing*. New York, NY, USA: The Guilford Press, 656 pp.

Camporeale, C., Perucca, E. and Gurnell, A.M., 2013. Modeling the interactions between river morphodynamics and rioparian vegetation. *Reviews of Geophysics*, 51(3):379-414.

Challice, A., 2007. *Common Reed (Phragmites australis): a Summary of Ecology and Management Techniques for the Ontario Federation of Anglers and Hunters Invasive Species Program*. Peterborough, ON, CA: Trent University Trent Centre for Community Based Education, 17 pp.

Chen, G., Hay, G.J. and St-Onge, B., 2012. A GEOBIA framework to estimate forest parameters from lidar transects, Quickbird imagery and machine learning: a case study in Quebec, Canada. *International Journal of Applied Earth Observation and Geoinformation*, 15:28-37.

Chu, H.-J. et al., 2014. Effect of point density and interpolation of LiDAR-derived high-resolution DEMs on landscape scarp identification. *GIScience and Remote Sensing*, 51(6):731-47.

Clerici, N., Weissteiner, C.J., Paracchini, M.L. and Strobl, P., 2011. *Riparian zones: where green and blue networks meet*. Scientific and Technical Research Series. Institute for Environment and Sustainability, Luxembourg: Publications Office of the European Union , 60 pp.

Cohen, J., 1960. A coefficient of agreement for nominal scales. *Educational and Psychological Measurement*, 20:37-46.

Congalton, R.G., Birch, K., Jones, R. and Schriever, J., 2002. Evaluating remotely sensed techniques for mapping riparian vegetation. *Computers and Electronics in Agriculture*, 37.

Congalton, R.G. and Green, K., 2009. *Assessing the Accuracy of Remotely Sensed Data - Principles and Practices*. 2nd ed. Boca Raton, FL, USA: CRC Press, Taylor and Francis Group, 183 pp.

Corenbilt, D., Steiger, J., Gurnell, A.M. and Naiman, R.J., 2009. Plants intertwine fluvial landform dynamics with ecological succession and natural selection: a niche construction perspective for riparian systems. *Global Ecology and Biogeography*, 18:507-20.

Décamps, H. et al., 2004. Riparian zones: where biogeochemistry meets biodiviersity in management practice. *Polish Journal of Ecology*, 52(1):3-18.

Desclée, B., Bogaert, P. and Defourny, P., 2006. Forest change detection by statistical object-based method. *Remote Sensing of Environment*, 102:1-11.

Dhore, A. and Veena, C.S., , 2014. A new pan-sharpening method using joint sparse FI image fusion algorithm. *International Journal of Engineering Research and General Science*, 2(4):447-55.

Dilts, T.E., Yang, J. and Weisberg, P.J., 2010. Mapping Riparian Vegetation with Lidar Data: Predicting plant community distribution using height above river and !ood height. *ArcUser*, Winter. pp.18-21.

Dixon, I., Douglas, M., Dowe, J. and Burrows, D, 2006. *Tropical Rapid Appraisal of Riparian Condition Version 1 (for use in tropical savannas)*. River Management Technical Guideline No. 7. Canberra, Australia: Land and Water Australia, 35 pp.

Dixon, I. et al., 2005. A rapid method for assessing the condition of riparian zones in the wet/dry tropics of northern Australia. In Rutherford, I.D., Wiszniewski, I., Askey-Doran, M. and Glazik, R., eds. *4th Australian Stream Managment Conference: Linking Rivers to Landscapes*. 19-22 October 2004, Launceton, Tasmania, 2005. Department of Primary Industries, Water and Environment.

Dowling, R. and Accad, A., 2003. Vegetation classification of the riparian zone along the Brisbane River, Queensland, Australia, using light detection and ranging (lidar) data and forward looking digital video. *Canadian Journal of Remote Sensing*, 29(5):556-63.

Drăguţ, , Tiede, D. and Levick, S.R., 2010. ESP: a tool to estimate scale parameter for multiresolution image segmentation of remotely sensed data. *International Journal of Geographical Information Science*, 24(6):859-71.

eCognition Developer, 2012. *eCognition Developer 8.7.2 Reference Book*. Munic, Germany: Trimble Germany GmbH, 418 pp.

Environment Canada, 2012a. *Climate Normals and Averages 1971-2000*. [Online] Available at: http://climate.weatheroffice.gc.ca/climate_normals/stnselect_e.html?pageid=1⟨=e&province=MAN&provBut=Search&page=1 [Accessed 26 October 2012].

Environment Canada, 2012b. *Hydrometric Data*. [Online] Available at: http://www.wsc.ec.gc.ca/applications/H2O/HydromatD-eng.cfm [Accessed 19 November 2012].

Eskelson, B.N.I., Madsen, L., Hagar, J.C. and Temesgen, H., 2010. Estimating riparian understorey vegetation cover with beta regression and copula models. *Forest Science*, 57(3):212-21.

ESRI, 2011. LiDAR analysis in ArcGIS 10 for forestry applications. *ESRI White Paper*, January. pp.1-32.

Farin, G., 2002. *Curves and Surfaces for CAGD: A Practical Guide*. Sandiego, CA, USA: Academic Press, 436 pp.

Ferreira, L. and Hitchcock, D.B., 2009. A compariason of hierarchical methods for clustering functional data. *Communications in Statistics - Simulation and Computation*, 38(9):1925-49.

Fischer, R.A., Martin, C.O., Ratti, J.T. and Guidice, J., 2001. *Riparian Terminology: Confusion and Clarification*. U.S. Army Corps of Engineers, Vicksburg, Mississippi, USA: Environmental Laboratory, 7 pp.

Fisher, R.A., 1936. The use of multiple measurements in taxonomic problems. *Annals of Eugenics*, 7:179-88.

Fitch, L. and Ambrose, N., 2003. *Riparians Areas: A User's Guide to Health*. Lethbridge, AB, Canada: Cows and Fish, 46 pp.

Fortier, J., 2014. *Agricultural Riparin Health: Theory, Concepts and Potential Indicators*. Monograph. Ottawa, Ontario, CA: Agriculture and Agri-Food Canada, 55 pp.

Forzieri, et al., 2011. Satellite multispectral data for improved floodplain roughness modelling. *Journal of Hydrology*, 407:41-57.

Forzieri, G. et al., 2010. Riparian vegetation mapping for hydraulic roughness estimation using very high resolution remote sensing data fusion. *Journal of Hydraulic Engineering*, 136(11):855-67.

Gebauer, A.D., 2013. *Ecohydrology Effects of an Invasive Grass (Phalaris arundinacea) on semi-arid Riparian Zones*. MSc Thesis. Cheney, Washington, USA: Eastern Washington University, 69 pp.

Gergel, E. et al., 2007. What is the value of a good map? an example using high spatial resolution imagery to aid riparian restoration. *Ecosystems*, 10:688-702.

Glaser, A. and Glick, P., 2012. *Growing Risk: Addressing the Invasive Potential of Bioenergy Feedstocks*. Washington, DC, USA: National Wildlife Federation, 51 pp.

Goetz, S.J., 2006. Remote sensing of riparian buffers: past progress and future prospects. *Journal of the American Water Resources Association*, 42(1):133–43.

Graveline, P.G. and Larter, J., 2006. *La Salle Redboine Conservation District: La Salle River Watershed Assessment Survey – with Emphasis on La Salle River, Elm River, Elm Creek Channel, and The King Drain – 2005*. Winnipeg, Manitoba, CA: North/South Consultants Inc., 107 pp.

Gregory, S.V., Swanson, F.J., McKee, W.A. and Cummins, K.W., 1991. An ecosystem perspective of riparian zones. *BioScience*, 41(8):540-51.

Gruen, A., 2012. Satellite versus aerial images -- not always a matter of choice! *GEOInformatics*, June. p.44.

Guo, Q., Li, W., Yu, and Alvarez, O., 2010. Effects of topographic variability and lidar sampling density on several DEM interpolation methods. *Photogrammetric Engineering and Remote Sensing*, 76(6):707-12.

Harris, R.R., 1988. Associations between stream valley geomorphology and riparian vegetation as a basis for landscape analysis in the eastern Sierra Nevada, California, USA. *Environmental Management* , 12(2):219-28.

Hay, G.H., Blaschke, T., Marceau, D.J. and Bouchard, A., 2003. A comparison of three image-object methods for the multiscale analysis of landscape structure. *ISPRS Journal of Photogrammetry and Remote Sensing*, 57:327– 345.

Hicken, E.J., 2003. Meandering Channels. In V. Middleton, ed. *Encyclopedia of Sediments and Sedimentary Rocks*. Dordrecht, Netherlands: Kulwer Academic Publishers. pp.430-34.

Holmes, K.L. and Goebel, P.C., 2011. A functional approach to riparian area delineation using geospatial methods. *Journal of Forestry*, 109(4):233-41.

Hudak, A.T., Evans, J.S. and Smith, A.M.S., 2009. LiDAR utility for natural resource managers. *Remote Sensing*, 1(4), p.934.

Hughes, F.M.R., 1997. Floodplain biogeomorphology. *Progress in Physical Geography*, 21(4):501-29.

Hupp, C.R. and Osterkamp, W.R., 1996. Riparian vegetation and fluvial geomorphic processes. *Geomorphology*, 14:277-95.

Ilhardt, B.L., Verry, E.S. and Palik, B.J., 2000. Defining Riparian Areas. In E.S. Verry, J.W. Hornbeck and C.A. Dolloff, eds. *Riparian Management in Forests of the Continental Eastern United States*. 1st ed. Boca Raton, Florida, USA: CRC Press LLC. pp.23-42.

Im, J., Jensen, J.R. and Tullis, J.A., 2008. Object-based change detection using correlation image analysis and image segmentation. *International Journal of Remote Sensing*, 29(2):399–423.

Jansen, A., 2005. Rapid appraisal of riparian condition: scaling up from on-ground measurement to remote sensing. In Rutherford, I.D., Wiszniewski, I., Askey-Doran, M.J. and Glazik, R., eds. *Linking rivers to landscapes*. 19-22 October 2004, Hobart, Tasmania, 2005. Department of Primary Industries, Water and Environment, pp 313-319.

Johansen, K. et al., 2010a. Mapping riparian condition indicators in a sub-tropical savanna environment. *Ecological Indicators*, p.10.

Johansen, K., Arroyo, L.A., Phinn, S. and Witte, C., 2008a. Object-oriented change detection of riparian environments from high spatial resolution multi-spectral images. In Hay, G.J., Blaschke, T. and Marceau, , eds. *GEOBIA 2008 - Pixels, Objects, Intelligence:*

GEOgraphic Object Based Image Analysis for the 21st Century. 5-8 August 2008. Calgary, Alberta, Canada, 2008a.

Johansen, K., Arroyo, L.A., Phinn, S. and Witte, C., 2010b. Comparison of geo-object based and pixel-based change detection of riparian environments using high spatial resolution multi-spectral imagery. *Photogrammetric Engineering and Remote Sensing*, 76(2):123-36.

Johansen, K., Coops, N.C., Gergel, S.E. and Stange, Y., 2007a. Application of high spatial resolution satellite imagery for riparian and forest ecosystem classification. *Remote Sensing of Environment*, 110:29-44.

Johansen, K. and Phinn, S., 2004. Mapping indicators of riparian vegetation health using IKONOS and Landsat-7 ETM+ image data in Australian tropical savannas. In *IEEE International Geoscience and Remote Sensing Symposium, Volume 3: 1559-1562*. 20-24 September 2004. Anchorage, Alaska, USA, 2004.

Johansen, K. and Phinn, S., 2006a. Linking riparian vegetation spatial structure in Australian tropical savannas to ecosystem health indicators: semi-variogram analysis of high spatial resolution satellite imagery. *Canadian Journal of Remote Sensing*, 32(3):228–43.

Johansen, K. and Phinn, S., 2006b. Mapping structural parameters and species composition of riparian vegetation using IKONOS and Landsat ETM+ data in Australian tropical savannahs. *Photogrammetric Engineering and Remote Sensing*, 72(1):71-80.

Johansen, K. et al., 2007b. Comparison of image and rapid field assessments of riparian zone. *Forest Ecology and Management*, 240:42-60.

Johansen, K., Phinn, S., Lowry, J. and Douglas, M., 2008b. Quantifying indicators of riparian condition in Australian tropical savannas: integrating high spatial resolution imagery and field survey data. *International Journal of Remote Sensing*, 29(23):7003-28.

Johansen, K., Phinn, S. and Witte, C., 2010c. Mapping of riparian zone attributes using discrete return LiDAR, QuickBird and SPOT-5 imagery: Assessing accuracy and costs. *Remote Sensing of Environment*, 114(11):2679–91.

Johansen, K. et al., 2011. Automatic geographic object based mapping of streambed and riparian zone extent from LiDAR data in a temperate rural urban environment, Australia. *Remote Sensing*, 3:1139-56.

Jolliffe, I.T., 2002. *Principal Component Analysis*. 2nd ed. New York, NY, USA: Spinger-Verlag, 488 pp.

König, A., 2000. Dimensionality reduction techniques for multivariate data classification, interactive vsualization, and analysis - systematic feature selection vs. extraction. In Howlett, R.J. and Jain, L.C., eds. *Proceedings of the Fourth International Conference on Knowledge-Based Intelligent Engineering Systems and Allied Technologies*. Brighton, UK, 30 August - 1 September, 2000. Institute of Electrical and Electronics Engineers, Inc.

De Kok, R., Scheinder, T., Baatz, M., and Ammer, U. 1999. Object based image analysis of high resolution data in the alpine forest area. *Proceedings of the Joint Workshop with ISPRS WG I/1, I/3 and IV/4: Sensors and Mapping in Space*. Bejing, China, 4-6 October 1, 1999. International Society for Photogrammetry and Remote Sensing, pp. 27-30.

Kollár, S., Vekerdy, Z. and Márkus, B., 2013. Aerial image classification for the mapping of riparian vegetation habitats. *Acta Silvatica and Lingaria Hungarica*, 9:119-33.

La Salle Redboine Conservation District, 2007. *La Salle River State of the Watershed Report*. Holland, Manitoba, CA: La Salle Redboine Conservation District, 295 pp.

La Salle Redboine Conservation District, 2012. *District Programs*. [Online] Available at: HYPERLINK "http://www.lasalleredboine.com/programs.html" http://www.lasalleredboine.com/programs.html [Accessed 18 November 2012].

La Salle River Watershed Planning Authority, 2010. *La Salle River Integrated Watershed Management Plan*. Holland, Manitoba, CA: La Salle Redboine Conservation District, 37 pp.

Lavergne, S. and Molofsky, J., 2007. Increased genetic variation and evolutionary potential drive the success of an invasive grass. *Proceedings of the National Academy of Sciences of the United States of America*, 104(10):3883-88.

Leclaire, C., 2011. *Dauphin Lake Watershed Integrated Watershed Management Plan - Water Quality Report*. Water Quality Management Section. Winnipeg, MB, Canada: Manitoba Water Stewardship, 27 pp.

Lefsky, M.A., Cohen, W.B., Parker, G.G. and Harding, D.J., 2002. LiDAR remote sensing for ecosystem studies. *BioScience*, 52(1):19-30.

Legendre, P. and Legendre, L., 2012. *Numerical Ecology*. 3rd ed. Amsterdam, The Netherlands, Amsterdam, : Elsevier B. V., 990 pp.

Lenhart, C.F. et al., 2013. The role of hydrologic alteration and riparian vegetation dynamics in channel evolution along the lower Minnesota River. *Transactions of the ASABE*, 56(2):549-61.

Levick, L.R. et al., 2008. *The Ecological and Hydrological Significance of Ephemeral and Intermittent Streams in the Arid and Semi-arid American Southwest*. Washington, DC , USA: U.S. Environmental Protection Agency and USDA/ARS Southwest Watershed Research, 116 pp.

Liu, X., 2008. Airborne LiDAR for DEM generation: some critical issues. *Progress in Physical Geography*, 32(1):31-49.

Lonard, R.I. et al., 2000. Evaluation of color-infrared photography for distinguishing annual changes in riparian forest vegetation of the lower Rio Grande in Texas. *Forest Ecology and Management*, 128:75-81.

Makkeasorn, A., Chang, N.-B. and Li, J., 2009. Seasonal change detection of riparian zones with remote sensing images and genetic programming in a semi-arid watershed. *Journal of Environmental Management*, 90:1069-80.

Manitoba Water Stewardship, 2011. *Dauphin Lake Watershed Integrated Watershed Management Plan - Water Quality Report*. Water Quality Report. Winnipeg, Manitoba, CA: Manitoba Water Stewardship, 27 pp Manitoba Water Stewardship.

Mason, L.A. and Maclean, A.L., 2007. GIS modeling of riparian zones utilizing digital elevation models and flood height data: an intelligent approach. In *Proceedings of the ASPRS 2007 Annual Conference*. Tampa, Florida, USA, 7-11 May , 2007.

May, C.W., 2003. *Stream-Riparian Ecosystems in the Puget Sound Lowland Eco-Region*. PSL Stream-Riparian BAS Review. Poulsbo, WA, USA: Watershed Ecology LLC, 76 pp.

Mayer, P.M., Reynolds, S.K. and Canfield, T.J., 2005. *Riparian Buffer Width, Vegetative Cover, and Nitrogen Removal Effectiveness: A Review of the Current Science and Regulations*. Cincinnati, Ohio, USA: United tates Environmental Protection Agency, 28 pp National Risk Management Research Laboratory, Office of Research and Development, United States Environmental Protection Agency.

McGaughy, R.J. and Carson, W.W., 2003. Fusing LiDAR data, photographs, and other data using 2D and 3D visualization techniques. In *Proceedings of Terrain Data: Applications and Visualization - Making the Connection*. 28-30 October 2003. Charleston, SC, USA, 2003. American Society for Photogrammetry and Remote Sensing.

Merritt, D.M. et al., 2010. Theory, methods and tools for determining environmental flows for riparian vegetation: riparian vegetation-flow response guilds. *Freshwater Biology*, 55:206-25.

Micheli, E.R., Kirchner, J.W. and Larsen, E.W., 2004. Quantifying the effect of riparian forest versus agricultural vegetation on river meander migration rates, central Sacramento River, California, USA. *River Research and Applications*, 20:537-48.

Millenium Ecosystem Assessment, 2005. *Ecosystems and Human Well-being: Synthesis*. Washington, DC, USA: Island Press, 137 pp.

Miller, T.W., Martin, L.P. and MacConnell, B., 2008. Managing reed canarygrass (Phalaris arundinacea) to aid in revegetation of riparian buffers. *Weed Technology*, 22:507–13.

Mitášová, H. and Mitás, L., 1993. Interpolation by regularized spline with tension: I. theory and implementation. *Mathematical Geology*, 25(6):641-55.

Mitás, L. and Mitášová, H., 1988. General variational approah to the interpolation problem. *Computers and Mathematics with Applications*, 16(12):983-92.

Moffatt, S.F. and McLachlan, S.M., 2004. Understorey indicators of disturbance for riparian forests along an urban–rural gradient in Manitoba. *Ecological Indicators*, 4:1-16.

Muller, E., 1997. Mapping riparian vegetation along rivers: old concepts and new methods. *Aquatic Botany*, 58:411-37.

Munro, N.T., Fischer, J., Wood, J. and Lindenmayer, D.T., 2009. Revegetation in agricultural areas: the development of structural complexity and floristic diversity. *Ecological Applications*, 19(5):1197–210.

Nagler, P.L., Glenn, E.P. and Huete, A.R., 2001. Assessment of spectral vegetation indices for riparian vegetation in the Colorado River delta, Mexico. *Journal of Arid Environments*, 49:91-110.

Naiman, R.J. and Décamps, H., 1997. The ecology of interfaces: riparian zones. *Annual Review of Ecology and Systematics*, 28:621-58.

Nanson, G.C. and Gibling, M.R., 2003. Rivers and Alluvial Fans. In V. Middleton, ed. *Encyclopedia of Sediments and Sedimentary Rocks*. Dordrecht, Netherlands: Kluwer Academic Publishers. pp.563-83.

Narumalani, S., Zhou, Y. and Jensen, J.R., 1997. Application of remote sensing and geographic information systems to the delineation and analysis of riparian buffer zones. *Aquatic Botany*, 58:393-409.

Nilsson, C. and Svedmark, M., 2002. Basic Principles and ecological consequences of changing water regimes: riparian plant communities. *Environmental Management*, 30(4):468–80.

Norris, R.H. and Thoms, C., 1999. What is river health? *Freshwater Biology*, 41:197-209.

Officer, R., 2012. *Establishing a Process for Wetland Vegetation Rehabilitation and Management Program Focused on Reed Canarygrass: a Parkland Mews Case Study*. MEnv Thesis. Winnipeg, MB, CA: University of Manitoba, 153 pp.

Osterkamp, W.R. and Hupp, C.R., 2010. Fluvial processes and vegetation — glimpses of the past, the present, and perhaps the future. *Geomorphology*, 116:274–85.

Pal, N.R. and Pal, S.K., 1993. A review on image segmentaion techniques. *Pattern Recognition*, 26(9):1277-94.

Pielou, E.C., 1984. *The Interpretation of Ecological Data: a Primer on Classification and Ordination*. New York, NY, USA: John Wiley and Sons, 263 pp.

Platt, R.V. and Rapoza, L., 2008. An evaluation of an object-oriented paradigm for land cover classification. *The Professional Geographer*, 60(1):87-100.

Podobnikar, T., Stancic, Z. and Oštir, K., 2000. Data Integration for the DTM Production. In Fras, M.K., Mussio, L., Crosilla, F. and Podobnikar, T., eds. *Bridging the Gap: ISPRS WG VI/3 and IV/3 Workshop*. Ljubljana, Slovenia, 2000. Institute of Geodesy, Cartography and Photogrammetry.

Pollen-Bankhead, N. and Simon, A., 2010. Hydrologic and hydraulic effects of riparian root networks on streambank stability: Is mechanical root-reinforcement the whole story? *Geomorphology*, 116:353–62.

Qiu, Z., 2009. Assessing critical source areas in watersheds for conservation. *Environmental Management*, 44:968-80.

Red River Regional Council, 2006. *Assess and Recommendations for Riparian Stabilization and Restoration of the Turtle River within the Grand Forks Air Force BaseNorth Dakota*. Grafton, ND, USA: Red River Regional Council, 33 pp.

Richards, K., Brasington, J. and Hughes, F., 2002. Geomorphic dynamics of floodplains: ecological implications and a potential modelling strategy. *Freshwater Biology*, 47:559–79.

Richards, J.H. and Chirman, D.B., 1994. *Establishment of understorey woody species of California Central Valley riparian habitats: nutrient dynamics and flooding tolerance*. UC Water Resources Center Technical Completion Report no. 786. Riverside County, California: University of California Water Resources Center University of California, 42 pp.

Roberts, J. and Ludwig, J.A., 1991. Riparian vegetation along current-exposure gradients in floodplain wetlands of the River Murray, Australia. *Journal of Ecology*, 79:117-27.

Saunders, E.J., 2000. *Riparian Areas and Endangered Species: A Summary of the Use of Riparian Habitats by Species at Risk in Canada*. Report No. 008. Lethbridge, AB, Canada: Cows and Fish, 9 pp.

Seebacher, L.A., 2008. *Phalaris arundincea Control and Riparian Restoration within Agricultural Watercourses in King County, Washington*. PhD Thesis. Seattle, WA, USA: University of Washington, 108 pp.

Skally, C. and Sagor, E., 2001. *Comparing Riparian Management Zones to Riparian Areas in Minnesota (Pilot Study): A Mid-Term Follow-Up Action in Response to the Riparian Peer Reviews from the Minnesota Forest Resources Council*. Minnesota Forest Resources Council, St. Paul, Minnesota, USA: Minnesota Forest Resources Council , 11 pp.

Smith, R.E. et al., 1998. *Terrestrial Ecozones, Ecoregions, and Ecodistricts: an Ecological Stratification of Manitoba's Landscapes.* Technical Bulletin 98-9E. Winnipeg, Manitoba, CA: Land Resource Unit, Agriculture and Agri-Food Canada, 319 pp.

Steiger, J. et al., 2005. Hydrogeomorphic processes affecting riparian habitat within alluvial channel-floodplain river systems: a review for the temperate zone. *River Research and Applications*, 21:719-37.

Sterling, D.L., 2003. *A Comparison of Spatial Interpolation Techniques For Determining Shoaling Rates of The Atlantic Ocean Channel*. MSc Thesis. Blacksburg, VA, USA, USA: Virginia Polytechnic Institute and State University, 94 pp.

Swanson, F.J., Gregory, S.V., Sedell, J.R. and Campbell, A.G., 1982. Land-water interactions: the riparian zone. In R.L. Edmonds, ed. *Analysis of Coniferous Forest Ecosystems in the Western United States*. Stroudsburg, PA, USA: Hutchinson Ross Publishing Company. pp.267-91.

Szumilas, M., 2010. Explaining odds ratios. *Journal of the Canadian Academy of Child and Adolescent Psychiatry*, 19(3):227-29.

Tabacchi, E. et al., 1998. Development, maintenance and role of riparian vegetation on the landscape. *Freshwater Biology*, 40:497-516.

Tabacchi, E. et al., 2000. Impacts of riparian vegetation on hydrological processes. *Hydrological Processes*, 14(16-17):2959- 2976.

Teller, J.T., 1984. *Natural Heritage of Manitoba*. Winnipeg, Manitoba, CA: Museum of Man and Nature, 208 pp.

Thompson, D., 2009. Ranking predictors in logistic regression. In *MWSUG XX Proceedings*. 11-13 October 2009, Cleveland, Ohio, 2009.

Tucker, C.J., 1979. Red and photographic infrared linear combinations for monitoring vegetation. *Remote Sensing of Environment*, 8:127-50.

USDA, 2004. *Appendices to the Chattahoochee-Oconee National Forests Land and Resource Managment Plan*. Management Bulletin. Forest Service, Southern Region, Atlanta, Georgia, USA: United States Department of Agriculture: C-1 - C-6.

Van Pelt, R., O'Keefe, T.C., Latterell, J.J. and Naiman, R.J., 2006. Riparian forest stand development along the Queets River in Olympic National Park, Washington. *Ecological Monographs*, 76(2):277-98.

Verry, E.S., Dolloff, C.A. and Manning, M.E., 2004. Riparian ecotone: a functional definition and delineation for resource assessment. *Water, Air, and Soil Pollution: Focus*, 4(1):67-94.

Wandinger, U., 2005. Introduction to LiDAR. In *LiDAR: Range-resolved Optical Remote Sensing of the Atmosphere*. New York, NY, USA: Springer Science+Business Media Inc. pp.1-18.

Wang, Y., Weinacker, H. and Koch, B., 2008. A lidar point cloud based procedure for vertical canopy structure analysis and 3D single tree modelling in forest. *Sensors*, 8:3938-51.

Ward, J.H., 1963. Hierarchical grouping to optimize an objective function. *Journal of the American Statistical Association*, 58(301):236-44.

Welsted, J., Everitt, J. and Stadel, C., eds., 1996. *The Geography of Manitoba: Its land and Its People*. Winnipeg, Manitoba, CA: The University of Manitoba Press, 352 pp.

Wenger, S., 1999. *A Review of the Scientific Literature on Riparian Buffer Width, Extent and Vegetation*. Athens, Georgia: Public Service and Outreach, Institute of Ecology, University of Georgia, 59 pp.

Wood, J.D., 1996. *The Geomorphological Characterization of Digital Elevation Models*. PhD Thesis. Leicester, UK: University of Leicester.

Wulder, M.A. et al., 2008. LiDAR in sustainable forest management. *Forestry Chronicle*, 84(6):807-26.

Wynn, T.M. and Mostaghimi, S., 2006. Effects of riparian vegetation on stream bank subaerial processes in southwestern Virginia, USA. *Earth Surface Processes and Landforms*, 31:399–413.

Yang, X., 2007. Integrated use of remote sensing and geographic information systems in riparian vegetation delineation and mapping. *International Journal of Remote Sensing*, 28(2):353-70.

Young, R.G. and Collier, J.K., 2009. Contrasting responses to catchment modification among a range of functional and structural indicators of river ecosystem health. *Freshwater Biology*, 54:2155–70.

Yu, et al., 2006. Object-based detailed vegetation classification with airborne high spatial resolution remote sensing imagery. *Photogrammetric Engineering and Remote Sensing*, 72(7):799–811.

Zaimes, G.N., Schultz, R.C. and Isenhart, T.M., 2008. Streambank soil and phosphorus losses under different riparian land-uses in Iowa. *Journal of the American Water Resources Association*, 44(4):935-47.